Enhancing Ballast Performance using Geocell Confinement

Ben Adam Leshchinsky

Submitted in partial fulfillment of the
requirements for the degree of
Doctor of Philosophy
in the Graduate School of Arts and Sciences

COLUMBIA UNIVERSITY

2012

ABSTRACT

Enhancing Ballast Performance through Geocell Confinement

Ben Adam Leshchinsky

In past years, railroad transportation has been of growing interest due to its efficiency and advancement in railway technologies. However, many issues arise due to the variability in subsurface conditions along the sizeable lengths of track that exist. One very important issue is the need for significant upkeep and maintenance for railways passing over areas of poor soil conditions due to continuous deformation and a lack of stiffness from the ballasted foundation. One general solution for lack of substructure integrity has been confinement, applied through a variety of reinforcement types, including geocell. To investigate the effectiveness of geocell confinement on ballasted substructure integrity, a series of embankment model tests with different configurations of geocell placement (one layer and two layers of geocell) were constructed and loaded monotonically and cyclically for comparison to unreinforced, control tests. Upon the completion of these tests, the model embankments were simulated numerically using finite element procedures. The results were then used as validation for a parametric study, observing the effects of less competent geocell material, ballast and foundation conditions and their implications. Further numerical simulations were then performed on railroad embankments reinforced with and without geocell to model realistic railroad conditions and the effects of confinement on performance.

The tests and numerical simulations demonstrate that geocell confinement effectively increased stiffness and strength of a ballast embankment, while reducing vertical settlement and lateral spreading. Additionally, the parametric study shows that the use of geocell provides a composite,

“mattressing” effect that distributes subgrade stress more uniformly than without reinforcement, increasing bearing capacity and reducing settlement, especially on soft foundations or when using weaker ballast. The results suggested that in some site conditions, use of geocell might be an economical alternative to frequent maintenance and/or lower train speeds. Additionally, it implies that geocell might be cost-effective when used in combination withed degraded, weaker ballasts, i.e. inferior local or recycled materials. The use of geocell in ballast stabilization could prove to a sustainable solution for a common and expensive problem.

TABLE OF CONTENTS

LIST OF FIGURES

LIST OF TABLES

ACKNOWLEDGEMENTS

First and foremost, I would like to extend my gratitude to my advisor, Dr. Hoe Ling, who has tirelessly taught and mentored me through all of the stages of learning and research. He has done this noble deed thanklessly, always ensuring that I never miss an opportunity. He has never turned me away from his office when I need help, no matter the circumstance. Much of my success is a reflection of Dr. Ling and the great advice and guidance he has always provided me. In addition to being an excellent advisor professionally, he has been like a father to me, and most importantly, he has been my friend. I will always appreciate the respect he has shown me despite being a mere graduate student, and the fact that we could connect on a personal level. I will never forget my studies at Columbia, one of the primary reasons being Dr. Hoe Ling.

Very little of this research could have been performed without funding to provide for testing. I would like to acknowledge funding by both PRS Mediterranean and the Federal Railroad Administration for financial support during my studies at Columbia. This support was essential to study of this project, and I am very grateful.

I would like to thank the Department of Civil Engineering and Engineering Mechanics at Columbia University in the City of New York. Much of initial fellowship was covered by the department for being a teaching assistant, which was the introduction into one of my favorite activites: teaching. Without this great opportunity, I would have never found the satisfaction (and anguish) that is teaching undergraduates Mohr's Circle.

I would like to appreciate the time and effort my committee has put forth in reviewing and offering feedback to me for my thesis. This tedious process is very difficult and your feedback, suggestions and time will never be forgotten.

I also would like to thank the Engineering School's Dean's Office, specifically Promiti Dutta. My latter fellowship exposed me to many areas that I would never have been exposed to otherwise, including entrepreneurship, architecture, mentorship and service. I will always be grateful for my teaching experiences at various schools in the Harlem area. These experiences have taught me to be grateful for my childhood and to be optimistic about the future of our society.

In addition to advising and organizations that made my research possible, there are many people who have been integral parts of many different stages of my studies. Dr. Liming Li has always been the expert with the know-how to help with my laboratory work. I have learned much from his meticulous nature, ingenuity, and extensive experience. Most of all, I appreciate his jovial nature and am glad to call him a friend. Additionally, I would like to thank Giulia Macaro and Alessandro Martucci for the invaluable help in one of the most difficult phases of my research: the laboratory testing stage. This involved many hours of dusty, dirty, and strenuous work with large amounts of ballast, a job that many would pass up on. However, they always showed up ready to work with a good attitude, and admittedly none of this work could have been finished without their help. Additionally, several patient people have had the burden of helping me learn the nuances of Finite Element modeling, a job with reward. However, they assisted me with patience and a smile, for which I would like to thank Arturo Montoya and Badri Hiruyir. I have had the pleasure of recently meeting Askar Zhusupbekov, and will always be grateful for his professional help throughout the last year. Additionally, I must thank Ching Hung for his

assistance with many of the mundane tasks necessary to maintain the Soils Lab and his great attitude to go along with it. I wish him the best of luck on finishing his studies.

It is, of course, impossible to ignore the support that my family has provided for me throughout my studies at Columbia University. Very few have had to deal with the highs and lows of my academic career like my parents. I am very fortunate that my father has been an incredible resource of knowledge, professional advice, and experience. He has always been my biggest critic for all of the right reasons. I appreciate his unwavering demands for performance and quality in all of my work and can only hope to emulate his astounding work ethic one day. My mother deserves just as much credit for her help through my time in New York. She has taken the painful job of dealing with my everyday complaints and the emotional rollercoaster that is life. She does so with love, care, patience and realism that I could not be more grateful for. I am so fortunate to have her as my mother. Also, my brother Nathan has always checked in on me from time to time, and for this, I am grateful. I am very lucky to have the dedication of a caring family. I am also very fortunate to have had the support of my father-in-law and mother-in-law, who have been nothing but thoughtful and supportive during this arduous process. Their kindness has been a great asset for which I am very grateful.

There is a common expression that could not bear any more truth: “An individual does not get a Ph.D., a couple gets a Ph.D.”. I can say with absolute certainty that my wife, Ariel, has been the foundation and primary reason I have made it this far in my academic career. Nobody else has had to deal with the weariness, the bad moods, the late nights, the early mornings, and the stress that has accompied my journey through this doctoral program. During this challenging part of my life, I have always depended on her, and she has always been there. For her endless support,

patience and help during a time where she deserved more attention, I can be nothing short of grateful, especially to call her my best friend.

DEDICATION

This dissertation is dedicated to my family, both old and new, both alive and passed away. Thank you for who you are and who you have made me.

CHAPTER 1: INTRODUCTION

1.1 Objective and Scope

The objective of this study is to observe the behavior of ballast reinforced with geocell and its effects on the performance and behavior of a railroad substructure. The implications of this project should provide insight into future design methods for railroad and geotechnical engineers. In order to make assertions on the behavior of such a geotechnical structure, experimental results followed by a series of numerical investigations would be employed.

In this study, laboratory experiments simulated the benefits of geocell on stiffness, strength and displacement under monotonic and cyclic loading in a controlled environment.

1.2 Background

In the past few decades, geosynthetics have been increasingly popular in construction and geotechnical ground improvement applications due to its ease of use and cost-efficiency. Their ease of installation and significant benefits has been a major factor in their increased use since the 1970's, especially in a variety of geotechnical structures, including earth retention, slopes, roadway construction, landfill lining, and coastal protection. To cater to this broad variety of geotechnical functions, geosynthetics have been developed in a multitude of forms and material combinations. These include geogrids, geomembranes, geotextiles, geonets, geocomposites and geocells (Koerner, 2005).

Geocell has long been used as means for improving soil conditions. It was originally developed by the US Army Corps of Engineers to increase vehicular mobility over loose, sandy subgrade through cellular confinement (Webster and Alford, 1977). Geocell has been shown to increase soil strength by confinement, reducing lateral spreading and causing the confined composite to behave as a more rigid mattress (Zhou and Wen, 2008). The higher stiffness of the geocell system reduces the stress applied to the subgrade due to bending stiffness of the mattress composite, similar to a slab (Pokharel et al., 2011). Several studies have shown that utilization of the cellular confinement mechanism significantly improves the strength and stiffness of a granular material; however a lack of generic design methodology has inhibited its implementation (Han et al., 2008).

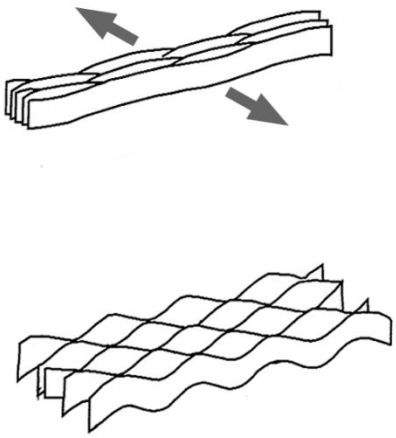

Figure 1.1 Common shape of geocell, when shipped (top) and outstretched (bottom), (credit, Koerner, 2005).

Geocell is generally sold in folded form, whereupon it can be outstretched into its three-dimensional shape and infilled with soil (*figure 1.1*). The soil, generally weaker at lower confining pressures has added strength due to the confinement effects of the reinforcement cells

surrounding it, providing a higher bearing capacity and stiffness. Geocell significantly increases the shear strength of the soil as shown by past triaxial tests (Koerner, 2005).The geocell also prevents excessive displacements of the infilled soil because of the cell confinement and the redistribution of stresses to the underlying soil. The composite action of the geocell and its fill is known as the "mattressing" effect and allows the reinforced soil to distribute loads much more uniformly to its subgrade, contributing to the aforementioned increase in bearing capacity, stiffness and reductions in displacements. These benefits are especially pronounced when used on soft subgrades.

Various shapes and sizes of geocell exist (*figure 1.2*), and they can be found in a multitude of materials. They are commonly found with heights varying from 75 mm to 200 mm, and with cell sizes ranging from 17 cm x 17 cm to 35 cm x 35 cm. Geocell is commonly made with High Density Polyethylene (HDPE), but can made with other polymers, including Novel Polymeric Alloy (NPA). In fact, the original geocell was made with Aluminum (Koerner, 2005). Geocell commonly has perforations along its walls to allow for rapid drainage laterally through the material, especially in soil reinforcement applications where water can initiate failure. Additionally, the holes can allow for further interlocking with granular materials, although the reduced nominal width of the cell walls does cause the wall tensile strength to be lower. This multitude of product specifications allows extreme versatility in its applications to soil reinforcement. This suggests that geocell could be beneficial in a ballasted railroad foundation as well.

Figure 1.2. Various Geocells: Strataweb (left, copyright: Strata Systems), Geoweb (middle, copyright: Presto), and Neoweb (right, copyright: PRS Mediterranean.

Despite the use of geocell reinforcement in a variety of geotechnical applications for decades, there is limited study on its use in railway engineering, possibly due to a combination of the sensitive, conservative nature of the field and a lack of design methodology for such an application, specifically for railroad embankments. Although the reinforcement has shown to improve performance under static and cyclic loading, optimal placement of geocell and its performance in a challenging environment such as train ballast is not well-studied, but has significant promise. Further insight into geocell and ballast behavior in a railroad application could provide incentive for the development of design methods in such an application. Such an application could have economical and environmental implications for future railroad design and track rehabilitation. Ballast functions as a base that absorbs energy, drains easily and resists forces acting vertically and laterally, providing a stiff, competent foundation for the repeated loading exerted by train passes (Selig and Waters, 1994). However, these important roles face significant technical issues that challenge the function of a working railroad. The pressures resulting from train loading can result in rearrangement and degradation of ballast over many loading cycles, reducing grain interlocking and facilitating lateral movement of particles (Lackenby et al., 2007). Track stability can decrease with the lateral spreading of ballast particles

due to decreasing frictional strength (Selig and Waters, 1994). Vertical and lateral deformations as a result of spreading or foundation problems result in loss of track geometry. Retention of ballasted foundation geometry is important; the cost of track maintenance due to geotechnical issues is significant when compared to other track expenses (Indraratna et al., 1998).

Ballasted railway foundations are supposed to be thick enough to ensure uniform loading of the subgrade at an acceptable intensity (Indraratna et al., 2006). Geocell confinement increases strength and stiffness of the infill, which in turn distributes the stress to a larger area, especially upon soft subgrades (Chrismer; 1997; Zhou and Wen, 2008; Yang, 2010). It is possible that geocell-ballast composite action could enhance this mechanism, which is especially advantageous under the high loading intensity of moving trains. In addition to the redistribution of vertical stresses (Chrismer, 1997), the confining behavior provided by reinforcements has been shown to reduce and/or re-disbribute shear stresses at the subgrade interface (Giroud and Han, 2004). Since ballast is generally a highly frictional material while the subgrade is often inferior, the reduction of shear stresses is highly beneficial. Some studies have suggested that use of geocell can improve ballast performance and stability, including a reduction in deformation (Raymond, 2001), sustained track geometry (Chrismer, 1997) and an increase in strength and resilience under cyclic loading (Indraratna et al., 2006). The increase in the confinement in the ballast due to geosynthetics would reduce the strains encountered in the foundation as well (Indraratna et al. 2010).

1.3 Organization of Dissertation

This dissertation is organized into six different chapters and two appendices that outline different phases of this work. Following this introductory chapter, a chapter describing preliminary

material testing and laboratory work is presented. Then, chapter three describes laboratory testing of large-scale ballast models. Chapter four describes numerical simulation of the laboratory tests and a parametric study based on the same model geometry. Chapter 5 consists of numerical modeling of geocell applied to an actual ballasted railway geometry. Finally, Chapter 6 consists of conclusions and recommendations based upon the study, as well as proposed areas for future research.

CHAPTER 2: MATERIAL CHARACTERIZATION

2.1 Introduction

It is vital to characterize materials before using them in laboratory tests, such as the ballast embankment models. Knowledge of material properties allows a better understanding of behavior and constraints that are relevant to the testing that will be performed. Therefore, various material tests were applied to both the ballast and geocell that were used in further experimentation.

A series of triaxial tests were performed to determine the strength and deformation properties of the ballast that was used in testing. In these tests, samples were loaded both monotonically and cyclically, since ballast is generally exposed to cyclic loads resulting from many train passes. The ballast specimens were loaded to shear failure in order to determine the material strength properties for use in further analyses.

During these tests, a variety of data was recorded, including axial stress, axial strain, volumetric strain and confining pressure. Before and after each test was performed, the material was put through a series of sieves in order to determine its gradation. The level of breakage and abrasion resulting from the triaxial loading was then evaluated. After each gradation analysis, any material passing a #4 sieve (equivalent aperture of 4.75 mm; retained material is defined as gravel) was removed from the sample.

In addition to determining the material properties of the ballast used in testing, the tensile strength and Young's Modulus of the geocell was determined. A series of tension tests were run

in both monotonic and cyclic loading conditions, where axial load and strain were recorded. The test specimen used was 6 inches in length, had a nominal width of 1 inch and maintained a "dogbone" shape in accordance with ASTM standards (ASTM D638).

2.2 Large-Scale Triaxial Specimen

A series of minimum and maximum density tests were performed on the ballast, composed of red granite, according to ASTM standards to attain its unit density. The maximum and minimum unit densities were 1535 kg/m^3 and 1330 kg/m^3, respectively. For poorly-graded materials, the difference between the minimum and maximum unit densities is usually small, as the material often reaches a higher relative density with placement alone.

Due to the large grain size of the ballast used in testing (*figure 2.1*), a traditional triaxial testing apparatus for normally-sized and medium-sized specimen (Diameter = 7 cm and Height = 14 cm, Diameter = 3.5 cm and Height = 7 cm, see *figure 2.2*) could not be used. This limitation is due to the interference caused by the gravel grain size compared to the actual specimen size. In order to effectively test the material strength properties and attain reliable data, a custom triaxial apparatus was constructed with larger dimensions to ensure no boundary interference and allow the ballast to behave as a continuum. Using a MTS loading actuator with a capacity of 450 kN, a triaxial specimen with a diameter of 30.5 cm and height of 61 cm was used. The specimen was confined by 1 cm thick latex membrane. Confining pressure was applied using a vacuum pump that applied negative pressure within the membrane, allowing confining pressures up to 1 atmosphere. The membrane was sealed and connected to the upper and lower platen using several hose clamps and high-quality vacuum grease (see *figure 2.3*). The use of these

precautions allowed for the confining pressure to remain constant throughout testing, ensuring reliable data and results.

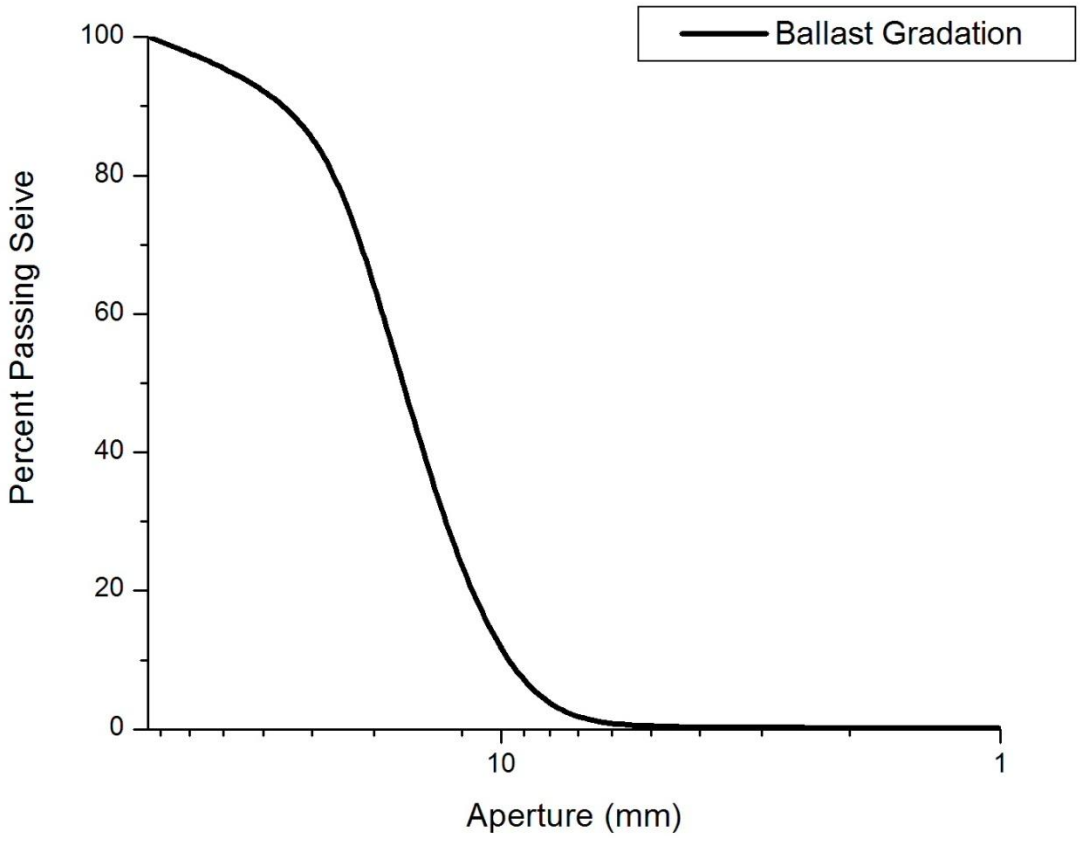

Figure 2.1. Gradation of ballast used in experimentation.

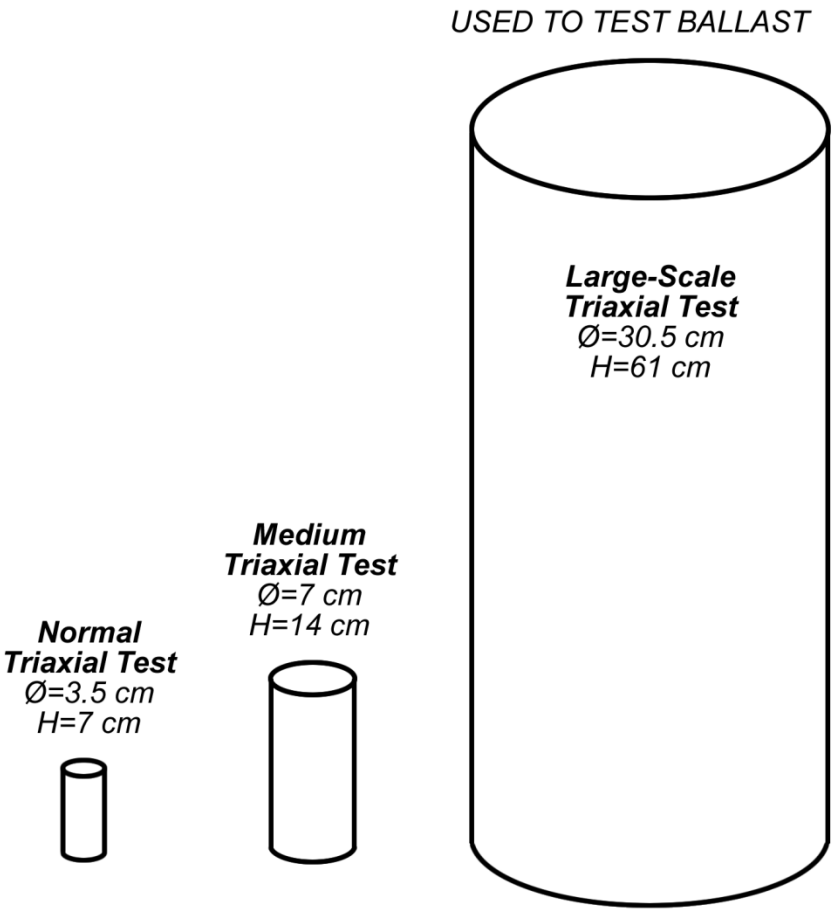

Figure 2.2. Comparison of large-scale triaxial specimen to commonly used triaxial test specimens.

Figure 2.3. Preparation of large-scale triaxial specimen.

2.2.1 Results of Monotonic Triaxial Tests

A series of four (4) large triaxial specimens were loaded monotonically at confining pressures of 95, 81, 91, and 61 kPa (*figure 2.4*). The strength properties for the material were determined from the triaxial test results. Additionally, degradation of the gravel was studied by performing a gradation analysis before and after the series of tests. Results are shown in table 2.1.

	Test 1	**Test 2**	**Test 3**	**Test 4**
Confining Pressure, σ_3 (kPa)	95	81	91	61
Axial Stress at 15% Strain,σ_1 (kPa)	420	360	420	300

Internal Angle of Friction	45°
Dilation Angle	15°

Table 2.1. Results of monotonically loaded triaxial tests.

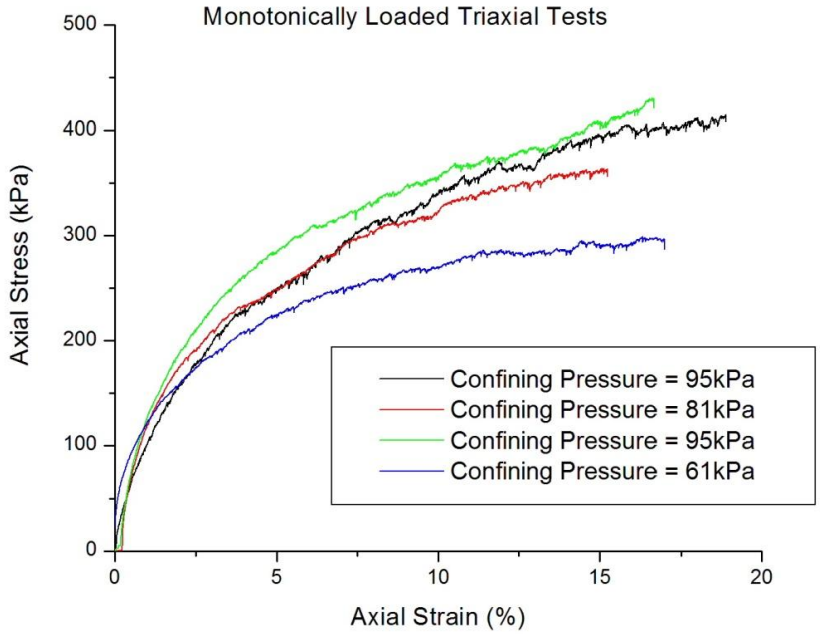

Figure 2.4. Monotonically loaded triaxial tests, Stress vs. Strain (top) and Volumetric Strain vs. Axial Strain (bottom) behavior.

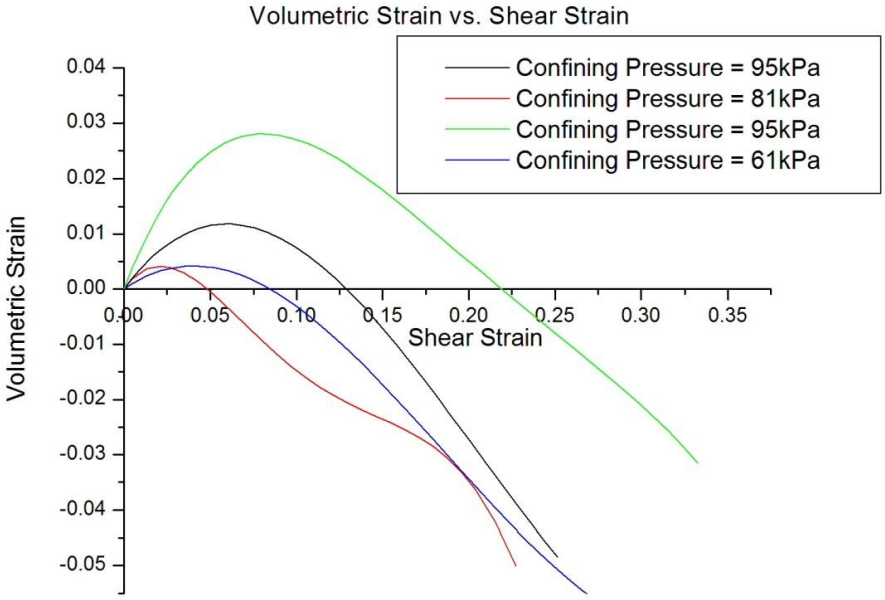

2.2.2 Material Degradation under Monotonic Loading

It is evident that in addition to the abrasion and crushing that resulted from the series of tests (2.97%), there was a shift in the gradation curve (see *figure 2.5*). This indicates that in addition to the degradation of the small particles, the larger pieces of gravel are fracturing into smaller, yet still coarse fragments. Qualitatively, one could see the change in shape of the gravel as the tests progressed. The undamaged gravel was rather angular, but several repeated heavy loadings caused the angular portions to fracture, creating rounder particles of gravel. It is apparent that the largest disparity in the gradation curves occurs within grains between 2.5 mm to 13 mm in diameter, suggesting that larger grains are crushing. Further testing under cyclic loading was pursued to obtain additional data on the material degradation when subject to limited repeated load cycles.

Table 2.2. Degradation of ballast from monotonic loading.

Degradation, % of Total Specimen Weight	2.97%
>#4 Sieve	2.58%
>#100 Sieve	0.11%
>#200 Sieve	0.11%
<#200 Sieve	0.27%

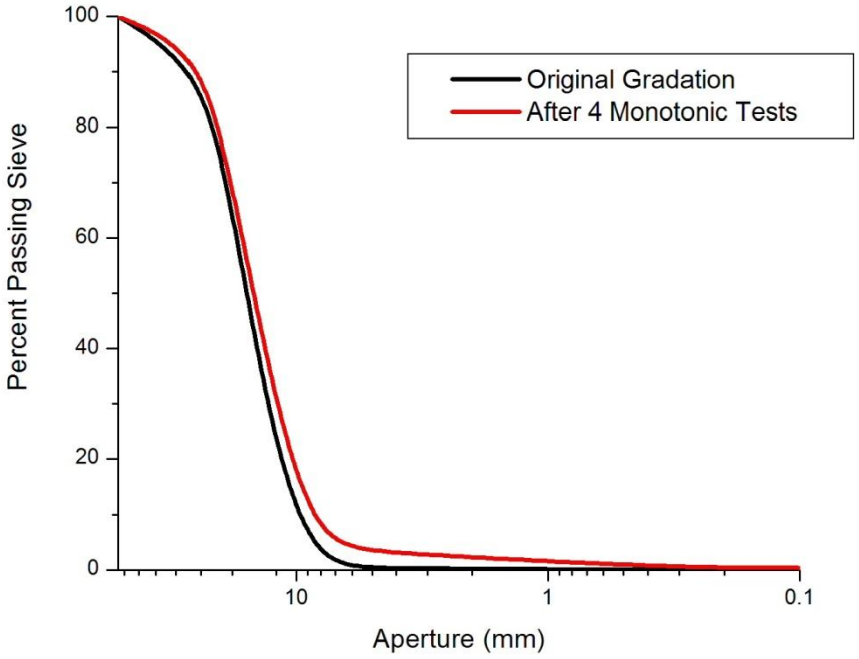

Figure 2.5. Gradation after 4 Monotonic Tests.

2.2.3 Results of Cyclic Triaxial Tests

A series of four (4) cyclic triaxial tests were performed. In each test specimens at varying confining pressures were loaded cyclically, and then failed monotonically. The confining pressures were 95, 95, 60, and 60 kPa for each respective test. Tests of either 100,000 or 250,000 loading cycles were chosen for each of different confining pressures. Degradation of the gravel was studied by performing a gradation analysis after each cyclic test. The testing began with unloaded, virgin material and a 100,000 cycle triaxial test confined at 95 kPa. The next loading included 250,000 cycles with a specimen confined at 95 kPa. *Virgin material* was then provided and the trials that followed were 100,000 and 250,000 cycles with specimens confined at 60 kPa.

Test Specifications

Any material passing a #4 sieve (opening size of 0.187 inches) was removed prior to the initial test and after each test. Material that was removed after each test was attributed to abrasion/crushing. The specimen was repeatedly loaded between 50 kPa and approximately 50% of the failure stress determined from monotonic testing. The loading frequency was 10 Hz.

Table 2.3. Test Results from Cyclically Loaded Triaxial Test

	Test 1	**Test 2**	**Test 3**	**Test 4**
Confining Pressure, σ_3 (kPa)	95	95	60	60
Stress at Failure, σ_1 (kPa)	450	440	350	300
Loading Cycles	250,000	100,000	100,000	250,000
Minimum Axial Stress, kPa	50	50	50	50
Maximum Axial Stress, kPa	280	280	170	170
Stress Amplitude, kPa	230	230	120	120
Relative Density, %	51%	35%	90%	95%
Abrasion, % of Total Specimen Weight	1.71%	1.60%	2.35%	0.70%

As evidenced in the following axial stress vs. axial strain curves, the load amplitude seemed to have an influence on the displacement over the course of the cyclic loading. Within the first few thousand cycles, the material densifies and the gravel matrix of the specimen becomes restructured and in turn, much stiffer. Note that due to a high frequency, the cyclic load amplitude stabilized when the material stiffened. This was dependent of the test conditions (*figures 2.6-2.9*) This is demonstrated by the fact that both 100,000 and 250,000 cycles of loading still cause the material to approach a constant strain (approximately 5% for confining pressure of 95 kPa; approximately 1.8% for confining pressure of 60 kPa). The possible reason for the different constant strains between the two different confining pressures is due to the load amplitudes. For non-linear materials, the amplitude has an effect on the strain resulting from cyclic loading.

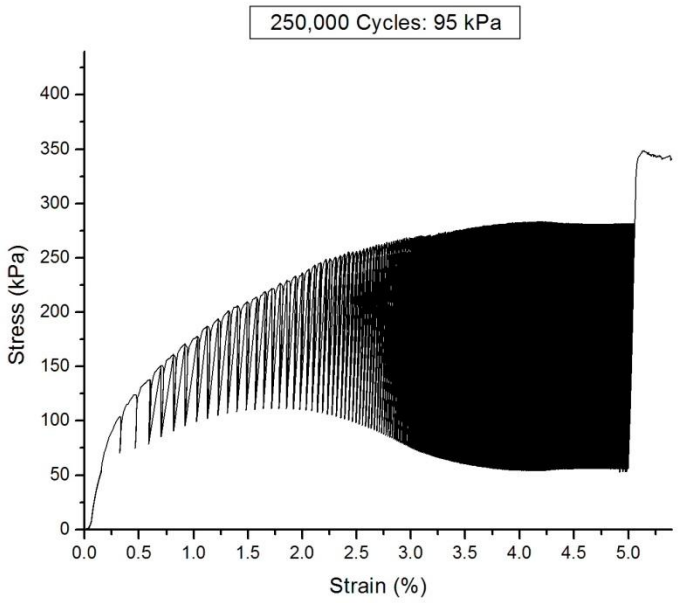

Figure 2.6. Cyclic Test 1, Axial Stress vs. Axial Strain, Confining Pressure of 95 kPa. 250,000 cycles loaded with a stress amplitude of 230 kPa.

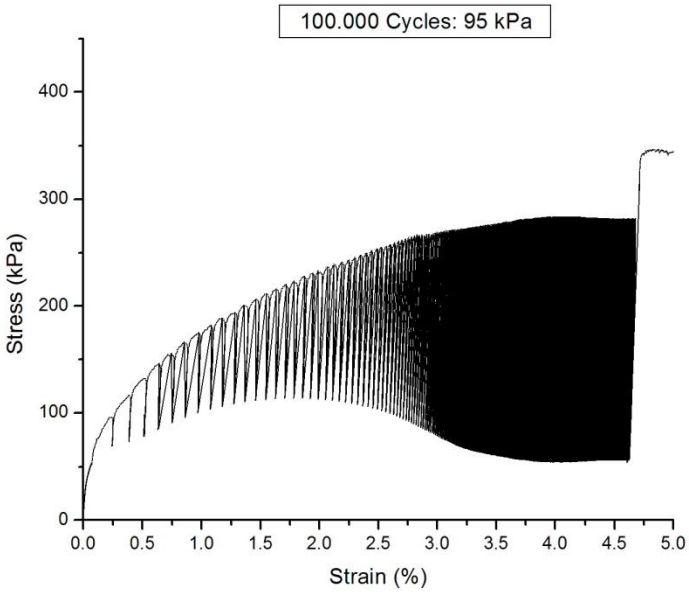

Figure 2.7. Cyclic Test 2, Axial Stress vs. Axial Strain, Confining Pressure of 95 kPa. 100,000 cycles loaded with a stress amplitude of 230 kPa.

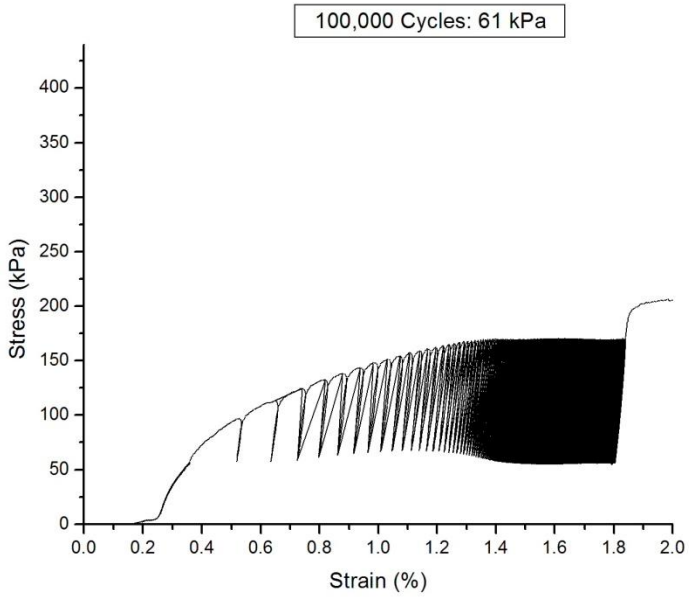

Figure 2.8. Cyclic Test 3, Axial Stress vs. Axial Strain, Confining Pressure of 60 kPa. 100,000 cycles loaded with a stress amplitude of 120 kPa.

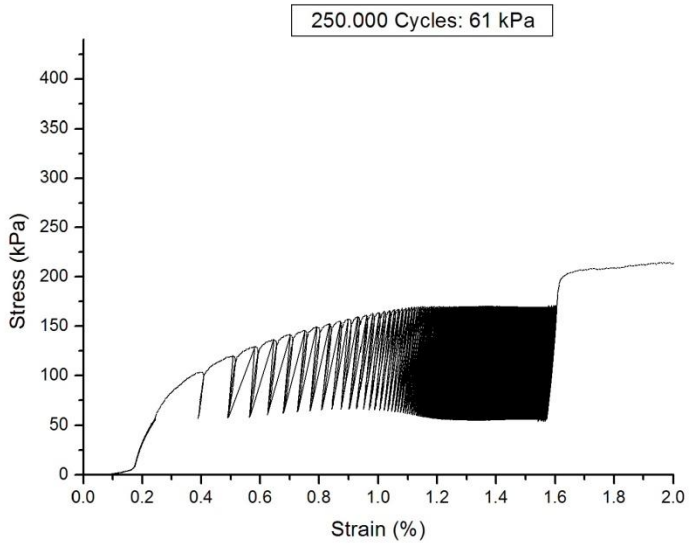

Figure 2.9. Cyclic Test 4, Axial Stress vs. Axial Strain, Confining Pressure of 60 kPa. 250,000 cycles loaded with a stress amplitude of 120 kPa.

2.2.4 Material Degradation under Cyclic Loading

The gradation analyses for the cyclic triaxial specimens indicated some interesting trends. From observation, it seems as if the confining pressure and corresponding stress amplitudes did not have a large influence on the abrasion rate. The specimen would always yield material passing a #4 sieve, with actual abrasion rates ranging between 0.7-2.35% by weight. However, despite no apparent trend for abrasion, the gradation curves indicate that most of degradation in the coarse grains happens rapidly, possibly within the first 100,000 cycles. This could be attributed to either the angularity of the untested material, or inherent cracks and weaknesses within the stone that fracture quickly under loading. This phenomenon is illustrated by the near-congruent curves for tests 1 and 2, and tests 3 and 4, respectively (*figure 2.10*). The first two tests used the same material, and then there was new, unloaded granite provided for the last two tests. When new material was used, the shift in the gradation curve is larger, especially for coarse grains. This seemed independent of the number of cycles or confining pressure. Generally, there is negligible damage to the ballast, as it is made of granite which is quite strong.

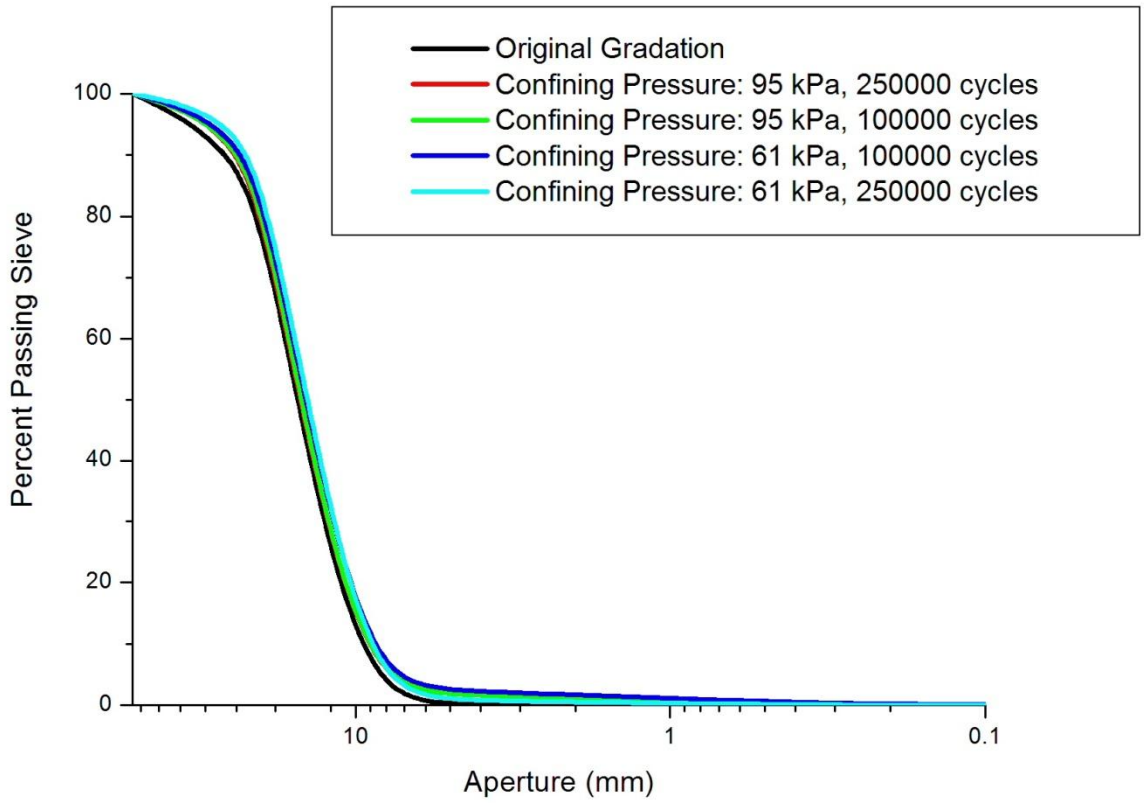

Figure 2.10. Grain size distribution for cyclically loaded triaxial tests.

2.3 Geocell Tensile Tests

The geocell was made of a material called Novel Polymeric Alloy (NPA), which was an alloy with a higher stiffness and resistance to creep than polyethylene. In order to attain its mechanical properties, several tests were performed, including tensile tests under both monotonic (0.025 mm/second loading rate) and cyclic conditions. The specimens used in tensile tests were "dogbone" shaped cutouts of the geocell walls, with a nominal width of 2.5 cm and nominal length of 12.5 cm. The material was found to have a higher stiffness (2.07 GPa) than HDPE (0.8-1.2 GPa). Its yield tensile strength was found to be approximately 26 MPa, and occurred at an approximate strain of 8% (see *figure 2.11*). However, it was found that the seams had significantly lower yield strength than the cell walls, rupturing at approximately 6.8 MPa and 15% strain (see *Figure 2.12*). This meant that the seams had only 25% of the strength of the walls, suggesting that they might be critical, especially when subjected to shear load.

The cyclically loaded tests showed significant creep in the geocell, especially under higher repeated load. Three tests were performed with 1000 loading cycles, each one having a load amplitude that went from 0 to 25% of tensile strength, 50% of tensile strength, or 75% of tensile strength (see *figure 2.13*). When the geocell encountered 25% of its load strength, it exhibited significantly less plastic strain, especially under repeated load. More of the strain occurred in the initial loading cycles as opposed to the final cycles. Under the higher loading amplitudes, significant plastic strain occurred. Additionally, the initial hundred cycles caused a significant amount of plastic strain before a gain of resilience. Generally, the geocell material would be safe under lower levels of repeated loading.

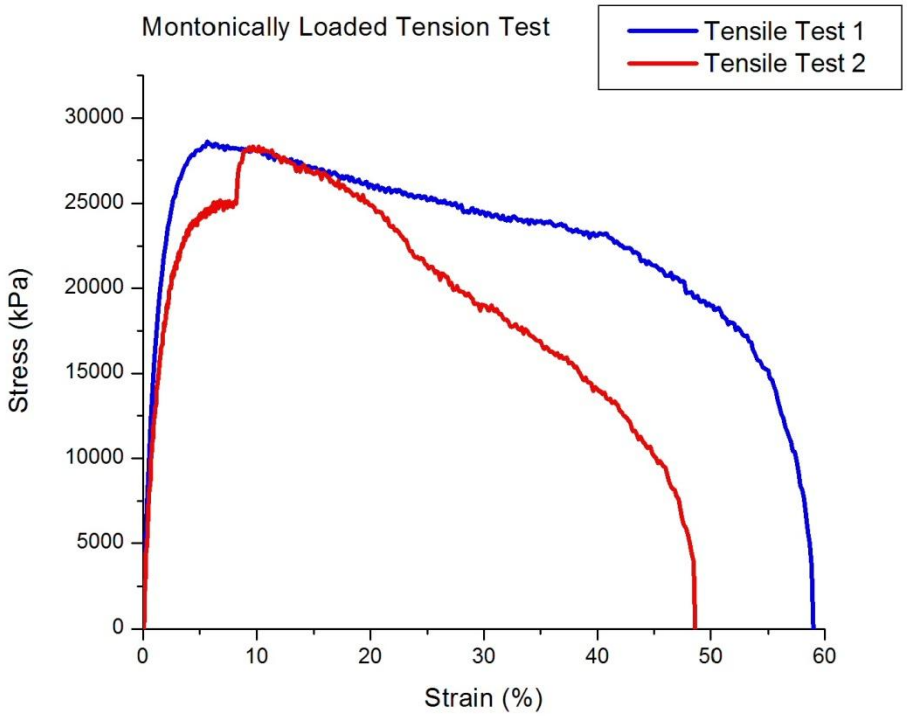

Figure 2.11. Tensile test results of NPA material used in Geocell.

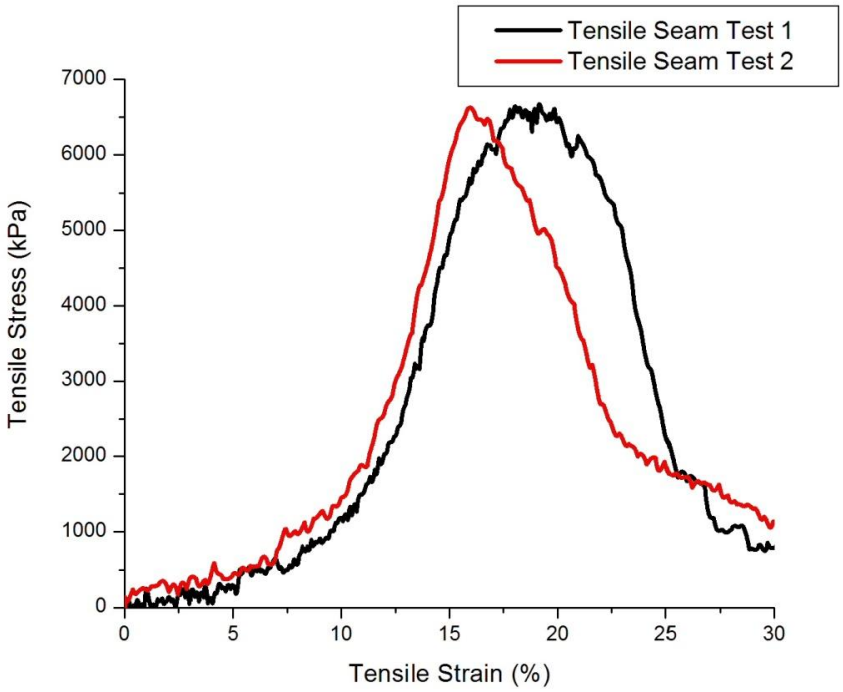

Figure 2.12. Tensile test results of welded seams in Geocell.

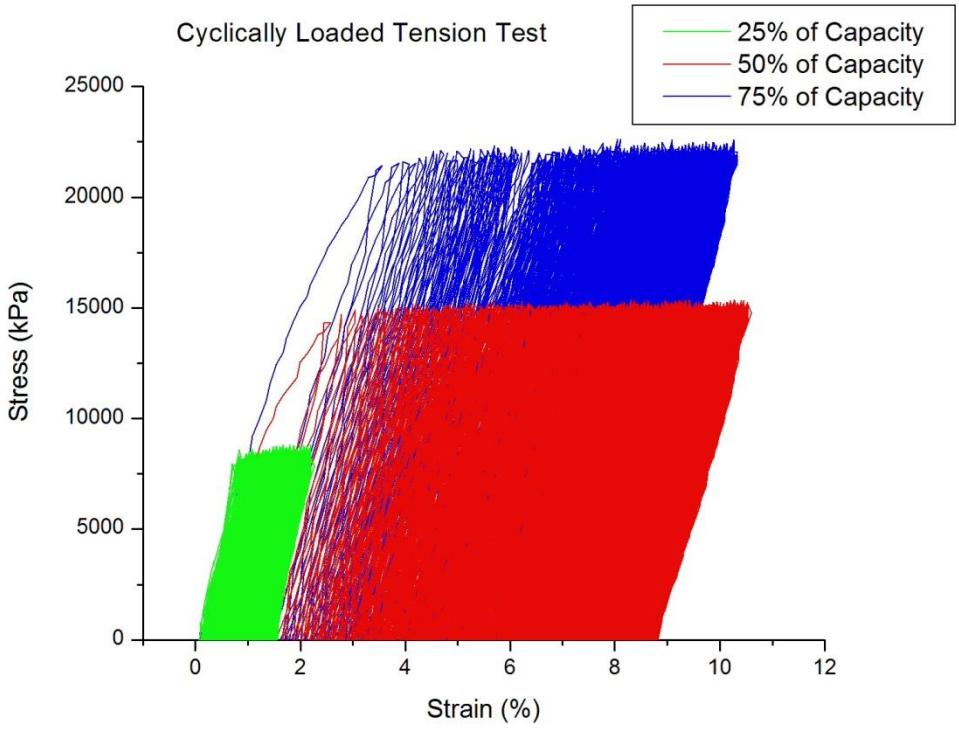

Figure 2.13. Cyclic tensile test results of NPA material used in Geocell.

2.4 Conclusions

The characterization of materials and their behavior is essential prior to full-scale testing. It allows for a better understanding of experimental constraints and expected behavior during testing. Characterization of ballast and geocell materials was performed and provided necessary data for full-scale models. The following conclusions were reached:

- Ballast degradation was limited under both monotonic and cyclic triaxial loading, as evidenced by the near congruent gradation curves provided. However, there is a slight shift, especially among medium sized to small grains, suggesting that there is some fracturing occurring among D_{50} grains (12.5 mm).

- The ballast stiffened up considerably after the first few cycles of loading, as one would expect for a poorly-graded granular material. This was also dependent on the confining pressure of the ballast.
- The geocell had a similar strength to HDPE, but a slightly higher Young's modulus. The seams of the geocell were much weaker than the walls of the geocell, as welds in geotextiles often are. Under cyclic loading, the geocell endured little plastic strain under lower loading (25% of capacity), but endured considerably more plastic strain under higher loading (75% of capacity).

CHAPTER 3: LABORATORY MODEL TESTS

3.1 Introduction

A series of six (6) loading tests were performed on the previously studied Granite ballast (see Chapter 2). These tests consisted of constructing an embankment, with and without reinforcement, and studying its behavior under loading. The reinforcement of choice was PRS Neoweb geocell. The reinforced model tests consisted of two different reinforcement configurations: a single, central reinforcement layer and a double-layer reinforcement. Each configuration was tested under two loading conditions: monotonic (static) and cyclic loading. The test results are provided and interpreted herein.

3.2 Test Setup

An H-frame was constructed to provide a reaction for the MTS actuator that loaded the constructed embankment. The test setup is shown schematically in *figure 3*.1. The MTS actuator had a 900 kN capacity and could load under both monotonic and cyclic conditions. The H-frame consisted of two 8 cm diameter steel rods, bolted to a meter-thick concrete floor for stability. The loading beam consisted of two steel channels, fastened together with 32 bolts.

The behavior that was studied during each test included lateral spreading, vertical deformation under the loading plate, bearing capacity of embankment, and strain in the reinforcement. Afterwards, a grain size distribution was performed to determine the degradation of the ballast

that may have taken place. The reinforcement was removed after testing and inspected for damage. After the tests were complete, data was compiled and analyzed.

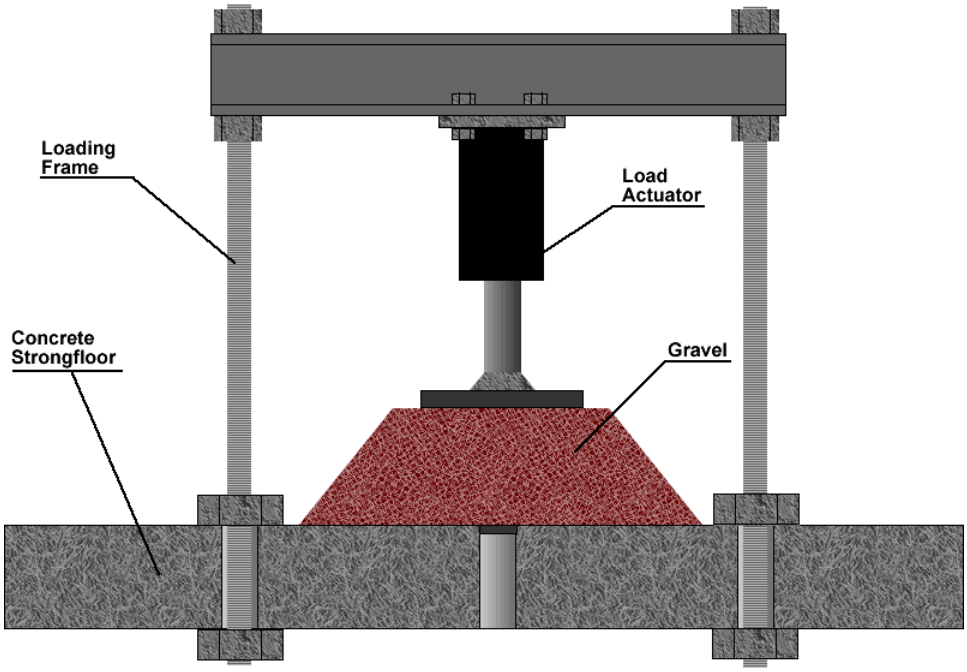

Figure 3.1. Model Test Schematic.

3.3 Unreinforced Model Tests

The control portion of the testing consisted of a model embankment that was constructed of the red granite ballast without any type of reinforcement (*figure 3.2*). This phase of the experimentation consisted of two tests: one monotonically loaded and one cyclically loaded.

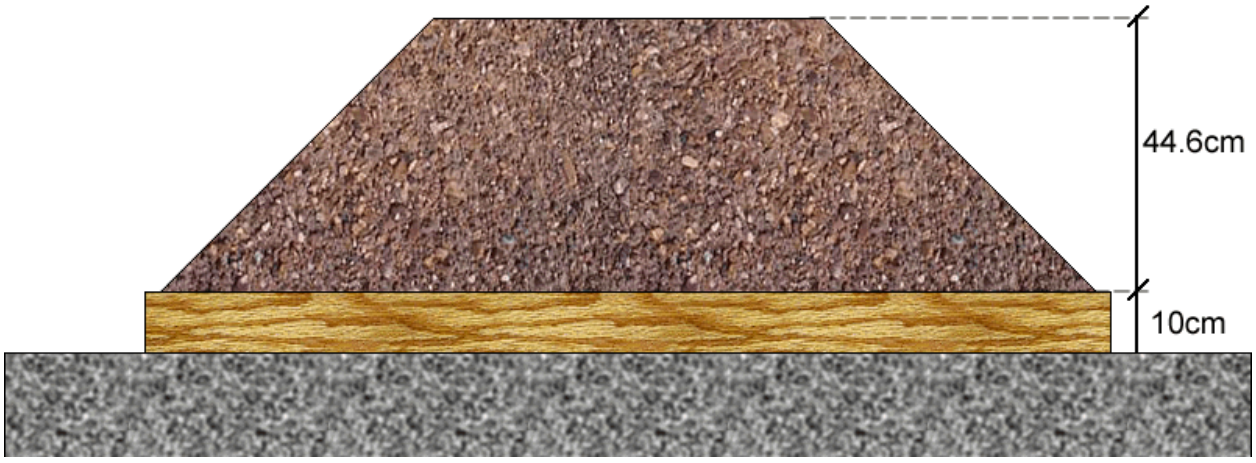

Figure 3.2. Schematic of embankment for tests 1 and 4.

3.3.1 Monotonic Loading: Test 1

The unreinforced ballast embankment was loaded monotonically under displacement-control conditions. That is, a displacement rate of 2.5 mm/minute was specified and the full loading was paused for every 6.35 mm of vertical displacement so measurements could be taken and data collected. This explains the "spikes" or seeming discontinuities in the loading curve (*figure 3.3*). Despite these jumps, the curve is rather unaffected, thus affording an estimate of apparent

stiffness. It seemingly required about 4.5 kPa of vertical stress to cause 1 mm of vertical displacement in the initial, elastic portion before "yield" occurs.

The test was stopped when it was apparent that a constant load was still causing displacement, which is classified as failure. This occurred at a vertical stress of 175 kPa.

Measurements of lateral deformation were made as the test was in progress. Considerable lateral deformations occurred at all heights, but the largest spreading occurred at the crest of the embankment (*figure 3.4*). The increase in cross-sectional widths at the recorded heights and main results are summarized in Tables 3.1 and 3.2.

Table 3.1. Lateral spreading of unreinforced, monotonically loaded embankment.

Height from Floor	**Percent Increase in Width (%)**
Top, 21.5" (54.6 cm)	31.5 %
Upper Middle, 18" (45.7 cm)	6.6 %
Lower Middle, 12" (30.5 cm)	3.0 %

Table 3.2. Summary of notable test results.

Failure Stress / Load	175 kPa (25.4 psi) / 22.1 kN (5000 lbf)
Yield Vertical Displacement	65 mm (2.56 in)
Apparent Stiffness	4.5 kPa/mm
Max. Lateral Spreading	31.5 % (Top)

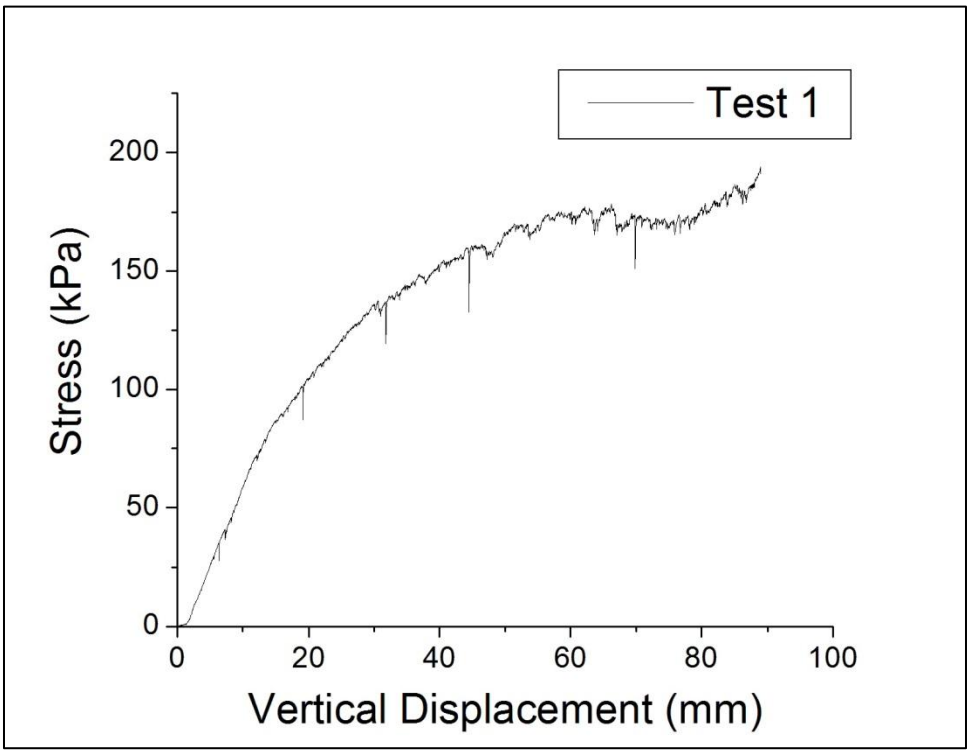

Figure 3.3. Load-Displacement Curve for unreinforced, monotonically loaded test.

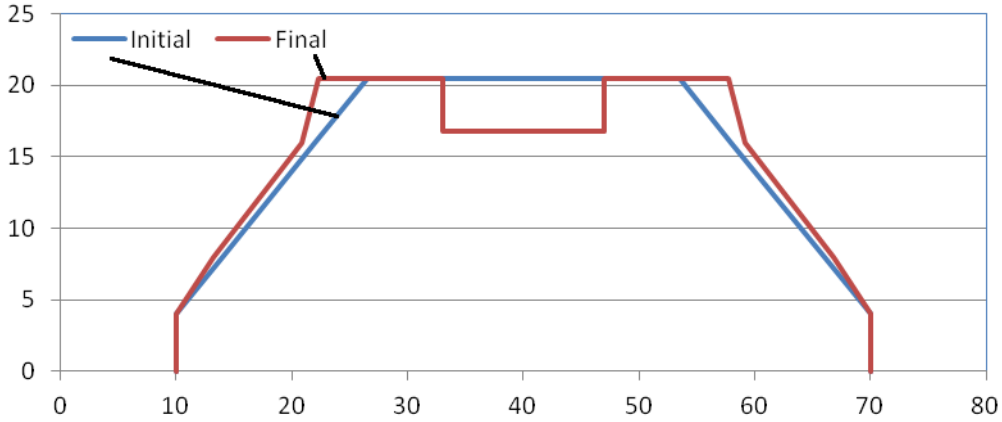

Figure 3.4. Schematic of initial shape and deformed shape of embankment after testing, all units in centimeters.

3.3.2 Cyclic Loading: Test 2

The unreinforced ballast embankment was loaded cyclically in load-control conditions. That is, a loading amplitude between 35 and 175 kPa was specified, and measurements of displacement were taken at 1000, 5000, 10000, 20000, 30000 and 50000 cycles (*figure 3.5*). The loading frequency was 10 Hz, simulating rapid loading.

The test was stopped when the load actuator reached its goal of 50,000 loading cycles. A considerable amount of vertical displacement occurred, totaling 118 mm, which is close to the maximum stroke allowed by the actuator. Much of the significant deformation occurred in the initial few hundred cycles. Although the material did seem to stiffen during the cyclic loading, the vertical displacement continued with every cycle.

As would be expected for such large vertical displacements, lateral spreading continued throughout the test and created a considerably different shape of the embankment (*figure 3.6*). Some of the most significant lateral spreading occurred in the upper-middle portion of the embankment, although there was also a very large amount of displacement at the crest. The increase in cross-sectional widths at the recorded heights and main results are summarized in Tables 3.3 and 3.4.

Table 3.3. Lateral spreading of unreinforced, cyclically loaded embankment.

Height from Floor	Percent Increase in Width (%)
Top, 21.5" (54.6 cm)	10.5 %
Upper Middle, 18" (45.7 cm)	12.1 %
Lower Middle, 12" (30.5 cm)	3.5 %

Table 3.4. Summary of notable test results.

Final Vertical Displacement	118 mm (4.65 in)
Vertical Displacement during Cyclic Loading	74 mm (2.91 in)
Max. Lateral Spreading	12.1% (Upper Middle)

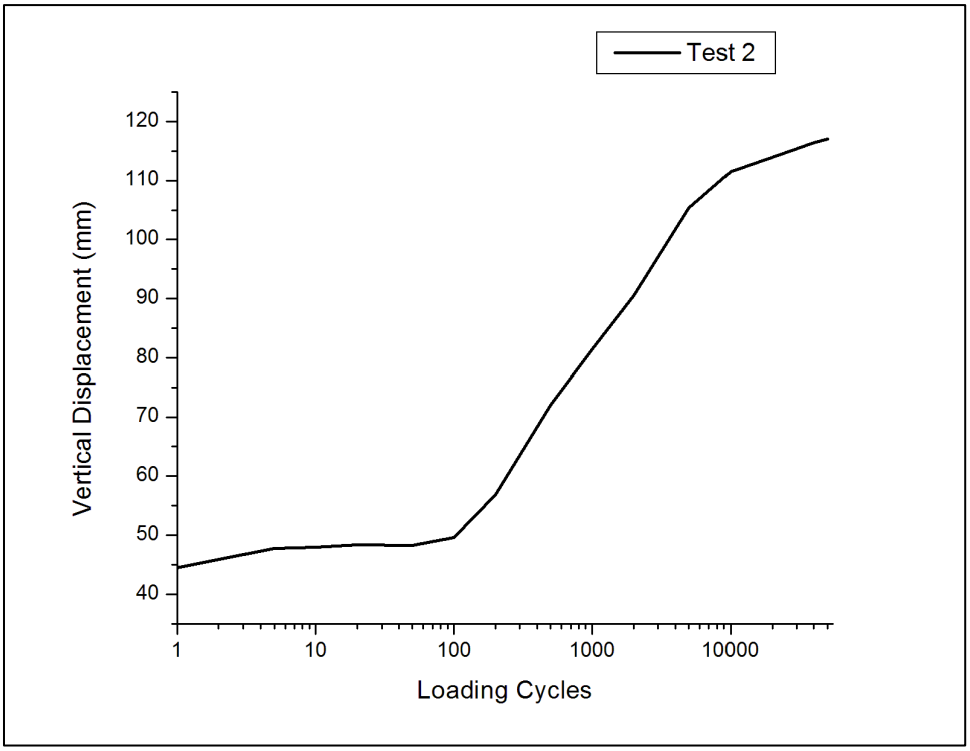

Figure 3.5. Cyclic Displacement Curve for unreinforced, cyclically loaded test.

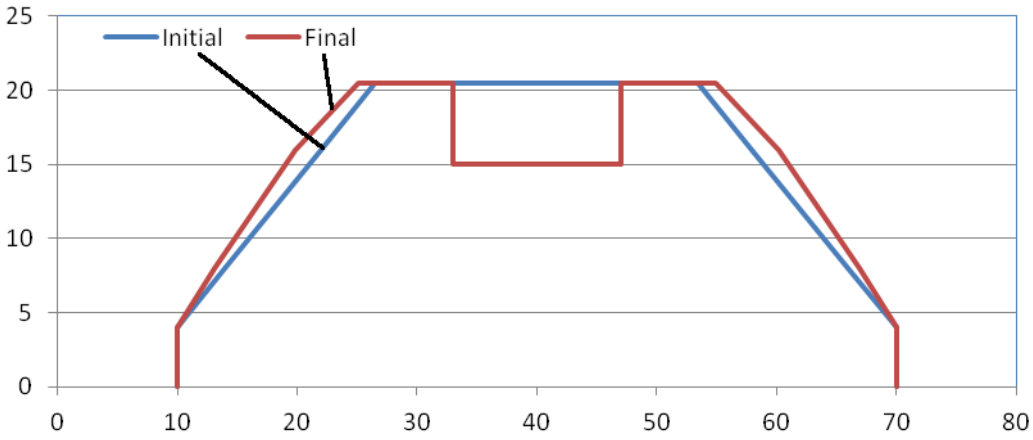

Figure 3.6. Schematic of initial shape and deformed shape of embankment after testing, all units in centimeters.

3.4 Reinforced Model Tests: One Layer of Geocell

The reinforced portion of the testing consisted of a model embankment constructed from granite, reinforced by a central layer of geocell placed 14.6 cm below the crest (*figure 3.7*). This section of the experimentation consisted of two tests: one monotonically loaded and one cyclically loaded. These tests were used to observe the behavior and strength of the ballast model and geocell *(figure 3.8)* under different loading conditions. The behavior that was observed was the apparent stiffness, deformation (laterally and vertically), and failure load. Strain gauges were place in the center and off-center cells to observe vertical and lateral strains in the geocell, Afterwards, its strength was quantified and a gradation analysis was performed.

Figure 3.7. Schematic of embankment for tests 3 and 4.

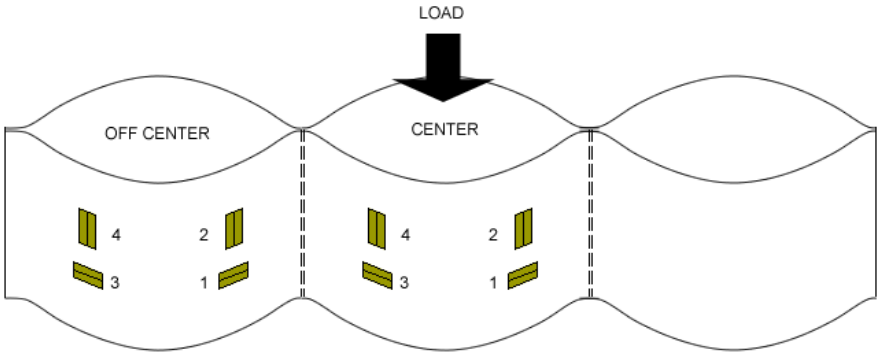

Figure 3.8. Schematic of strain gauge configuration in Geocell.

3.4.1 Monotonic Loading: Test 3

The reinforced ballast embankment was loaded monotonically in displacement-control conditions. That is, a displacement rate of 2.5 mm/minute was specified and the full loading was paused for every 6.35mm of vertical displacement so measurements could be taken and data

collected. This explains the “spikes” or seeming discontinuities in the loading curve. Despite these jumps, the curve is still rather linear, allowing an estimate of apparent stiffness (*figure 3.9*). It seemingly required about 10.9 kPa of vertical stress to cause 1 mm of vertical displacement. This apparent stiffness is higher than the unreinforced model, as expected.

In addition to a higher apparent stiffness, the reinforced model had much more strength than the unreinforced, likely due to the confinement and stiffening of the ballast from the geocell reinforcement. The test was stopped when the loading frame neared its allowable loading capacity (approximately 16,350 lbf, or 72.7 kN) of about 575 kPa. It seemed evident that the reinforced model could mobilize more strength before failure, but had already evidenced its effectiveness by doing more than tripling the carried load without excessive vertical deformation.

The confinement of the single reinforcement layer was also very effective in preventing lateral spreading. This lateral displacement was greatly reduced and mostly limited to the crest of the embankment, where no reinforcement existed (*figure 3.10*). This is very evident from the results, which indicate very little lateral deformation from the level of the reinforcement and below. The vertical displacement that occurred within the 175 kPa range of the single reinforcement test was 31% of the displacement that occurred in the same range for the unreinforced, monotonically loaded test. The increase in cross-sectional widths at the recorded heights was effectively reduced by geocell confinement. The main results are summarized in Tables 3.5 and 3.6.

Table 3.5. Lateral spreading of single-reinforced, monotonically loaded embankment.

Height from Floor	Percent Increase in Cross-Sectional Area (%)
Top, 21.5" (54.6 cm)	18.5 %
Upper Middle, 18" (45.7 cm)	3.0 %
Lower Middle, 12" (30.5 cm)	1.8 %

Table 3.6. Summary of notable test results.

Final Stress / Load	575 kPa (83.4 psi) / 72.7 kN (16350 lbf)
Final Vertical Displacement	60 mm (2.36 in)
Apparent Stiffness	10.9 kPa/mm
Max. Lateral Spreading	18.5 % (Top)

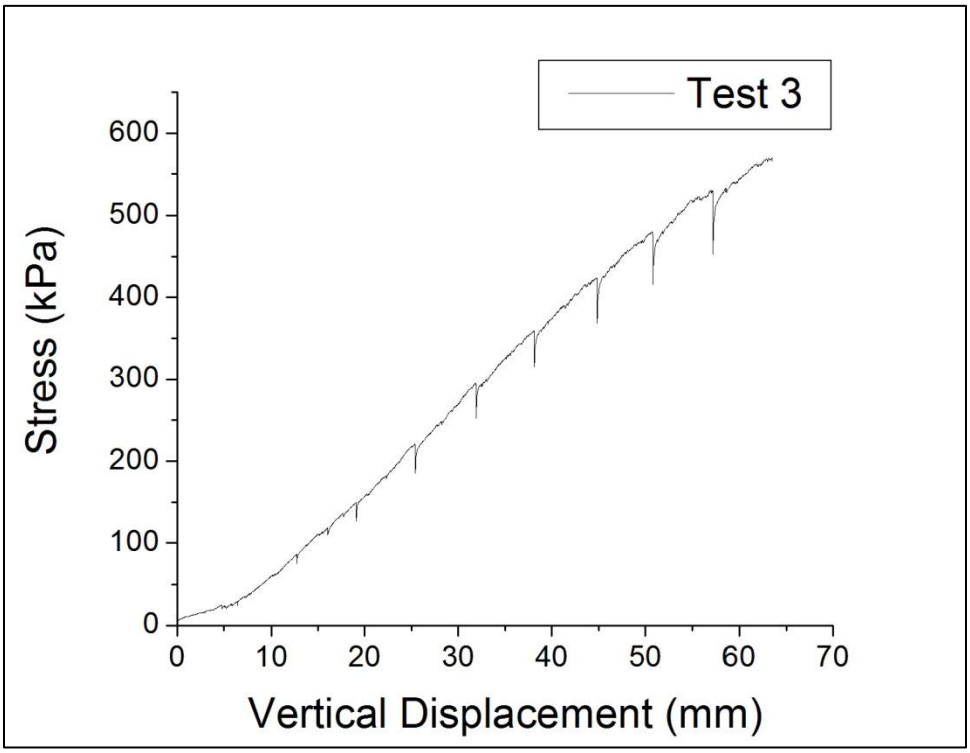

Figure 3.9. Load-Displacement Curve for single-reinforced, monotonically loaded test.

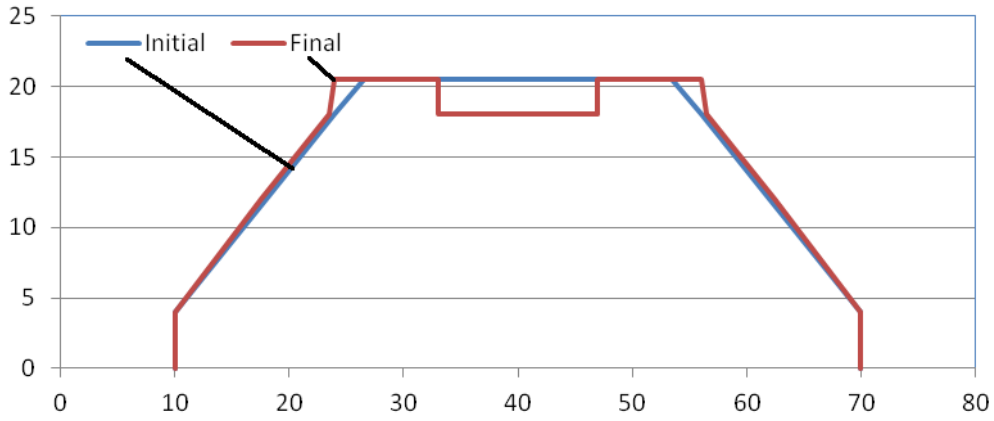

Figure 3.10. Schematic of initial shape and deformed shape of embankment after testing, all units in centimeters.

3.4.2 Cyclic Loading: Test 4

The reinforced ballast embankment was loaded cyclically under load-control conditions. That is, a loading amplitude between 75 and 350 kPa was specified and measurements of displacement were taken at 1000, 5000, 10000, 20000, 30000 and 50000 cycles. The loading frequency was 10 Hz, simulating rapid loading.

The reinforced model had much more strength than the unreinforced one, likely due to the confinement and stiffening of the ballast from the geocell reinforcement. The test was stopped when the actuator reached its goal of 50,000 loading cycles. The test indicated that it prevented almost 60% of the total vertical displacment that would have occurred if the ballast had been unreinforced (*figure 3.11*). This reduction could possibly have been much more if the cyclic amplitude for the reinforced test was the same as the lower loading amplitude used in the unreinforced test.

The confinement of the single reinforcement layer was also very effective in the preventing of lateral spreading (*figure 3.12*). This lateral deformation was greatly reduced and mostly limited to the crest of the embankment, where no reinforcement existed. This is evident from the results, which indicate that very little lateral deformation from the level of the reinforcement and below. The increase in cross-sectional widths at the recorded heights was effectively reduced by geocell confinement.The main results are summarized in Tables 3.7 and 3.8.

Table 3.7. Lateral spreading of single-reinforced, cyclically loaded embankment.

Height from Floor	Percent Increase in Cross-Sectional Area (%)
Top, 21.5" (54.6 cm)	10.7 %
Upper Middle, 18" (45.7 cm)	3.3 %
Lower Middle, 12" (30.5 cm)	1.3 %

Table 3.8. Summary of notable test results.

Final Vertical Displacement	62 mm (2.44 in)
Vertical Displacement during Cyclic Loading	36 mm (1.41 in)
Max. Lateral Spreading	10.7 % (Top)

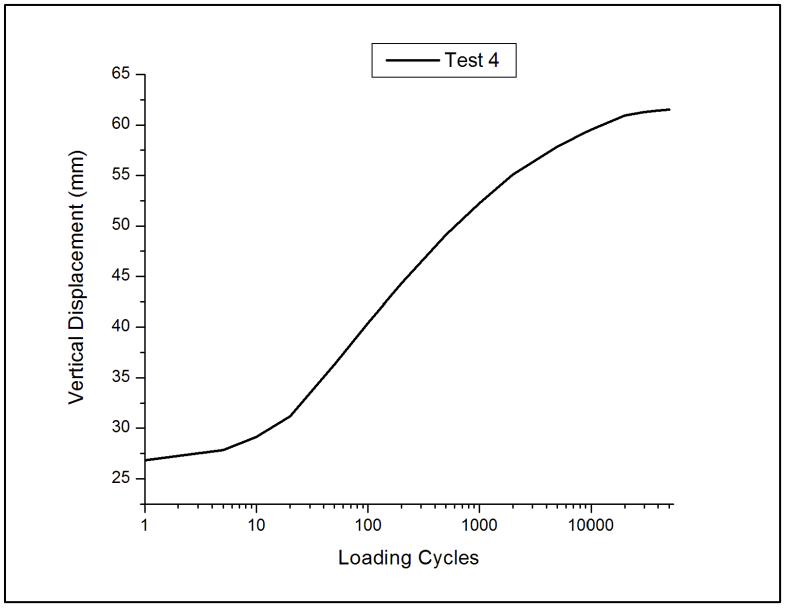

Figure 3.11. Cyclic Displacement Curve for single-reinforced, cyclically loaded test.

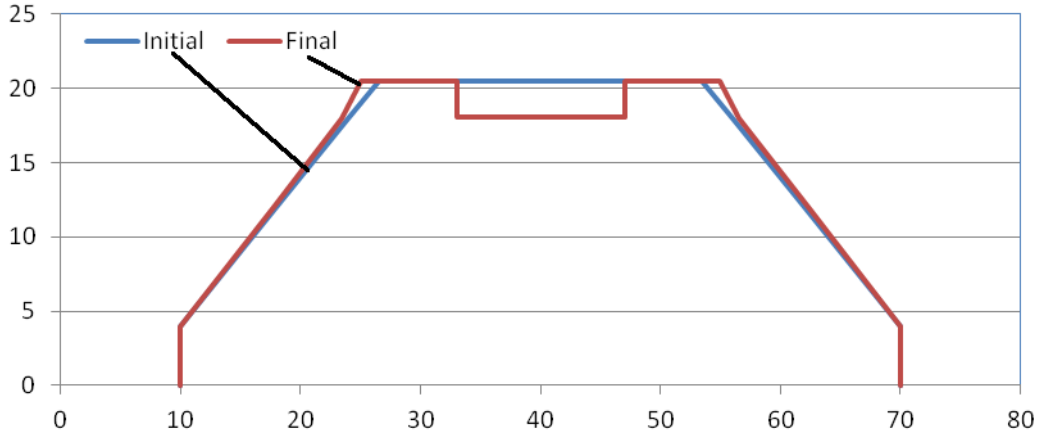

Figure 3.12. Schematic of initial shape and deformed shape of embankment after testing. Shape shown in centimeters.

3.4.3 Behavior of Geocell during Tests 3 and 4

Despite the success in preventing lateral spreading, significant damage occurred to the geocell at the seams under and around the center of the loading plate. Strain gauges placed on the geocell seem to suggest excessive deformation and possible rupture due to sudden shifts between compression and extension.

Upon dismantling the model after testing, the geocell was examined for damage. It was damaged significantly, with tearing and rupture at all 4 of the seams beneath the loading plate. Unfortunately, the strain gauge data beneath the center of the plate cuts off approximately 28 minutes into the test. This prevents any observation of sudden shifts or changes from compression to extension. These shifts are an effective means of determining any events within geocell during the test.

The off-center strain gauges managed to capture data throughout the course of the test. It seems to imply that there was increasing tension laterally and compression vertically in the near off-center gauges (1 and 2) as the load was increased. The further off-center strain gauges showed little to no reaction to the load. However, all gauges indicate strains within the elastic range of the geocell loading (*figures 3.15* and *3.16*).

The geocell encountered some damage during the cyclic loading test, but not nearly as much tearing at the seams as during the monotonic test (*figure 3.14*). In fact, most of the damage occurred as bending and compression of the top portion of the Geocell walls. This lack of tearing could possibly be a result of the lower load amplitude.

More problems occurred with the on-center strain gauges, as they only started recording at about 2 hours and 20 minutes into the test. However, there are no sudden shifts and the strain is relatively constant, suggesting that the previous data was likely similar. Further supporting this notion is the strain gauge data from the off-center cell (*figures 3.18 and 3.19*). It shows a relatively constant strain throughout the test, suggesting that no serious failures or localizations occurred within the geocell.

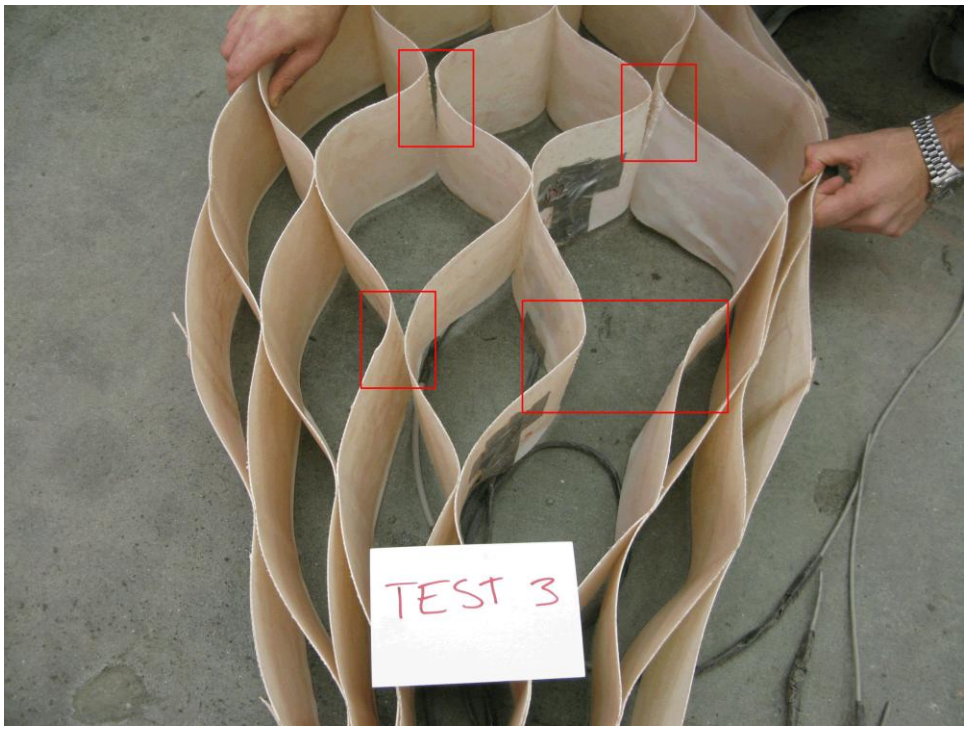

Figure 3.13. Damage in the Geocell after test 3.

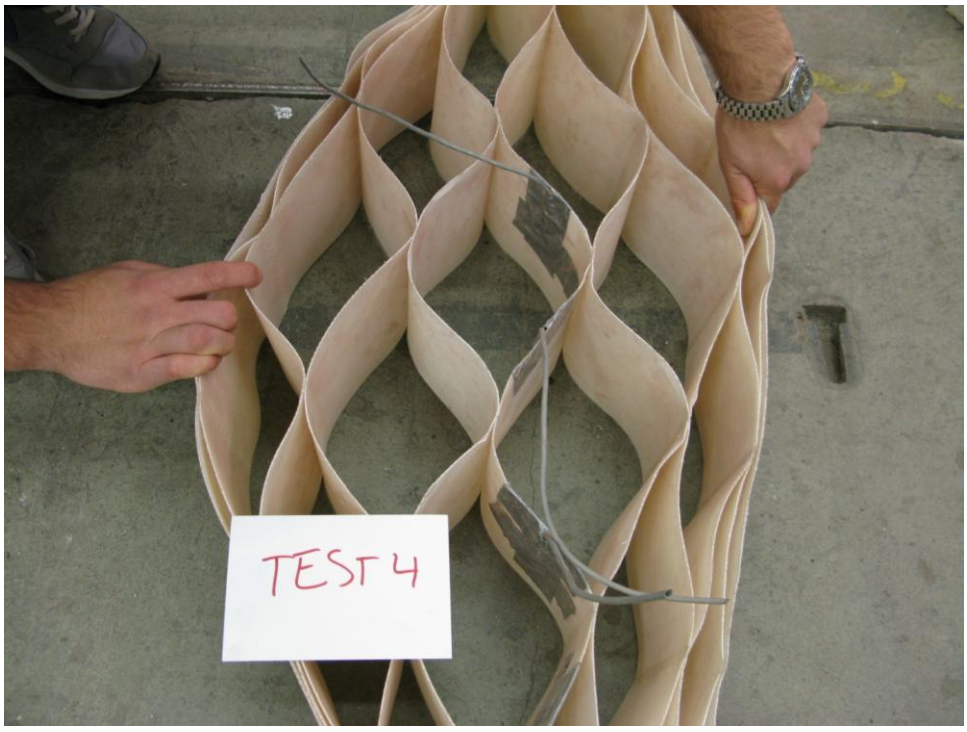

Figure 3.14. Condition of Geocell after test 4.

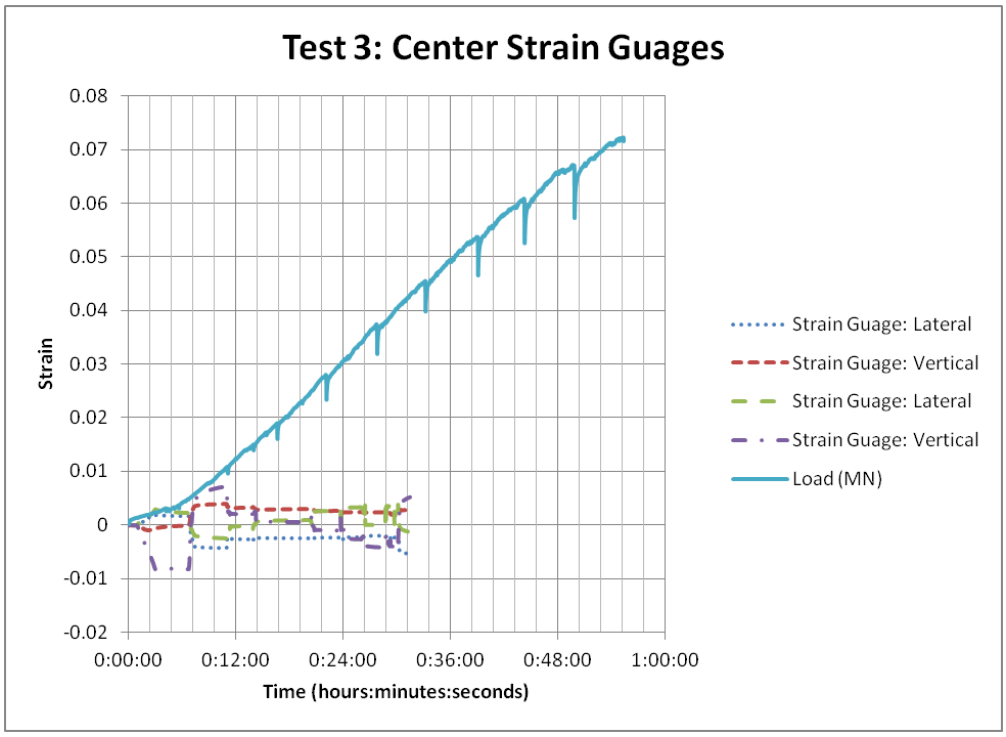

Figure 3.15. Limited strain data for on-center strain gauges.

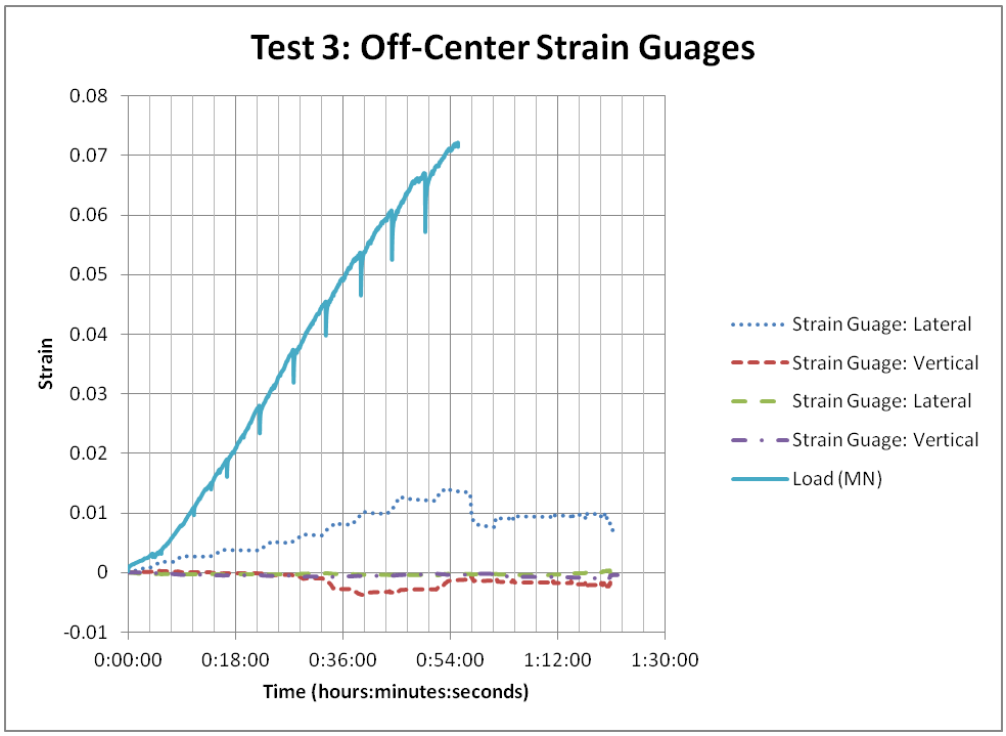

Figure 3.16. Full strain data for off-center strain gauges.

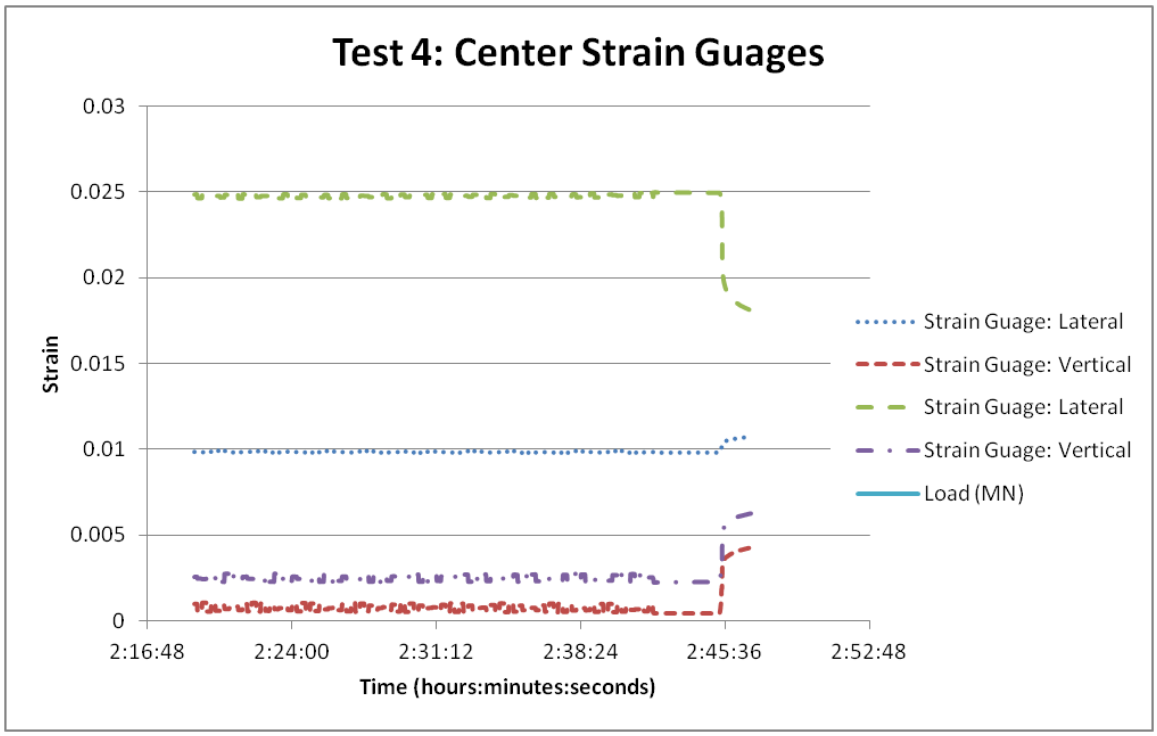

Figure 3.17. Limited strain data for on-center strain gauges.

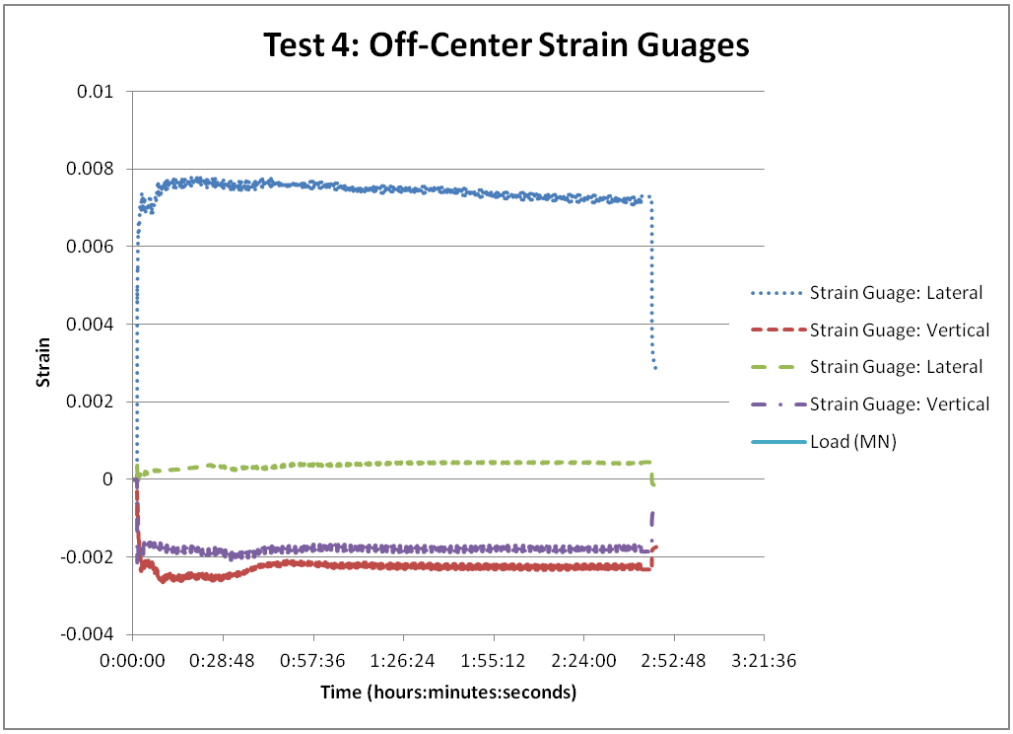

Figure 3.18. Full strain data for off-center strain gauges.

3.5 Reinforced Model Tests: Two Layers of Geocell

The reinforced portion of the testing consisted of a model embankment constructed from granite ballast, reinforced by a two layers of geocell: a top layer and a bottom layer. This section of the experimentation consisted of two tests: one monotonically loaded and one cyclically loaded. Similar to previous tests the strength of the ballast model under different loading conditions was observed, along with apparent stiffness, deformation (laterally and vertically), and failure load. Again, a gradation analysis was performed before and after testing.

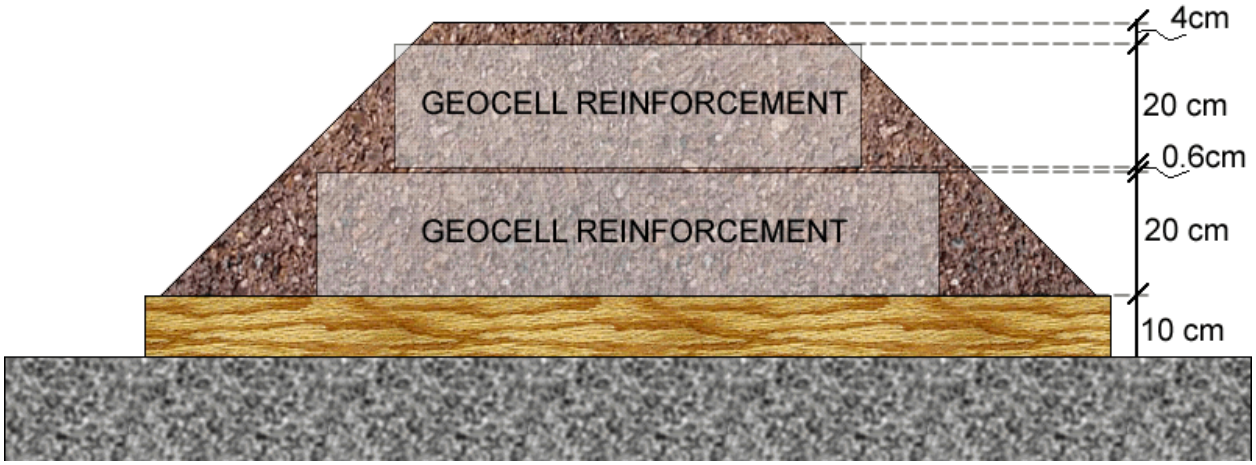

Figure 3.19. Schematic of embankment for tests 5 and 6.

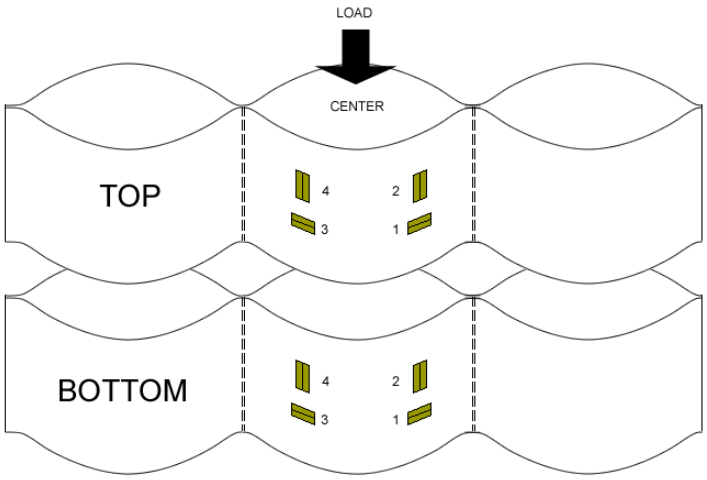

Figure 3.20. Schematic of strain gauge configuration in layers of Geocell.

3.5.1 Monotonic Loading: Test 5

The reinforced ballast embankment was loaded monotonically in displacement-control conditions. The loading curve is rather linear, allowing an estimate of apparent stiffness (*figure 3.21*) with its loading rate of 2.5 mm/minute. It seemingly required about 11.9 kPa of vertical stress to cause 1 mm of vertical displacement. This apparent stiffness is higher than the unreinforced model and the model with a central reinforcement layer. This increase in stiffness is expected as the whole model is a reinforced composite.

This model test was able to support more load than the unreinforced case and possibly the case of just the central reinforcement. Like the test with a single reinforcement, this test was stopped when the loading frame reached its allowable loading capacity (approximately 17,780 lbf, or 79.1 kN) of about 625 kPa. This model handled more load because no significant damage in the geocell occurred and the composite model was significantly stiffer.

The confinement of the double reinforcement layer was also very effective in the prevention of lateral spreading. This lateral deformation was greatly reduced throughout the height of the model as the top layer of reinforcement prevented spreading at the crest (*figure 3.22*). The vertical displacement that occurred within the 175 kPa range of the double-reinforcement test was 28% of displacement that occurred in the same range for the unreinforced, monotonically loaded test. The increase in cross-sectional widths at the recorded heights was effectively reduced by geocell confinement and the main results are summarized in Tables 3.9 and 3.10.

Table 3.9: Lateral spreading of double-reinforced, monotonically loaded embankment.

Height from Floor	**Percent Increase in Cross-Sectional Area (%)**
Top, 21.5" (54.6 cm)	6.5 %
Upper Middle, 18" (45.7 cm)	3.4 %
Lower Middle, 12" (30.5 cm)	1.8 %

Table 3.10: Summary of notable test results.

Final Stress / Load	625 kPa (90.7 psi) / 79.1 kN (17780 lbf)
Final Vertical Displacement	53 mm (2.08 in, calibrated)
Apparent Stiffness	11.9 kPa/mm
Max. Lateral Spreading	6.5 % (Top)

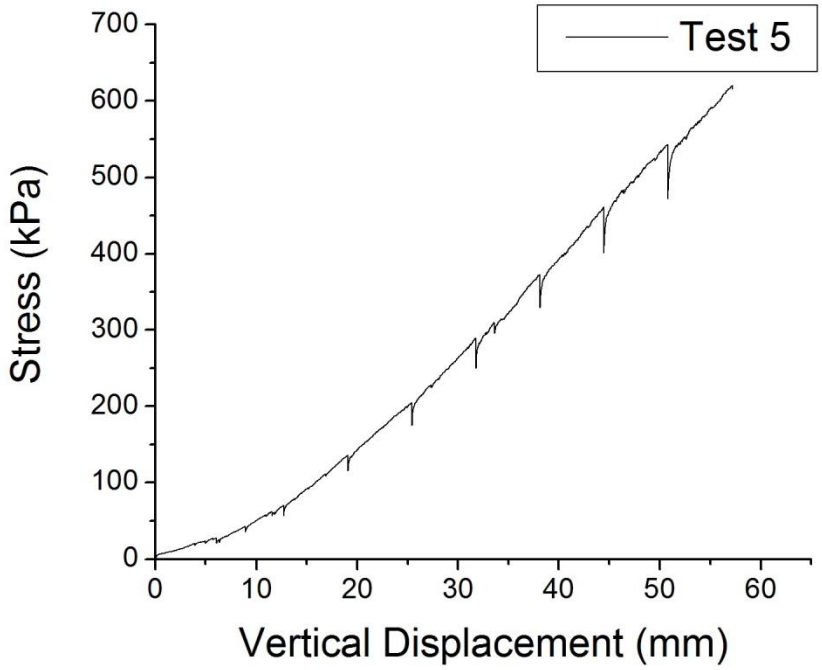

Figure 3.21. Load-Displacement Curve for double-reinforced, monotonically loaded test.

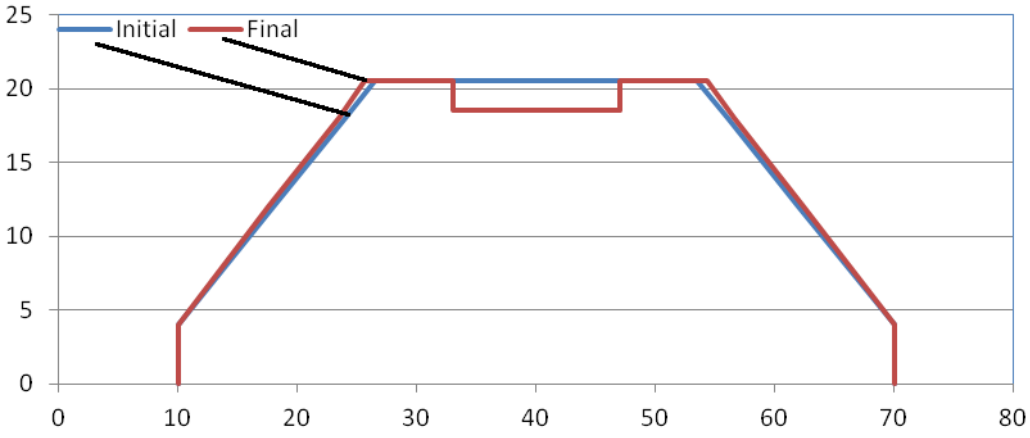

Figure 3.22. Schematic of initial shape and deformed shape of embankment after testing. Dimensions given in centimeters.

3.5.2 Cyclic Loading: Test 6

The double-reinforced ballast embankment was loaded cyclically in load-control conditions. That is, a loading amplitude between 75 and 350 kPa was specified and measurements of displacement were taken at 1000, 5000, 10000, 20000, 30000 and 50000 cycles (*figure 3.23*). Similar to before, the loading frequency was 10 Hz.

The test was stopped when the actuator reached its goal of 50000 loading cycles.

The confinement of the double-reinforcement layer was very effective in the prevention of lateral spreading (*figure 3.24*). This lateral deformation was greatly reduced and mostly limited to the crest of the embankment, where no reinforcement existed. This is evident from the results, which indicate very little lateral deformation from the level of the reinforcement and below. The final vertical displacement was 48% of displacement that occurred in the unreinforced, cyclic test. The increase in cross-sectional widths at the recorded heights was effectively reduced by geocell confinement. The main results are summarized in Tables 3.11 and 3.12.

Table 11: Lateral spreading of double-reinforced, cyclically loaded embankment.

Height from Floor	Percent Increase in Cross-Sectional Area (%)
Top, 21.5" (54.6 cm)	7.4 %
Upper Middle, 18" (45.7 cm)	2.5 %
Lower Middle, 12" (30.5 cm)	0.9 %

Table 12: Summary of notable test results.

Final Vertical Displacement	57 mm (2.24 in)
Vertical Displacement during Cyclic Loading	34 mm (1.34 in)
Max. Lateral Spreading	7.4 % (Top)

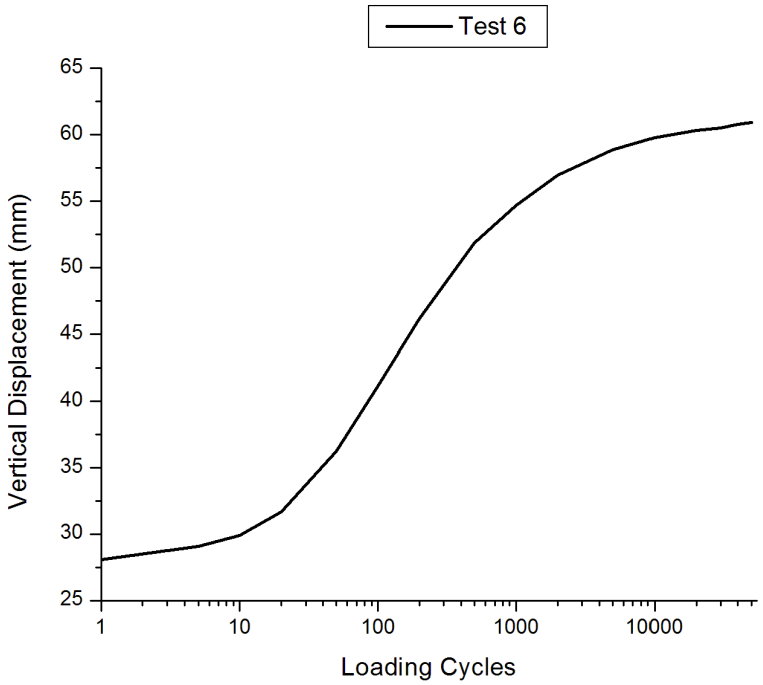

Figure 3.23. Cyclic Displacement Curve for Double-Reinforced, Cyclically Loaded test.

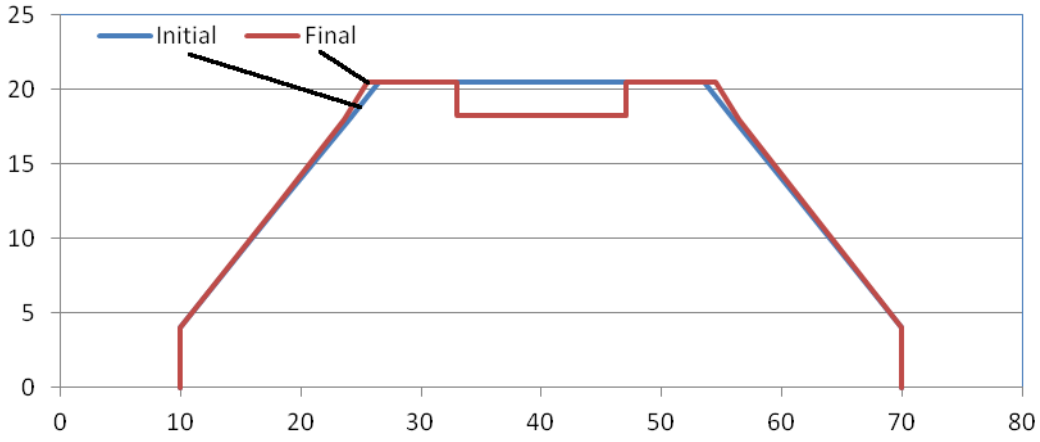

Figure 3.24. Schematic of initial shape and deformed shape of embankment after testing. Dimensions given in centimeters.

3.5.3 Behavior of Geocell during Tests 5 and 6

Both layers of geocell were essentially undamaged from the monotonic loading of the model. Both encountered no tearing at the seams and joints, unlike in the single reinforcement layer test (*figure 3.25*). This could likely be due to a higher stiffness of the embankment acting as a composite and in turn, a lower deformation of the geocell. The only observed consequence, which was negligible, was slight superficial bending and compression of the geocell walls.

Further problems occurred with the strain gauges as no data was recorded in the bottom layer, but was not critical. Full data was available for the top layer (*figure 3.27*), which indicated increasing strain correlating to each increasing load, as expected. The general return of the strains to the initial level after the test was completed suggests that strain was elastic and minimal damage (plastic strain) occurred.

Both layers of geocell were undamaged from the cyclic loading of the model. Both encountered no tearing at the seams and joints (*figure 3.26*).

To avoid some of the issues with the strain gauges that had been previously encountered, both data collection devices were connected to both layers for redundancy. As expected, one of the devices failed during the test, but the other collected data throughout, giving an accurate representation of what was occurring in both layers. As expected, the lower layer encountered less lateral, tensile strain than the top layer (*figure 3.28*). However both were relatively constant throughout the test, suggesting that no rupture occurred. The vertical, compressive strain was

rather similar throughout the test, suggesting that the compressive stresses were transferred rather evenly through the model, possibly due to the high stiffness of the model.

Figure 3.25. Condition of geocell layers after test 5. They were relatively undamaged.

Figure 3.26. Condition of geocell layers after test 6.

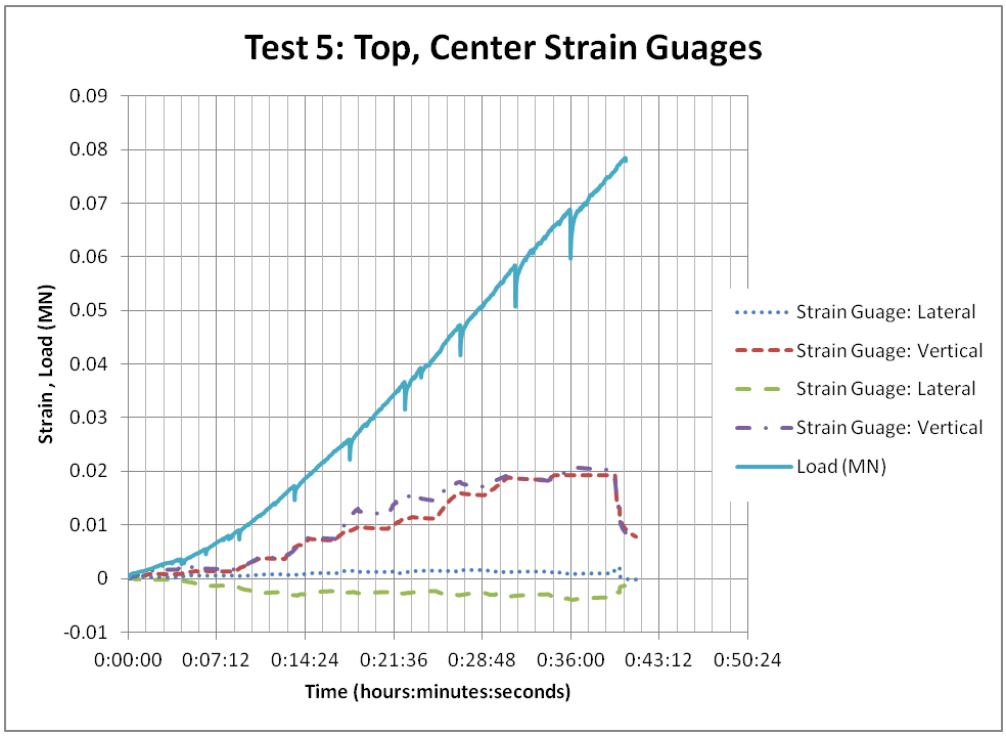

Figure 3.27. Full strain data for top, on-center strain gauges.

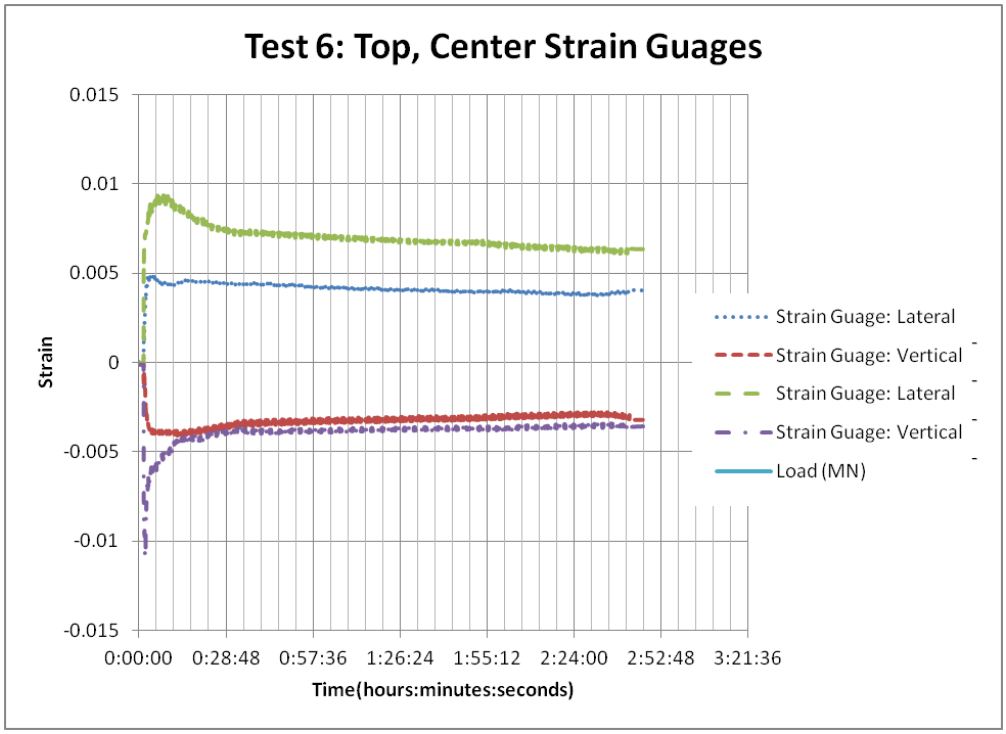

Figure 3.28: Full strain data for top and bottom, on-center strain gauges.

3.6 Summary and Discussion

The monotonic and cyclic tests performed demonstrate that the geocell is very effective in increasing ballasted embankment bearing capacity, increasing embankment stiffness and preventing excessive deformation (laterally and vertically). The reinforcement seems to handle cyclic loading well under sustainable load amplitudes and could be a cost-effective method for strengthening granular embankments under an optimized configuration and loading.

Geocell increased the strength of the embankment considerably, as evidenced by the much higher loads sustained by the reinforced models (*Table 3.13. and 3.14*). In the unreinforced model, vertical displacement of the loading plate at failure (175 kPa) was about 65 mm. For the same load in both the single- and double-reinforced tests, the displacements were much smaller (20 mm and 18 mm, respectively). Hence, the single- and double-reinforcements prevented about 69% and 72%, respectively of the vertical displacement of the load-bearing footing. This difference in vertical displacement between the reinforced configurations is negligible, suggesting that perhaps one layer of reinforcement is more cost-effective than two. However, before making this conclusion, it is important to consider what the working load of the embankment or foundation would be. Both configurations could easily support the load from the unreinforced test, but when exposed to much higher loads, damage can occur in the geocell, affecting the structural integrity of the embankment. Both of the reinforced configurations were exposed to loads in excess of 575 kPa, but the single-reinforcement configuration resulted in geocell with torn seams. This is possibly the result of excessive deformation and very high lateral stresses in each cell due to stiffening of the confined material below it. The confining behavior of the geocell causes a concentration of lateral stresses that places the reinforcement in tension.

The double-reinforcement configuration negated nearly all of the damage, possibly because more strength was mobilized from the entire embankment. That is, the vertical/lateral stresses were likely distributed more evenly throughout the whole model, as opposed to being heavily concentrated in a single layer of reinforcement. The high concentration of lateral stresses in conjunction with the large vertical stresses in the center of the embankment could very possibly have caused the rupture in test 3 (single-reinforcement, monotonically loaded). It seems evident that the cyclic load amplitude for the single reinforcement test was not enough to cause tearing at the seams, although long-term strength of the geocell should be a design concern.

The application of geocell reinforcement to the monotonically loaded tests was very effective in preventing lateral spreading with increased load. When compared to the unreinforced case, the single-reinforcement reduced the lateral spreading at the crest by 45%. This reduction is significant, but the lateral spreading still occurs since the ballast above the reinforcement is shearing. Similarly, the double-reinforced configuration reduced lateral spreading at the crest by 82%. This highly effective prevention of lateral spreading is due to the whole model being reinforced and confined by the geocell.

Table 3.13. Summary of Monotonically Loaded Tests in All Reinforcement Setups.

	Test 1	Test 3	Test 5
	Unreinforced	Single-Layer	Double-Layer
Failure Stress / Load	175 kPa / 22 kN	575 kPa / 72.7 kN	625 kPa / 79.1 kN
Yield Vert. Disp.	65 mm	60 mm	53 mm
Apparent Stiffness	4.5 kPa/mm	10.9 kPa/mm	11.9 kPa/mm
Max. Lateral Spreading	72.78 % of Area (Top)	40.46 % of Area (Top)	13.38 % of Area (Top)

	Displacement (mm)			Percent Increase in Width[2]		
	Test 1	Test 3	Test 5	Test 1	Test 3	Test 5
Top, 54.6 cm[1]	108.0	63.5	22.2	31.48 %	18.52 %	6.48 %
Upper Middle, 45.7 cm[1]	30.0	12.2	13.6	6.56 %	3.00 %	3.35 %
Lower Middle, 30.5 cm[1]	20.1	10.2	10.2	3.04 %	1.82 %	1.83 %

[1]Height measured from concrete strongfloor.
[2]Percentage increase as compared to initial width.

Table 3.14. Summary of Cyclically Loaded Tests in All Reinforcement Setups.

	Test 2	Test 4	Test 6
	Unreinforced	Single-Layer	Double-Layer
Final Vert. Disp.	118 mm	62 mm	57 mm
Cyclic Vert. Disp.	74 mm	36 mm	34 mm
Max. Lateral Spreading	25.69 % of Area (Upper Middle)	22.43 % of Area (Top)	15.36 % of Area (Top)

	Displacement (mm)			Percent Increase in Width[2]		
	Test 2	Test 4	Test 6	Test 2	Test 4	Test 6
Top, 54.6 cm[1]	36.1	36.5	25.4	10.52 %	10.65 %	7.41 %
Upper Middle, 45.7 cm[1]	55.3	13.3	10.2	12.11 %	3.27 %	2.52 %
Lower Middle, 30.5 cm[1]	23.4	7.0	4.9	3.54 %	1.25 %	0.88 %

[1]Height measured from concrete strongfloor.
[2]Percentage increase as compared to initial width.

In addition to strengthening the monotonically-loaded models, the geocell was very effective in strengthening the cyclically loaded embankments. Vertical displacement of the loading place occurred continuously when the unreinforced model was loaded cyclically (between 35 and 175 kPa). In fact, during the 50,000 cycles of loading, over 74 mm of vertical displacement occurred. The cyclic loading for the reinforced models was double the amplitude (between 75 and 350 kPa) due to the higher strength of the model. Despite the higher loads in the single- and double-reinforced models, only 36 and 34 mm of vertical displacement occurred during the cyclic loading, respectively. The difference in vertical displacements between the two reinforcement configurations was negligible. In both configurations, the damage to the geocell was very light, suggesting that the single reinforcement might be more cost-effective for cyclic loading of this amplitude. However, for larger loads, the double-reinforcement might be necessary. It is evident that the seams in the single-reinforcement configuration rupture under larger loading, as witnessed in the monotonically loaded test.

The application of geocell reinforcement to the cyclically loaded tests was effective in preventing lateral spreading. The spreading at the crest was similar for the unreinforced and single-reinforced models because the spreading was largely local, being confined to above the reinforcement. This is evidenced by the significant reduction is lateral deformation in the center (reduction from 25.7% to 6.6%) and base (reduction from 7.2% to 2.5%) of the embankment. In the case of the double-reinforced configuration, lateral spreading was reduced throughout the model due to the confinement from the geocell. Both reinforced cases prevented significant lateral spreading by reducing the vertical deformation that could occur.

Unfortunately, recurring problems with the strain gauges restricted inferences that could be made during the tests. The geocell did strain during the tests, but the strain level was not critical during most of the tests, as it never exceeded the elastic range. Generally, compressive strain occurred vertically in the geocells and tensile strain occurred laterally. This tensile strain was due to the confining nature of each cell, as expected. Buckling in the geocell wall was not noted.

The durability of the geocell was impressive, but was dependent on the configuration of the embankment. In the monotonically loaded case with single reinforcement, the damage was considerable due to high lateral stresses within the confined cells. However, the geocell only encountered light damage in the cyclically loaded test of 50,000 repetitions, possibly due to the lower load amplitude. In the double-reinforcement configuration, damage was insignificant for both monotonic and cyclic loading applications, monotonic and cyclic. This is due to the more even distribution of stresses and the composite behavior of the model and confining reinforcements. The double-reinforcement configuration could handle a higher load, or likely sustain the cyclic load for a longer time with less damage at the seams. Load, and expected

cycles of the life of the embankment should be important considerations when designing with the geocell.

Gradation analyses performed after each model test suggested that the geocell had little impact on the degradation of the ballast due to loading. The grain size distribution of the ballast remained relatively constant throughout each of tests, although considerable dust was created as a by-product of abrasion between particles (*figure 3.29*). Quality ballast and a limited number of cycles could explain the lack of degradation. Testing of inferior ballast could provide more insight into the deteriorative properties of the ballast under loading.

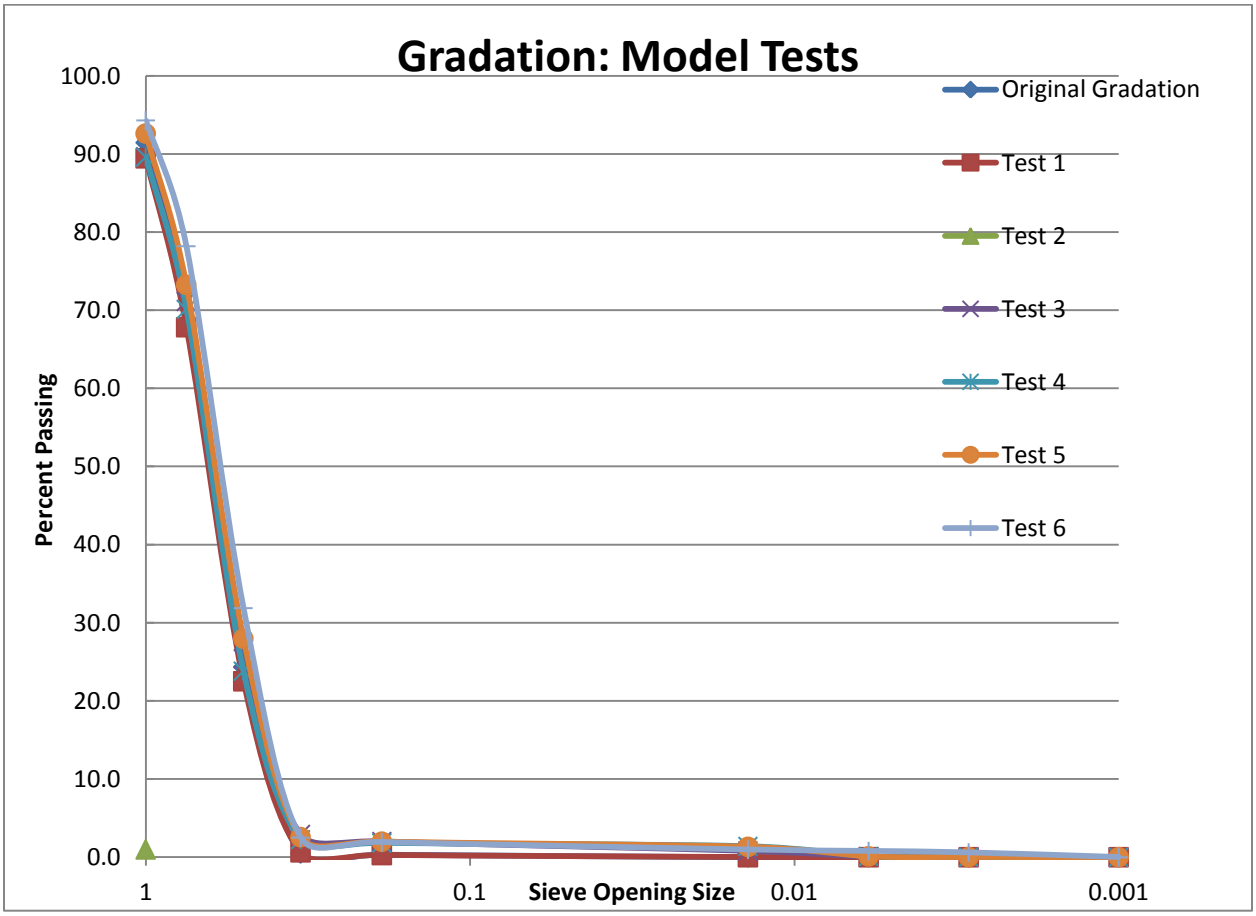

Figure 3.29: Comparison of gradation analyses for each test.

3.7 Conclusions

A series of laboratory tests were performed on ballast embankments with and without geocell reinforcement. During these tests, actuator load, vertical displacement, lateral displacements along side slopes, and strain in the geocell were measured. There were three different configurations for embankment construction: no geocell, a single, centrally placed layer of geocell, and two layers of geocell. The application of confinement to the model embankment was very effective in improving its behavior under loading. The following conclusions are drawn from the experiments:

1) The monotonically loaded tests indicated that application of geocell to the gravel embankment significantly increased the effective apparent stiffness under loading. The apparent stiffness of the embankment under loading from the MTS actuator was increased by 140% and 165% for the single- and double-layer reinforced embankments, respectively. The vertical settlement that occurred during cyclic loading was reduced by 48% and 52% for the single- and double-layer reinforced embankments.

2) Geocell confinement effectively reduced the vertical settlement that occurred under the loading plate. In comparison to the unreinforced embankment, the reinforced embankments reduced vertical settlement at a monotonic actuator load of 175 kPa by 69% and 72% for the single- and double-layer reinforced embankments, respectively.

3) Geocell confinement effectively reduced lateral spreading of ballast, especially in material below or at level with the reinforcement. Lateral displacements at the crest of the

embankment were 38% and 79% for the single- and double-layer reinforced embankments, respectively.

4) Under cyclic loading, the reinforced embankments attained stabilization and exhibited structural resilience more rapidly than without reinforcement. When geocell was absent, vertical settlement and lateral settlement continued despite a lower stress amplitude than that applied in the reinforced cases. With geocell confinement, a stable and final settlement and lateral spreading was attained quite rapidly, which implies mobilization of the reinforcement.

5) Strain gauges placed on the walls of the geocell showed low tensile and compressive strains during loading, both monotonically and cyclically. The strains remained within the elastic range for the geocell, rarely exceeding 1%. Upon removal of loads, the strain in the geocell wall returned back to its initial state, suggesting negligible plastic strain or creep during the loading phase.

6) Generally, the condition of the geocell upon exhumation after testing was good, with only minor, superficial damage. However, in the monotonically loaded case, where high loads and bending occurred in the cells below the loading plate, rupture occurred at the cell seam. Despite relatively low tensile strains in the material, the significantly weaker seams yielded. Therefore, excessive stress concentrations, especially at the welded seams of the cell are more of a structural concern than the tensile strength of the cell walls. Due to this

issue, it is suggested that clearance be provided between the area of load application and geocell location.

CHAPTER 4: NUMERICAL SIMULATION OF LABORATORY TESTS

4.1 Introduction

A commercially available finite element (FE) software, ABAQUS (Hibbit et al., 2007) was used in the analysis. The 6 model tests were simulated using material properties obtained from laboratory tests and the actual geometry and boundary conditions, and the stress and deformation behavior was compared. Similar to the laboratory tests, these simulations consisted of 3 static and 3 cyclic loading conditions. Validation through numerical modeling adds credibility for further analyses simulating more practical applications. A 3-dimensional (3-D) analysis is necessary to accurately simulate the confining mechanism of geocell reinforcement as well as ballasted railroad foundations.

4.2 Numerical Simulation of Model Tests

4.2.1 Material Properties

In order to correctly characterize the materials used in testing and attain reasonable results in the FE analysis, reliable material data must be used. The data was obtained from prior laboratory material testing.

The ballast was modeled as a non-associative elastic-plastic material, obeying a 3-D Drucker-Prager yield criterion (see *Appendix B*), which is commonly used to simulate granular materials as its strength and yield is dependent on volumetric strain. Although the ballast is a cohesionless material, it was given a small cohesion (1 kPa) to assist with convergence issues, while not critically affecting the results (*Table 4.1*). The Drucker-Prager model was chosen for simplicity in modeling the elastic-plastic behavior of the ballast using a rounded yield surface as opposed to

the sharp, drastic yield surface that exists in the stress space when using Mohr-Coulomb failure criteria. Additionally, the material parameters for the Drucker-Prager model can be determined in a straight-forward manner. Material models exist that could capture the behavior of the ballast with slightly more accuracy, especially under cyclic conditions, but would require considerably more parameters (some difficult to attain), introducing potentially less accurate results. The circumscribed, circular Drucker-Prager yield surface was used for the compressive strength properties of the ballast. The inscribed circle is used to describe extensive properties of soil under triaxial extension

The geocell was modeled as an elastic material since only minimal damage and plastic strain was encountered during the tests (*Table 4.1*). The shape of the geocell was modeled with a rhomboidal shape as opposed to the actual pseudo-sinusoidal shape that is used in the tests. This was done to simplify meshing, while still maintaining the basic mechanical function of confinement. Other 3-D FE models of multiple cells of geocell have represented the cells in a diamond, rhomboidal shape (Yang, 2010). The loading plate was modeled as a rigid material because the stiffness of the steel is orders of magnitude larger than the ballast.

Table 4.1. FE properties of ballast and geocell.

Ballast	**Value**
Mass Density, ρ (kg/m^3)	1520
Elastic Modulus, E (kPa)	2000
Poisson's Ratio, ν	0.35
Internal Angle of Friction, ϕ	45°
Angle of Dilation, ψ	15°
Cohesion, c' (kPa)	1
Geocell	**Value**
Elastic Modulus, E (GPa)	2.07
Poisson's Ratio, ν	0.35
Mass Density, ρ (kg/m^3)	2000

4.2.2 Boundary Conditions

A quarter of the embankment was modeled to simulate the deformations as accurately as possible, while only requiring reasonable computational time. To ensure that the geometrical symmetry can allow this computational advantage, boundary conditions must be modeled correctly. Several displacement restrictions were applied to the embankment. Both of the interior, side faces were restrained from moving laterally, but allowed to move vertically since they lie in the center of the symmetrical embankment, where no lateral deformation is expected (*Figure 4.1)*. Also, the base of the embankment was fixed from displacing in the z-direction, modeling the rigid concrete foundation underlying the ballast in the model tests.

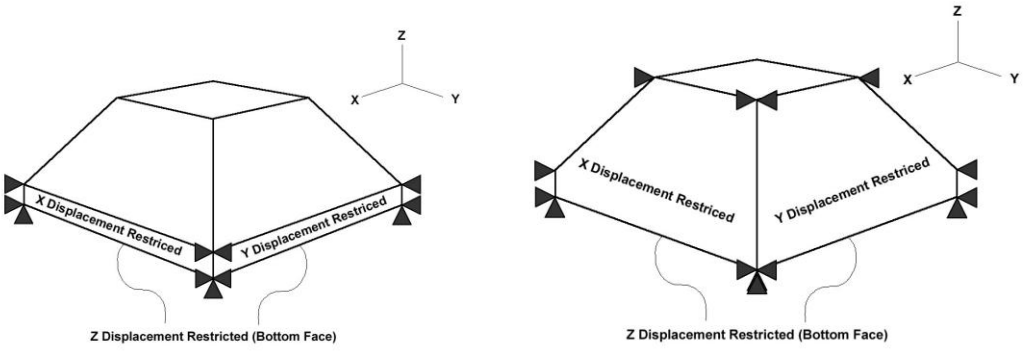

Figure 4.1. Boundary conditions for quarter embankment geometry.

4.2.3 Elements/Mesh

The baseline tests (1 and 2) were meshed using a structured pattern made up of 9500, hexahedral, 8-noded, reduced integration elements (C3D8R). Coarser meshes generally provided large underestimates in displacement. The general simplicity of the embankment shape, in addition to the absence of a complex embedded 3-dimensional reinforcement allowed for the use of a simple meshing pattern (*figure 4.3a*).

The single-reinforced tests (3 and 4) were meshed using a semi-structured pattern that consisted of 17520, tetrahedral, 4-noded, reduced integration elements (C3D4R), which modeled both the gravel and geocell (*figures 4.2* and *4.3b*). The irregular geometry that arises from the use of a 3-dimensional reinforcement with a complex structure requires tetrahedral elements due to the wide variety of angles and dimensions encountered. The shape of this element serves a competent alternative to the 8-noded brick element used in the unreinforced test, but requires many more nodes in the mesh and subsequently more computational time.

The double-reinforced tests (5 and 6) were also meshed using a semi-structured pattern that consisted of 14630, tetrahedral, 4-noded, reduced integration elements (C3D4R), which modeled both the gravel and geocell (*figures 4.2* and *4.3c*). Again, similar to the previous simulations with one layer of geocell, the irregular geometry that arises from the use of a 3-dimensional reinforcement with a complex structure requires tetrahedral elements due to the wide variety of angles and dimensions encountered.

Despite the lack of perfectly congruent meshes used for the three reinforcement configurations, all of the elements were generally meshed to a similar size (about 1.5 cm in diameter). This is an

important consideration since meshing too finely might misrepresent the coarse gravel used in the actual test ($D_{50} \approx 1.5$ cm), while meshing coarsely could have a similar, detrimental effect.

The geocell was initially modeled with shell elements due to its high aspect ratio. However, due to significant meshing difficulties, it was eventually modeled using solid elements.

Planar interface elements were assigned to the surfaces where ballast and geocell were in contact, including the inside, outside, top and bottom of the geocell-ballast interface. They were modeled as a contact surface where tangential properties were frictional (i.e. $\delta=(2/3\Phi)=30°$) and normal contact was “hard”, that is the walls of geocell could not be penetrated. Contact was defined by contact pairs using a penalty kinematic constraint algorithm. Consequently, contact surfaces were defined, then normal and tangential stresses were determined based on nodal pairs.

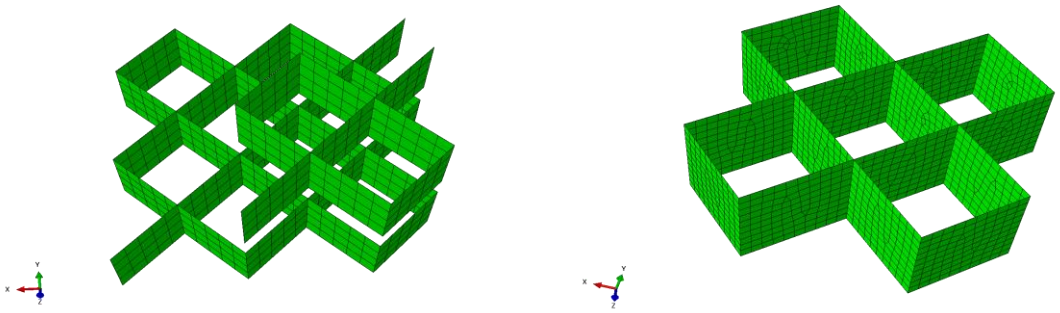

Figure 4.2. Discrete meshing of quarter of Geocell.

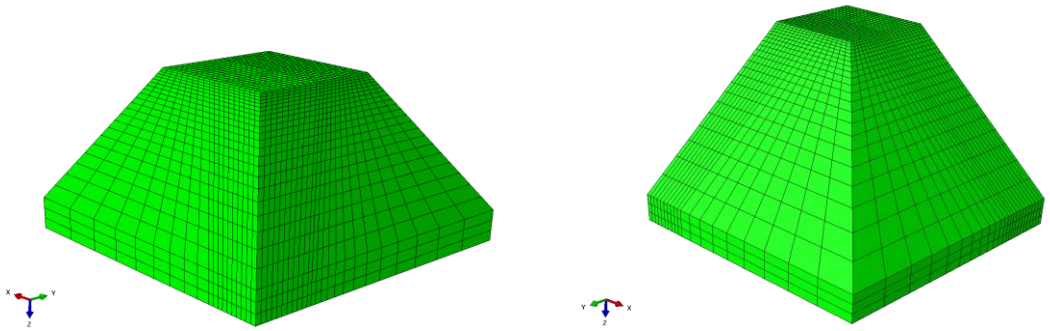

Figure 4.3a. Meshing of unreinforced embankment.

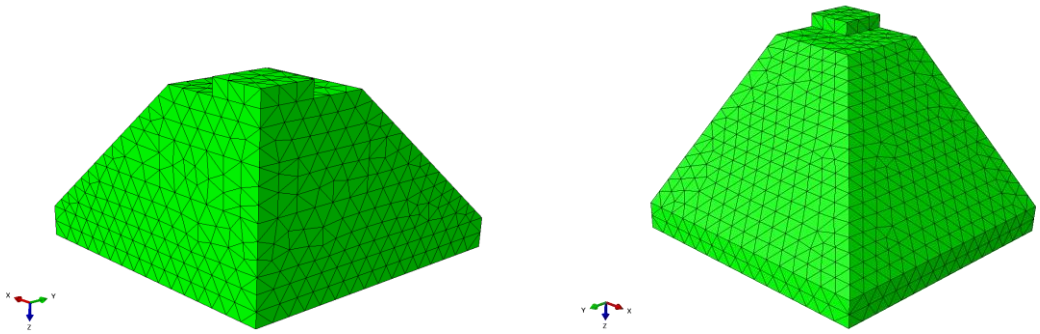

Figure 4.3b. Meshing of single-reinforced embankment.

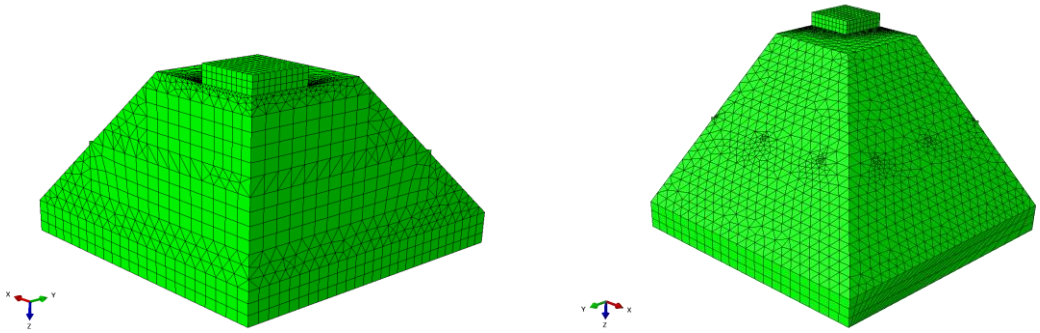

Figure 4.3c. Meshing of double-reinforced embankment.

4.2.4 Loading Stages

4.2.4.1 Static Loading

Two loading stages were applied to the embankment quarter to simulate the loading conditions. First, gravity was applied to simulate construction and in-situ conditions of model test. It also allows the ballast to gain frictional strength as overburden pressure enables mobilization of its internal strength.

The next loading stage consisted of applying pressure to the crest of the model using a steel loading plate. ABAQUS/Explicit was used to simulate the static loading applied to the embankment in displacement-control conditions, while maintaining computational stability. ABAQUS/Explicit was an important choice since it is used to model highly non-linear behavior of materials (like soil) in a stable and efficient manner. An Implicit analysis (ABAQUS/Standard), cannot capture the yield behavior of soil, often having convergence errors and infinitesimally small time increments. In this stage, the displacement was slowly and steadily increased at a rate of 0.1 mm/second to those attained in the actual experiments. The vertical stress/displacement behavior was monitored throughout the simulation for comparison.

4.2.4.2 Cyclic Loading

Two loading stages were applied to the embankment quarter to simulate the cyclic loading conditions. First, gravity was applied to simulate construction and in-situ conditions of lab test, in a manner identical to the static case.

Next, dynamic conditions were simulated using ABAQUS/Explicit in order to expedite the simulation by reducing computational time and to account for the inertial effects of the ballast. In this situation, a vertical pressure was applied to a loading plate placed on top of the crest, similar to static conditions. However, the load was applied cyclically, with the same load amplitudes and

frequency as used in the lab tests. The simulations required approximately 30 hours to run on 32GB RAM, 2.66 GHz server.

4.3 Numerical Modeling of Experiments

4.3.1 Monotonically Loaded Tests

The three statically loaded embankment tests were simulated using similar loading conditions and model geometry. Two geocell configurations were used: a single, centrally placed layer of geocell, and two layers of geocell placed within the embankment. The actual experiment and the FE simulation were run in displacement-control conditions. Throughout the duration of these simulations, the vertical displacement and stress under the loading plate, as well as the lateral displacement along the profile of the embankment were compared with the actual test results.

While comparing the vertical displacement to the vertical load, it is shown that the results match reasonably well (*Figure 4.4a, 4.6a,b,c)*. This is likely due to the use of quality laboratory data (triaxial tests results for the ballast, tensile tests results for the geocell) to characterize the material properties required by the FE analysis. These tests allowed an accurate determination of properties such as the internal friction angle, ballast stiffness, and geocell stiffness which are necessary for analyzing this behavior.

However, the lateral displacements did not match entirely. This could be due to the difficulties in predicting the plastic deformation behavior in anisotropic cohesionless materials that are subject to low confinement pressures, such as much of the ballast at the crest or along the profile where much of the lateral spreading occurred. Often, numerical models yield acceptable results, especially when considering lateral displacements. Despite the imperfect modeling of the lateral

spreading occurring along the profile of the embankment, the general trends matched, and the displacement simulations were all within the same order of magnitude of the experimental results (*Figure 4.5a,b,c*).

Preliminary modeling was done using Mohr-Coulomb plasticity for ballast, but was neglected as ABAQUS would not accept the material model for cyclic loading. The monotonic testing matched reasonably well (*figure 4.4b*), but was ignored for consistency in modeling throughout all phases of study. Additionally, Mohr-Coulomb plasticity has convergence errors stemming from the shape of its yield surface, further justifying the choice of Drucker-Prager as a material model.

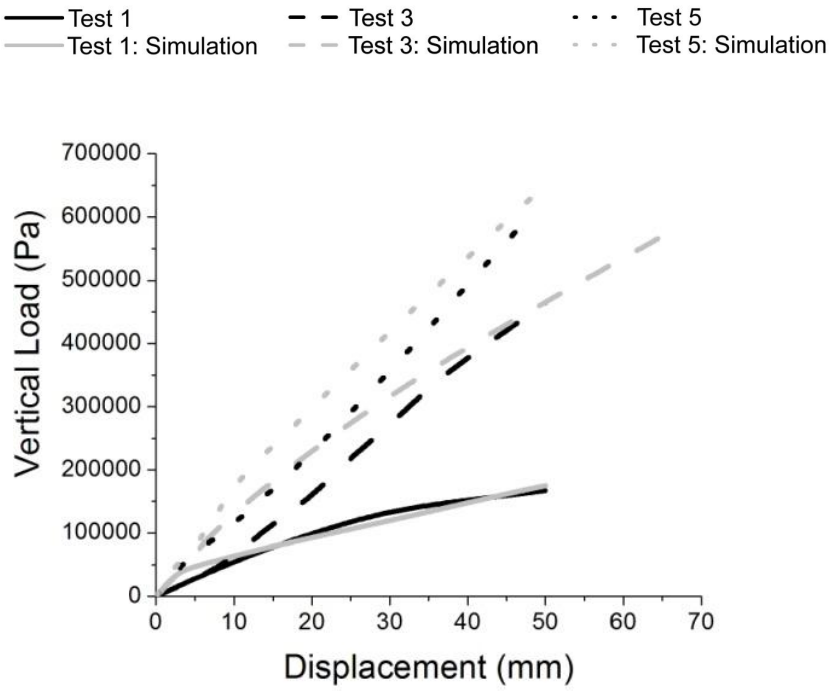

Figure 4.4a. Comparison of vertical displacement from experiments and FE simulations for monotonically loaded tests using Drucker-Prager plasticity.

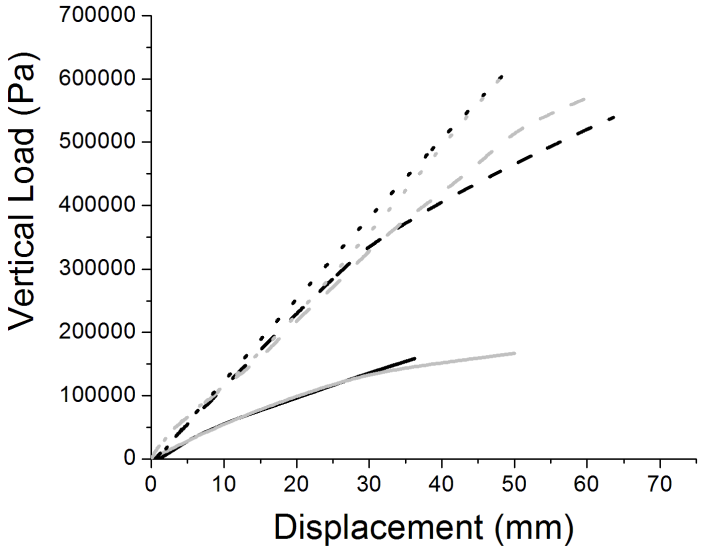

Figure 4.4b. Comparison of vertical displacement from experiments and FE simulations for monotonically loaded tests using Mohr-Coulomb plasticity.

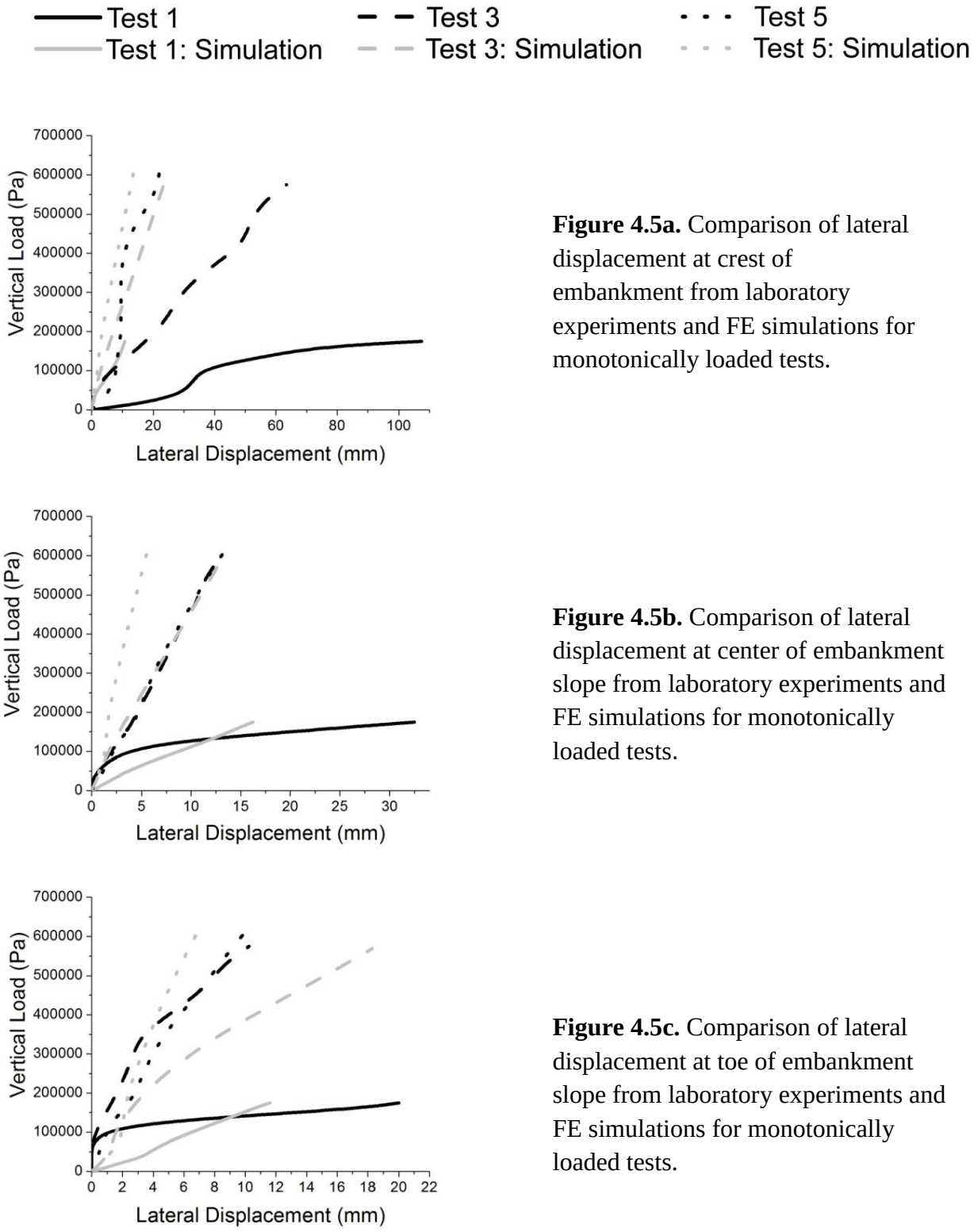

Figure 4.5a. Comparison of lateral displacement at crest of embankment from laboratory experiments and FE simulations for monotonically loaded tests.

Figure 4.5b. Comparison of lateral displacement at center of embankment slope from laboratory experiments and FE simulations for monotonically loaded tests.

Figure 4.5c. Comparison of lateral displacement at toe of embankment slope from laboratory experiments and FE simulations for monotonically loaded tests.

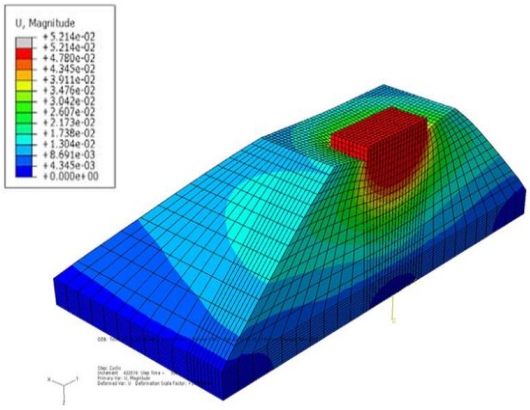

Figure 4.6a. Displacement in unreinforced case at end of loading.

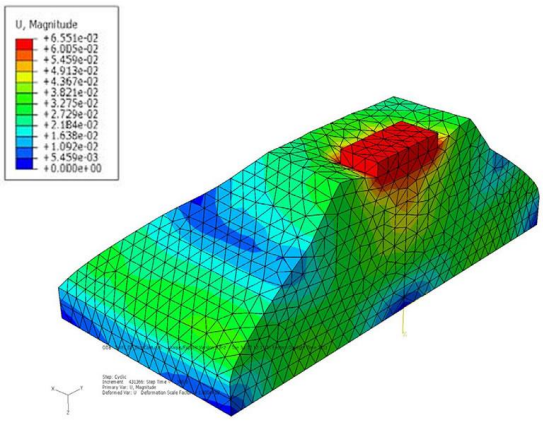

Figure 4.6b. Displacement in single-reinforced case at end of loading.

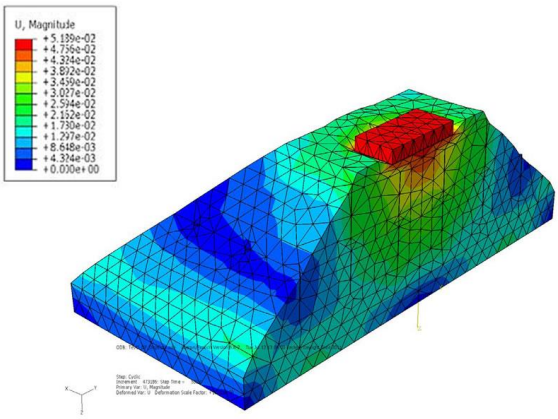

Figure 4.6c. Displacement in double-reinforced case at end of loading.

The FE analysis is particularly useful in observing the stresses and strains in the geocell in order to examine possible weaknesses. As observed during the experiment and afterwards, when the geocell was exhumed, the highest concentrations of stresses and strains occurred at the bottom corners of the diamond-shaped cells, under the loading plate. Intuitively, this makes sense since the bending of the ballast-geocell composite places significant tensile stresses on the lower part of the geocell, especially in the center region that happens to be some depth under the loading plate. This observation is important because although the geocell underwent mainly elastic deformations during the testing, the polymer material can yield throughout the cell wall or the seam under higher loading. The stress concentration observed at the cell corners accentuates the need for higher seam strength, which is often critically weak in comparison to the tensile strength of the walls forming the cells. Despite these concerns, strain gages used in the geocell during experimentation implied that the geocell exhibited mostly elastic strain (i.e., recoverable strains), allowing the assumption of elastic behavior in the geocell for the FE analysis. The strains encountered in the critical regions of the geocell during the simulation were in the same range of magnitude as those found in the experiments. In the single-layer reinforced test, the strains encountered in the geocell under the loading plate were 3.5% and 2.1% at bottom corner seam and central cell wall, respectively. Computed at the same geocell locations in the double-layer reinforced test, the strains encountered in the geocell under the loading plate in the top layer were 2.4% and 1.4%, and 1.8% and 1.1% in the bottom layer (*Figure 4.7).*

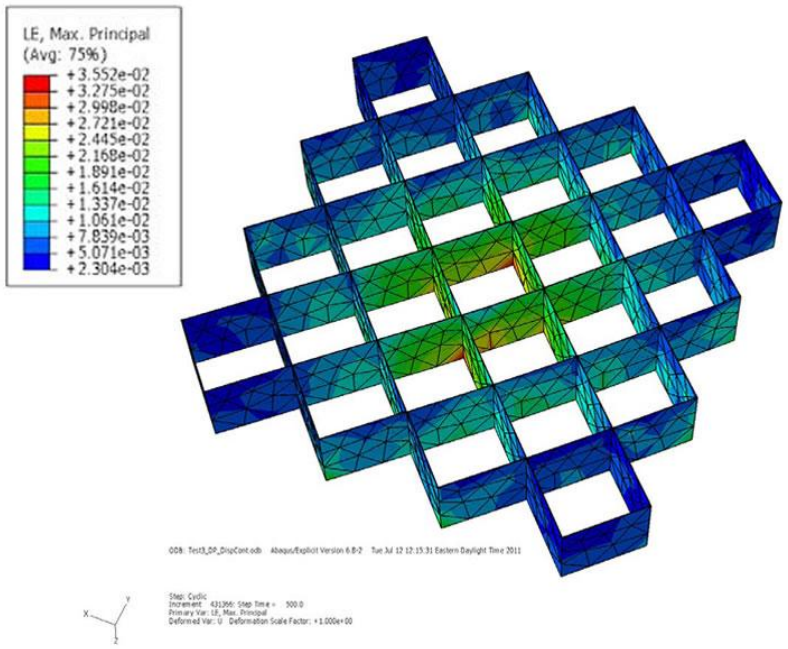

Figure 4.7. Strain in Geocell from FE simulation (single-layer, top; double-layer, bottom).

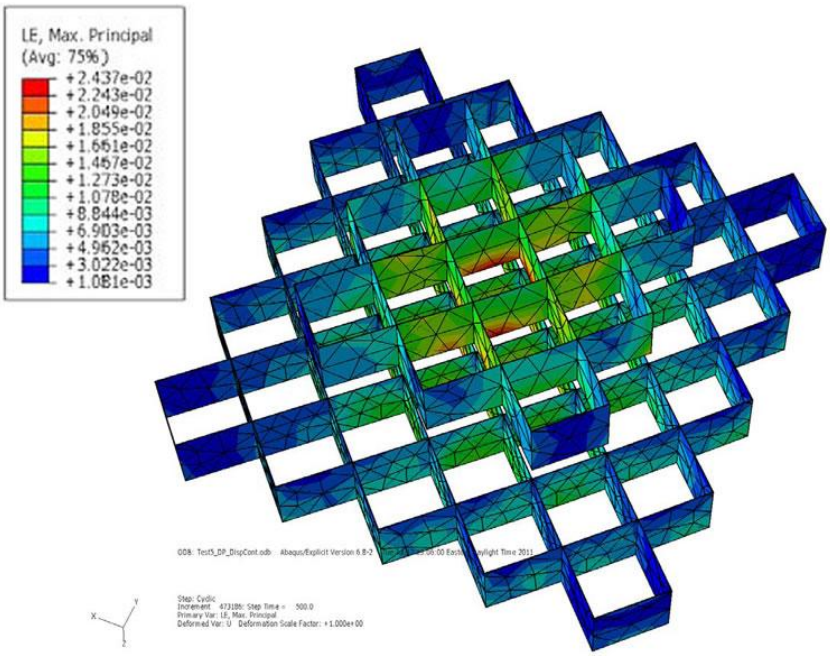

Excluded from the analysis of the geocell was any simulation of creep, which can be a very complex and difficult process to simulate or predict. The material used for the geocell is an alloy that contains materials to inhibit creep behavior over time. However, the long-term creep might be a key concern, depending on material properties or a specific geocell application.

Although some of the simulated displacements did not match very well, the simulations and experiments were a good indicator to the advantages attained from using geocell confinement, including lower deformations and higher strength and stiffness. The lack of accurate matching for lateral displacements was not deemed critical since similar advantageous trends were still observed due to the confining mechanism in the geocell.

4.3.2 Cyclic Tests

The three cyclically loaded embankment tests were simulated using similar loading conditions and model geometry. That is, the pressure was applied to the plate under load-control conditions, using a specified maximum and minimum load. An unreinforced control test and two reinforcement configurations were used: a single, centrally placed layer of geocell, and two layers of geocell placed within the embankment. Throughout the duration of these simulations, the vertical displacement and stress under the loading plate, as well as the lateral displacement along the profile of the embankment, were compared with the actual test results.

Again, it was shown that the comparison of vertical displacement to vertical load matched reasonably well, at least for the unreinforced configuration (*Figure 4.8*). However, the high stiffness of the geocell yielded relatively low estimates for vertical settlements encountered in either of the geocell model simulations. Generally, the cyclic hardening encountered by both of the reinforced models in the later loading stages was captured (as implied by the flattening of the

curves in the later cycles), while the unreinforced configuration still underwent some cyclic deformation in both the experiment and the simulation. However, the magnitudes of the final vertical settlements simulated for both of the reinforced cyclic tests were not accurate. The fact that both Tests 4 and 6 encountered the same vertical displacement at the end of the test, a counterintuitive observation, was difficult to account for in the simulation. Despite this disagreement for the reinforced tests, the experimental results and simulations still demonstrate the benefits of using the geocell confinement in the ballast.

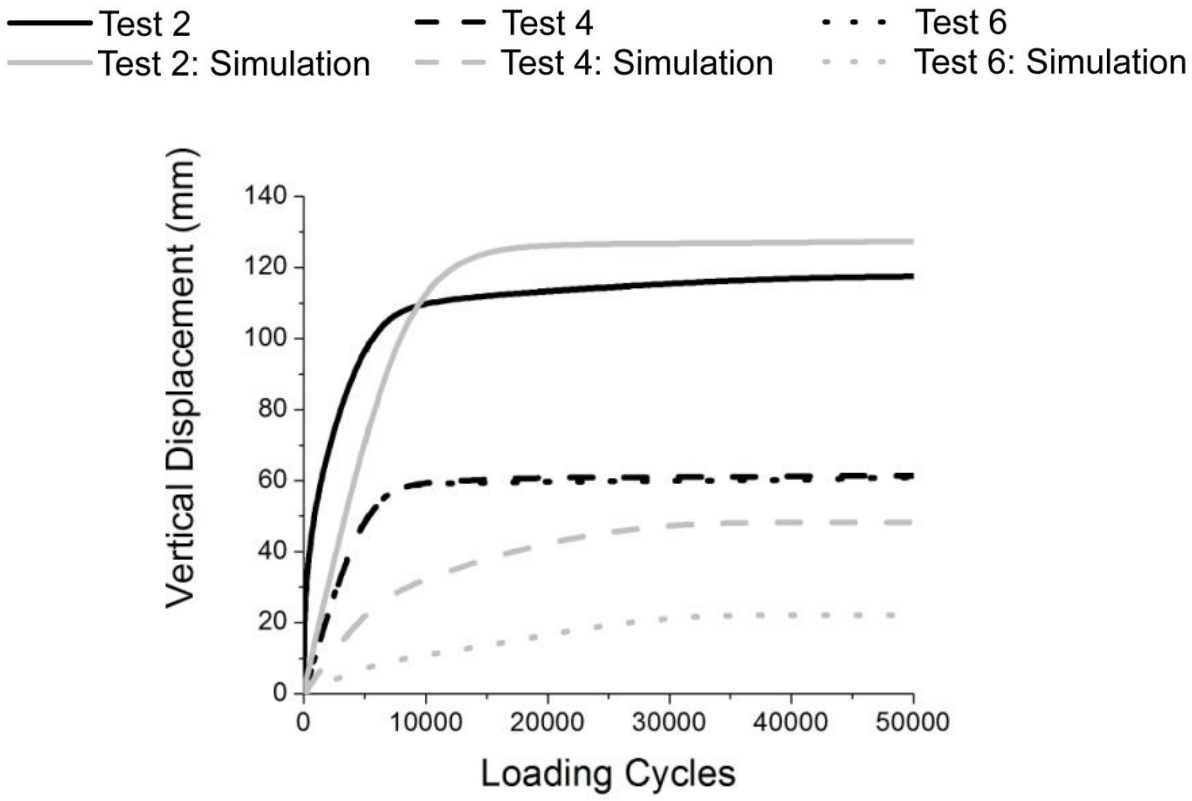

Figure 4.8. Comparison of vertical displacement from experiments and FE simulations for cyclically loaded tests, unreinforced (test 2), single-layer (test 4), and double-layer (test 6).

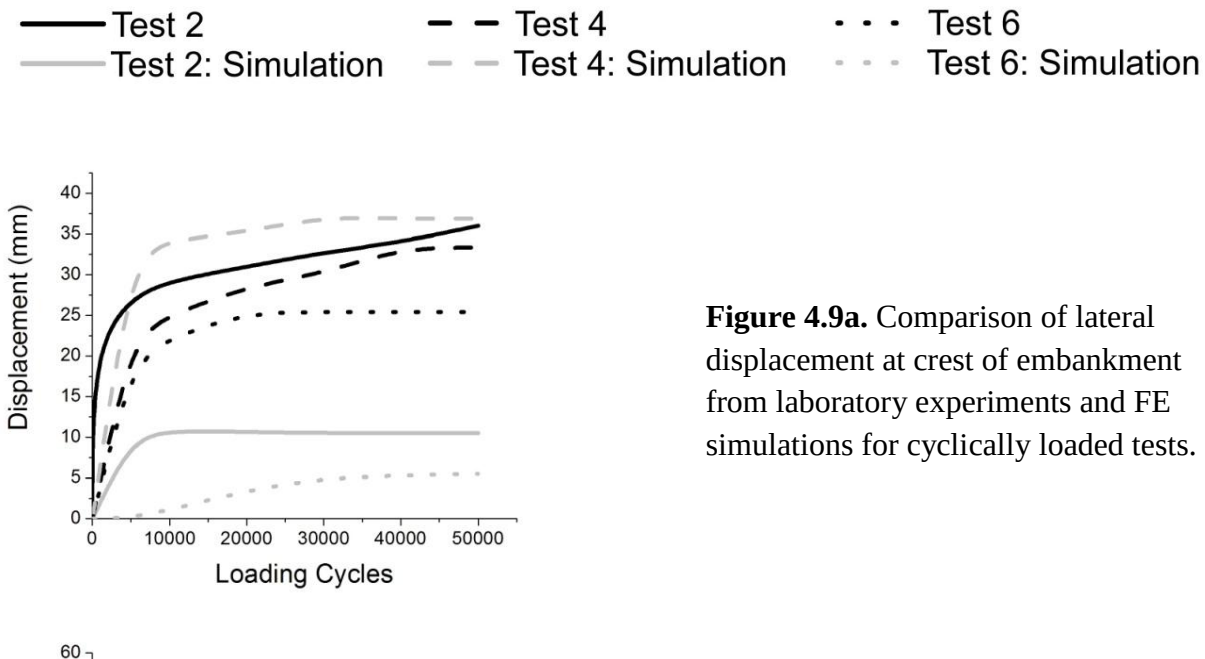

Figure 4.9a. Comparison of lateral displacement at crest of embankment from laboratory experiments and FE simulations for cyclically loaded tests.

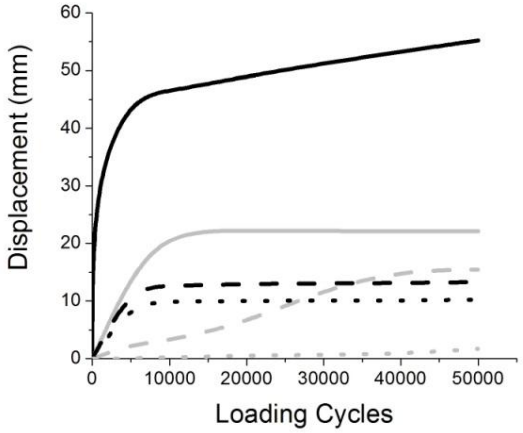

Figure 4.9b. Comparison of lateral displacement at center of embankment slope from laboratory experiments and FE simulations for cyclically loaded tests.

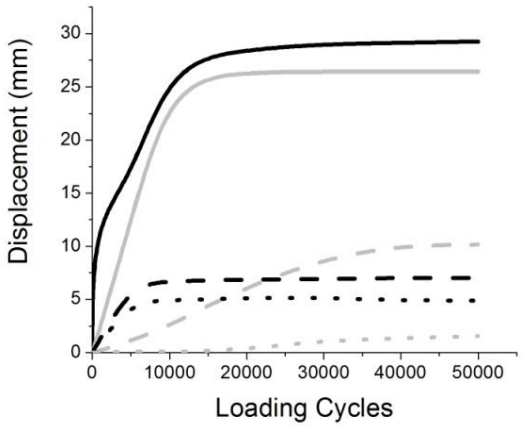

Figure 4.9c. Comparison of lateral displacement at toe of embankment slope from laboratory experiments and FE simulations for cyclically loaded tests.

Regardless of some numerical discrepancies, the FE analysis did capture the advantageous trend that the single- reinforcement configuration prevented further lateral spreading throughout the embankment profile, and even more so with the double-reinforcement configuration. The actual simulated amounts of lateral displacement from the FE analysis did not match entirely, although they were reasonable (*Figure 4.9a,b,c*). Despite this, the simulated and experimental results indicate the significant reduction in deformation attained by using geocell confinement.

Strains observed in the geocell during experimentation were in the same range (<4%) with those found in the FE analysis, both of which exhibited elastic behavior. Similar to the monotonic testing, the highest stresses and strains were found in the lower corners of the geocell that were located beneath the loading plate. In the single-layer reinforced test, the strains encountered in the geocell under the loading plate were 3.6% and 2.3% at bottom corner seam and central cell wall, respectively. Measured at the same geocell locations in the double-layer reinforced test, the strains encountered in the geocell under the loading plate in the top layer were 1.2% and 1.1%, and 1.1% and 0.8% in the bottom layer. Creep was not modeled. It would be difficult to observe creep under the limited amount of loading cycles applied and the duration of the experiment.

4.3.3 Summary of Numerical Modeling of Experiments

In order to validate further full-scale finite element simulations using more relevant geometry, materials and scenarios, the experimental results were simulated and calibrated using data from the model tests and material testing in the lab. Using the Drucker-Prager elastic-perfectly plastic model for the ballast and modeling the appropriate geometry and boundary conditions of the

embankment, numerical simulations were performed to attain acceptable results in both monotonic loading and cyclic loading.

1) Although the agreement between the actual and simulated lateral displacements was not perfect in either the monotonic or cyclic cases, the simulations still effectively demonstrated a trend of reduced deformation as a result of geocell confinement. In the cyclically loaded, reinforced tests, the vertical displacements did not match exactly, but again indicated the reduced deformations due to use of geocell while still matching the loading curve for the unreinforced case.

2) The lateral deformations that occurred in the experiments were difficult to simulate with FE analysis, especially with a simplified plasticity model using Drucker-Prager yield criterion. This could be due to the anisotropy and low confinement pressures encountered outside the geocell confinement (i.e. crest of embankment, outer profile of slope). However, many of the benefits attained from geocell are captured using the material model, including the confining mechanism, the ‘mattressing effect” and expedited resilience under cyclic loading. This is demonstrated by reduced lateral spreading and settlements as well as increased loading capacity.

3) Observations of stresses and strains in the geocell in both the experiments and simulations generally agreed, especially in indicating the elastic behavior and low strains in the geocell. Additionally, the highest concentrations of stress and strain were found to be in the lower corners of the cell underlying the loading plate, likely due to high tensile stresses in the reinforcement as a result of the significant vertical settlement under the loading plate and resultant bending behavior of the geocell/ballast composite. This

suggests the importance of strong geocell seams, which could be critical under increased loading and/or more loading cycles.

4) General matching between the monotonic loading curves and acceptable matching for the cyclically loaded curves was promising and warrants further analyses studying the effects of various scenarios and material properties. However, significant discrepancies were noted when comparing lateral spreading between laboratory tests and numerical simulations. These in turn, warrant further study of accurate modeling of lateral displacements.

5) The greatest discrepancies in displacement behavior occurred in the double-layer case, as well as lateral displacements in many cases, likely due to shortcomings in the chosen constitutive model (Drucker-Prager). Some possible sources of these shortcomings could be a lack of consideration for anisotropy and an overestimate in angle of dilation and lack of consideration of anisotropy, causing excessive lateral displacements as well as the inability to capture degradation or fatigue.

4.4 Parametric Study

A numerical parametric study was performed on the model geometry to observe its performance under varying geocell stiffness, ballast strength, and overlying over a soft foundation (*Figure 4.10*). Each time a parameter was varied; the model was in three configurations: an unreinforced control test, one layer of centrally placed geocell confinement, and two layers of geocell confinement. The model meshes were the same as used in the FE simulations for each respective setup, with the exception of an additional 8603 C3D4 tetrahedral elements used to model the underlying foundation in all the cases. Insight into the resulting behavior demonstrates the benefits of using geocell confinement in ballasted foundations. Under each condition, the vertical settlement under the loading plate and the maximum stress at the ballast-subgrade interface (to demonstrate the improvement in the stress distribution) was monitored when vertical load of the plate had reached 150 kPa. The settlement and subgrade stress behavior for each reinforced case (under each changed parameter) was normalized to using the related, unreinforced case through the following relationships:

$$\frac{S}{S_u} = Normalized\ Settlement$$

$$\frac{q}{q_u} = Normalized\ Maximum\ Stress$$

S and q is the vertical settlement under the loading plate and the maximum stress at the ballast-subgrade interface, respectively. Similarly, S_u and q_u is the vertical settlement and the maximum stress at the ballast-subgrade interface for the unreinforced model embankment, respectively (*Figure 4.11*).

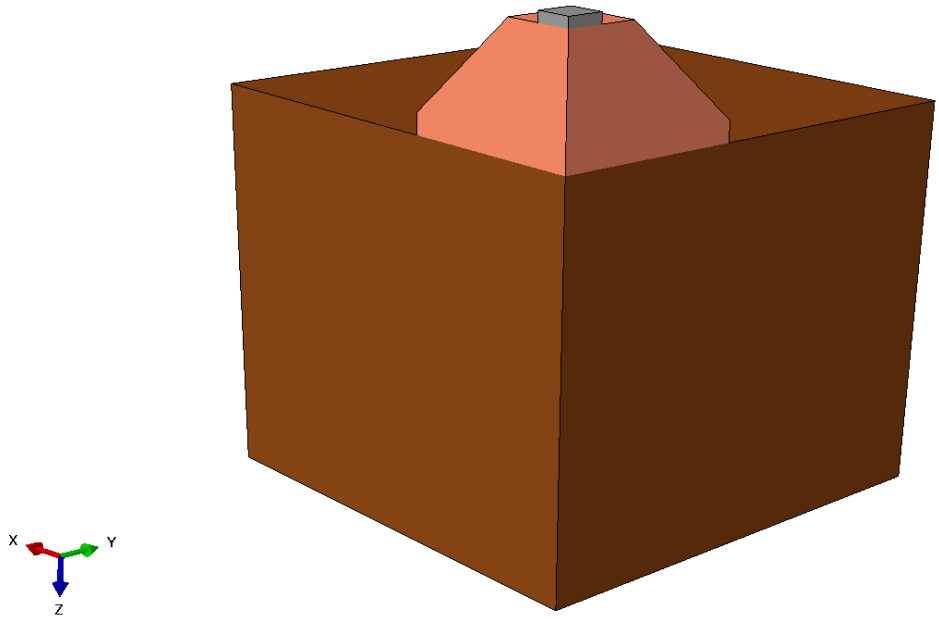

Figure 4.10. Geometry of model used for parametric study.

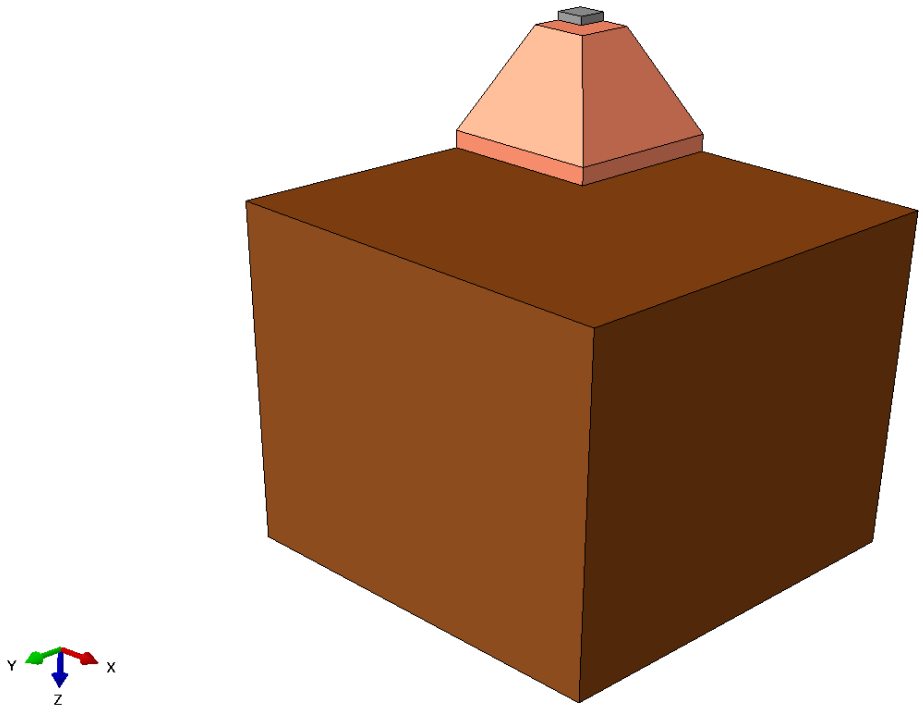

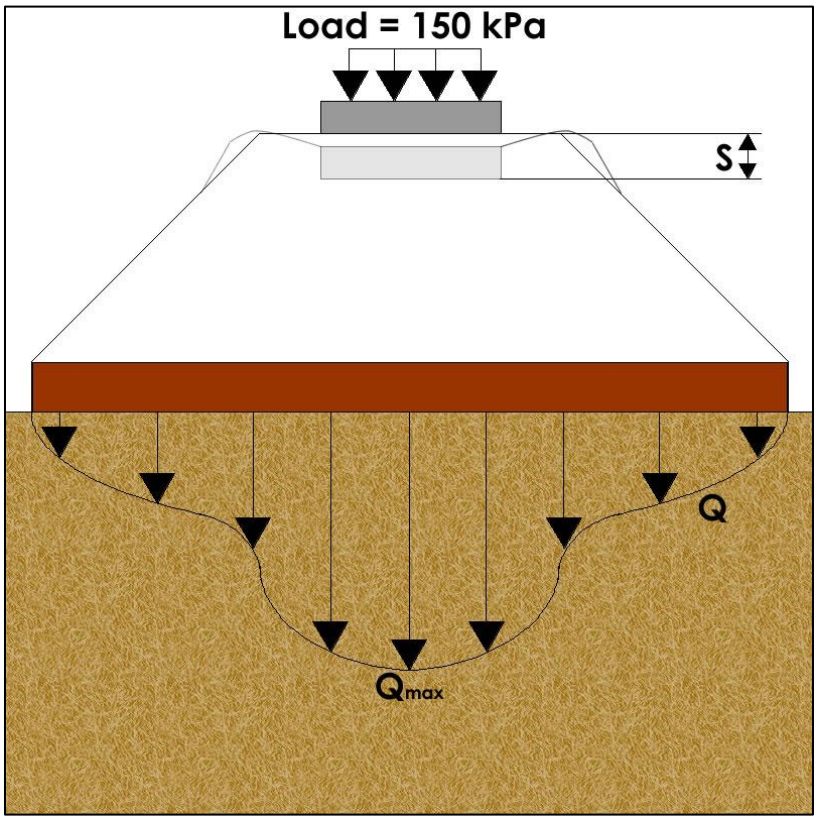

Figure 4.11. Observed behavior in parametric study.

The effects of geocell stiffness were demonstrated by placing the model over a 2 m deep, soft foundation (simulated by a stiffness of 1 MPa). Then, all three embankment setups were run using geocell stiffness of 0.1, 1, 2.07, and 200 GPa to demonstrate a variety of materials including HDPE, NPA, and structural steel (*Figure 4.12*). Use of HDPE, NPA and steel in test 2 and 3 displayed significant added performance as the results show a significant reduction in settlement (75% and 82%, respectively) and maximum subgrade stress (35% and 40%, respectively) with the increasing geocell stiffness (*Figure 4.12*).

The effects of foundation stiffness were demonstrated by placing the model (reinforced with NPA geocell) over a 2 m deep foundation with varying stiffness. The foundation stiffnesses of 1,

10, 100, and 100 MPa were used to demonstrate a range from soft to very stiff subgrades. The subgrade was modeled as an elastic material. The generation of pore pressure and consolidation behavior was ignored. The benefit of confinement was significant upon a soft foundation as it decreased settlement and maximum stress at the subgrade significantly. As the foundation stiffness increased, the uniformity in stress distribution was lost (reductions of 3% and 20% for tests 2 and 3, respectively), but settlement was still greatly reduced (87% and 90% for tests 2 and 3, respectively) by preventing lateral spreading (*Figure 4.13).* This is likely because the foundation stiffness was higher than that of the ballast, and the geocell-ballast composite action due to confinement provides a more competent soil structure. Geocell reinforcement was beneficial on both soft and stiff foundations as it reduces settlement.

After many loading cycles, ballast deteriorates, becoming rounded, contaminated by fines and losing some of its strength (Indraratna and Salim, 2002) eventually, requiring replacement or maintenance. Thus, it was important to study the effects of ballast quality by altering the angle of internal friction (the governing strength parameter for a cohesionless material like ballast) between 25° and 55°, representing both very weak and very strong ballast. The embankment was placed above a 2 m deep, soft foundation (stiffness was 1MPa).

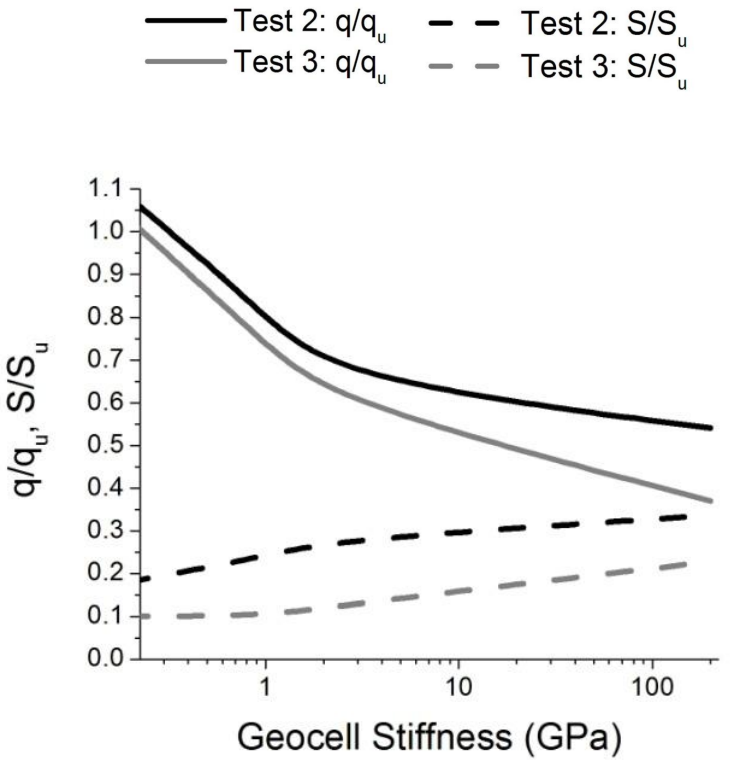

Figure 4.12. Results of varying Geocell stiffness.

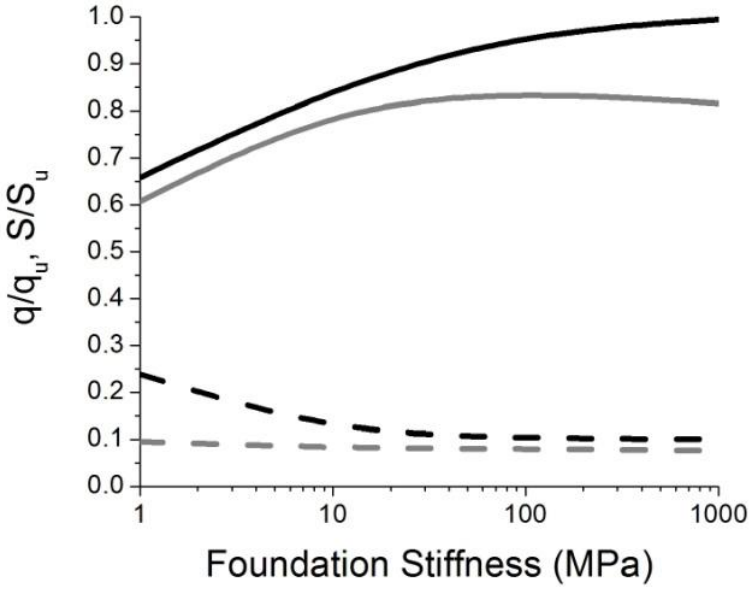

Figure 4.13. Results of varying subgrade compressibility.

The vertical settlement with a soft subgrade (1 MPa) is greatly reduced (between 60-75%) using a single layer of geocell and even more so with two layers. This benefit is attained for a range of frictional strengths in the ballast for double layer configuration and above approximately 33 degrees for single layer (*Figure 4.14)*. However, it did not vary greatly as the use of geocell confinement allowed the embankment to act as a composite, providing dimensional stability that is less dependent on ballast strength properties. Considering that all of these simulations occurred on a soft subgrade as opposed to a rigid subgrade, the benefit of geocell is shown by the great disparity between unreinforced and the reinforced cases.

The ballast friction angle had a significant effect on the subgrade stress distribution. At higher strengths, both geocell configurations provided a similar decrease in maximum subgrade stress (28% and 33% for Tests 2 and 3, respectively) in comparison to the unreinforced case. At lower strengths, there was little change in maximum stress at the subgrade interface (3% and 25% reduction for Tests 2 and 3, respectively). As expected, the double reinforced case yields a significant benefit here as it maintains a more uniform distribution even under very low strength because the entire embankment acts a composite. However, the plot suggests that it may not be an economical choice to use two layers of geocell as opposed to a single layer for reasonable ballast properties (40° and above) as the two reinforcement cases have similar benefits over the unreinforced case (*Figure 4.12)*. Despite this, both reinforcement configurations demonstrate a considerable gain in performance due to geocell confinement under several different conditions.

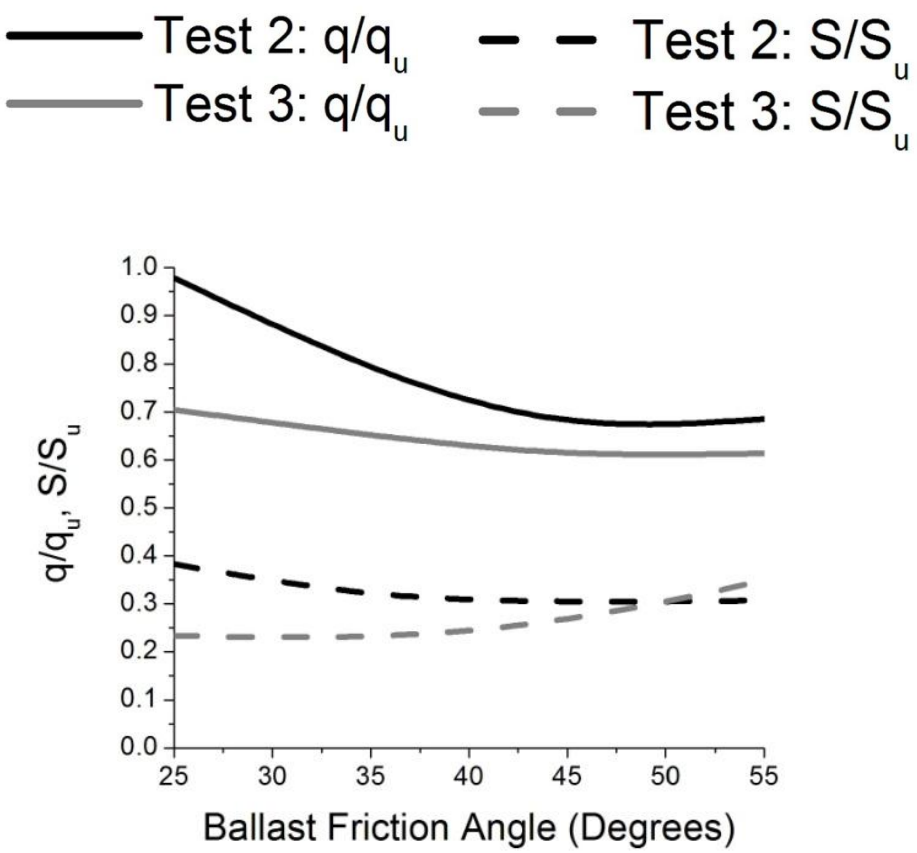

Figure 4.14. Results of varying ballast strength.

The strains in the geocell were in the recoverable, elastic range of values in the models discussed at a vertical load of 150 kPa. The compressibility of the foundation had a marginal effect on strain, yielding a range of maximum strain between 0.4% to 0.6% and 0.4% to 0.6% for the single- and double-reinforced configurations, respectively. Changing the stiffness of the geocell had a larger effect, as expected. Lowering the stiffness of the material allows much more strain for the same load. The range of strains varied between 4.5% to 0.02%, 3.2% to 0.01% for the single- and double-reinforced configurations, respectively. However, for HDPE and NPA, the maximum strain was in 0.6% range, well within elastic behavior for both materials. The strength

of the ballast had an effect on the strain in the geocell, although it was not critical. Larger strains, 1.1% and 0.7% for the single and double-reinforced tests, respectively, occurred when using weaker ballast (ϕ=25°). When using stronger ballast that mobilized less confinement from the geocell, smaller strains occurred in the geocell (0.4% and 0.3%, single- and double-reinforced).

Table 4.2. Tabulated Results of Parametric Study.

Unreinforced Tests: Foundation Stiffness Varied					
$\mathbf{E_{foundation}}$	[MPa]	**1**	**10**	**100**	**1000**
$\mathbf{q_u}$	[kPa]	26.8	39.1	38.3	38.1
$\mathbf{S_u}$	[mm]	98.9	98.6	97.8	97.6
Unreinforced Tests: Geocell Stiffness Varied					
$\mathbf{E_{geocell}}$	[GPa]	**0.1**	**1**	**2.07**	**200**
$\mathbf{q_u}$	[kPa]	26.8	26.8	26.8	26.8
$\mathbf{S_u}$	[mm]	98.9	98.9	98.9	98.9
Unreinforced Tests: Ballast Strength Varied					
$\mathbf{\phi_{ballast}}$	[°]	**25°**	**35°**	**45°**	**55°**
$\mathbf{q_u}$	[kPa]	34.1	32.8	26.8	26.5
$\mathbf{S_u}$	[mm]	142.8	126.2	98.9	43.6

4.4.1 Implications of Numerical Analysis

Reasonable matching between the actual and simulated tests warrants further studies, such as behavior in a ballasted foundation for railways. Additionally, the effects of geocell stiffness or soil strength and stiffness can be observed, which could have significant economic implications in design. Future simulation of geocell confinement applied to actual railroad ballasted geometry could provide some useful predictions and insight on the effectiveness of such an application.

In the case of railroad construction, geocell would be installed no closer than 150 mm from the base of the tie in order to facilitate ballast construction and tamping. This clearance also assists

in the maintenance process. Additionally, the upper portion of the ballasted foundation is exposed to high dynamic loads that could be damaging in proximity to the geocell. The minimum clearance between the geocell and the tie is reliant on maximum ballast grain size (typically below 63.5 mm in diameter according to industry standards). This constraint needs to be considered when modeling a ballasted railway foundation accurately, an aspect that further FE simulation could elucidate.

Actual field testing of such an application of geocell would also allow for observation of other relevant concerns, like creep, installation damage, higher amounts of loading cycles, ballast degradation, and foundation/subgrade effects. With actual field data, a FE analysis can again be validated and applied to a larger variety of applications with confidence.

4.4.2 Conclusions of Parametric Study

In order to demonstrate the effects of various factors on the performance of the embankment, a parametric study was performed on geometry similar to that used in the experiment and simulation, except that foundation was no longer modeled as rigid. Various material properties were changed in order to observe their influence on the behavior of the model. These properties included geocell stiffness, ballast strength, and foundation compressibility. Implications of the simulations included:

1) This study demonstrates that implementation of geocell confinement demonstrates a significant benefit by distributing subgrade stresses more uniformly, as supported by previous field tests (Chrismer, 1997). This is due to the “mattress” effect that the geocell

composite displays when under loading (Zhou and Wen, 2008). The reduction in maximum stress was especially pronounced in situations where the embankment was placed upon a softer foundation. This reduction in maximum stress reduces settlement and increases bearing capacity.

2) The application of geocell significantly reduced vertical settlement under the loading plate. This was especially true when the embankment overlaid softer foundations or was applied to weaker ballast. Upon stiffer foundations, vertical settlement was also reduced due to a prevention of lateral spreading applied to the ballast due to the confining effects of the geocell. The behavior of the geocell-ballast composite also prevents excessive settlement and shear from occurring when inferior material is used, like recycled, deteriorated or rounded ballast.

3) The use of one layer of geocell as opposed to two (whole embankment reinforced) generally provides similar benefits in a more cost-efficient manner. Generally, the single-layer reinforcement geometry performed similarly to the double-layer scenario, if only providing 15% less strength improvement and/or deformation reduction, a benefit unlikely to justify application of such a considerable additional amount of geocell. In addition to constructability issues and economics, it is recommended that use of a single layer of geocell in ballasted foundation applications as opposed to excessive reinforcement for little benefit.

4) The strains that occurred in the geocell under the various ballast strengths and foundation stiffnesses were well within the elastic, recoverable range for the material. This suggests

that the geocell would have remained in working conditions under the adverse conditions presented in the parametric study.

5) Generally, for materials commonly used as geosynthetic reinforcements, the benefit of using superior geocell materials are not pronounced, suggesting that the confinement mechanism does not necessitate expensive, top-grade polymers or alloys to function adequately.

CHAPTER 5: NUMERICAL MODELING OF RAILWAY WITH GEOCELL

5.1 Introduction

General validation of experimental results from Finite Element modeling and intriguing implications from parametric studies intuitively led to the numerical modeling and simulation of geocell reinforcement with actual ballasted railway foundation geometry and conditions.

Future work and correspondence with AMTRAK (National Railroad Passenger Corporation) engineers, in addition to consultation of current AREMA (American Railway Engineering and Maintenance-of-Way Association) code has resulted in standard railroad ballast design and geometry specifications, allowing numerical studies of the effects of Geocell on track settlement, lateral spreading, squeeze and subgrade stress distribution under various conditions.

Since the 3-dimensional modeling procedures have been validated by full-scale experimental testing, it is acceptable to apply it to the parametric studies conducted in this chapter. A plane-strain slice of the cross-section of a half of a ballasted railway substructure was modeled with a finite element mesh refined to observe important behavior of the foundation under loading, with or without geocell reinforcing the subgrade-ballast interface. Behavior observed during the numerical simulation included vertical displacement, lateral displacement, vertical stress, subgrade stress and strain in the geocell. The parametric studies examined the effects of subgrade stiffness, geocell stiffness, and ballast strength.

5.2 Geometry and Cross-Section

5.2.1 Cross-Section

The embankment was 5.2 meters in width at the base, 2.7 meters at the crest, and 0.6 meters in height (see *figure 5.1a*). The slopes did not exceed the specified slope of 2:1 as indicated by various rail design manual (i.e. *USACE track design manual, 2000*). Based to on proposed constructability issues and prior research, the geocell would have to be placed in the ballast/subballast layer at a minimum of 25 centimeters below the ties in order to avoid construction damage and stress concentrations from heavy axle loads from trains (see *figure 5.1b*). Additionally, design specifications provided by AMTRAK for standard railway substructure geometry with and without geocell provided a basis for a parametric study, where the benefits of the confining mechanism could be explored.

The simulated tie was assumed to be made of concrete, had a width of 2.7 meters and was beveled with a maximum height of 0.2 meters at the ends and 0.15 meters at its center. They were spaced at every 0.5 meters on-center.

The rail head had a width of 7.5 cm, the web a width of 1.75 cm and the base had a width of 15 cm.

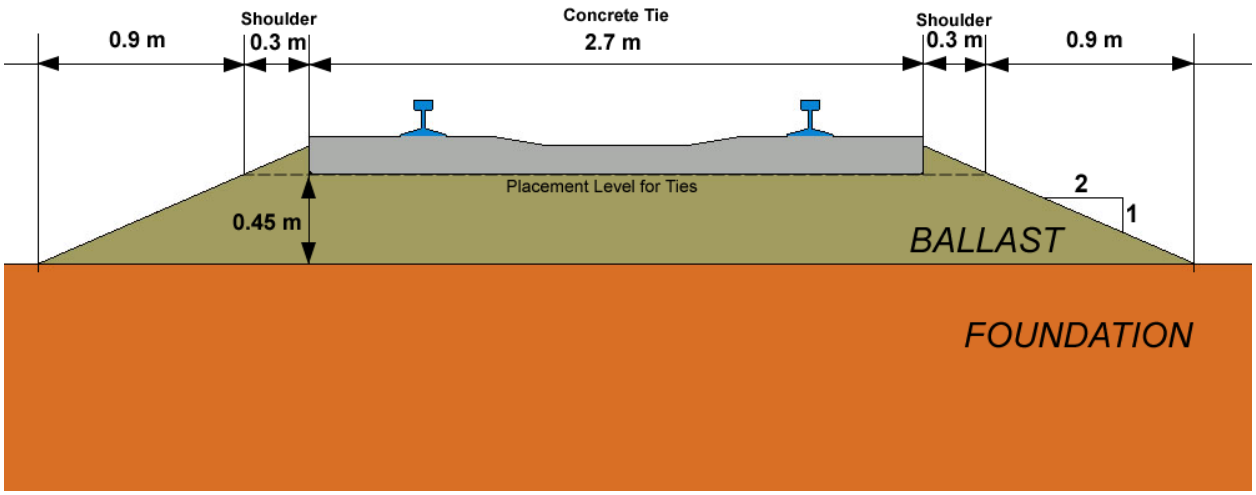

Figure 5.1a. Railway geometry without geocell.

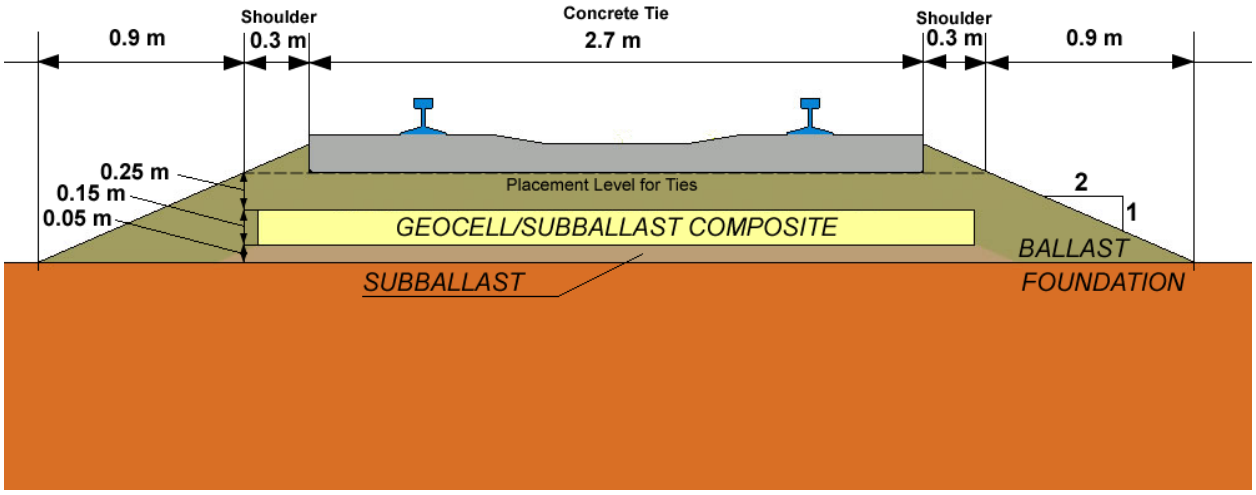

Figure 5.1b. Railway geometry with geocell confinement.

5.2.2 Selection of Three- Dimensional Model Geometry

Due to the computational requirements of running a larger or more refined mesh, the width of the plane-strain slice was limited to 1.8 meters in thickness; that is, enough width to have three ties with the full thickness of ballast infill in between each. The boundary effects were generally considered small due to the symmetry, even loading and large depth of the foundation. The USACE railroad design manual assumes that the point load attained from the wheel of the railcar is distributed among 5 ties, emphasizing the highest load on the tie below the wheel (*figure 5.2a*). The FE simulation is modeled with three ties that is slightly more conservative, contributing higher loads on the two adjacent ties, but not allowing a stress higher than 40% of the wheel load for a tie, which is representative of the assumptions in the manual (*figure 5.2c*) and the conclusions stated in literature (*figure 5.2d,* Selig and Waters, 1994). However, these slightly more adverse conditions still demonstrate the advantages of geocell reinforcement because the conditions and stress distributing behavior of the ties assumed are not as favorable as assumed in the the manual. Additionally, the deflection profile of track subject to a wheel load from Selig and Waters (1994) suggests that only three ties carry the load, while the further ties are actually suspended due to the deflection of the track.

In order to assure that the boundary effects of the model used are not vastly unconservative or misrepresentive of realistic distributions, a FE model with 5 ties was analyzed for comparison (*figure 5.2b*). It was shown that the distribution was more even and hence, unconservative, while the “three-tie” system matched the assumed distribution in a conservative fashion. That is, the five-tie model had a maximum stress underlying the point load, as expected, however it was only 25% of the applied load, which is significantly less than the manual suggests. Such an under-

representation of loading only impedes demonstrating the effects of geocell confinement within the embankment. The wheel load was applied statically as a point load (due to the small area of stress application and large load).

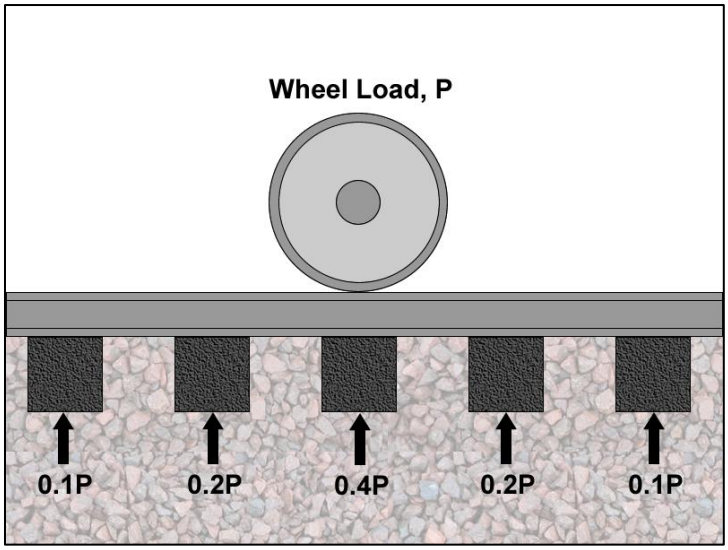

Figure 5.2a. Assumed ballast-tie reaction from wheel load.

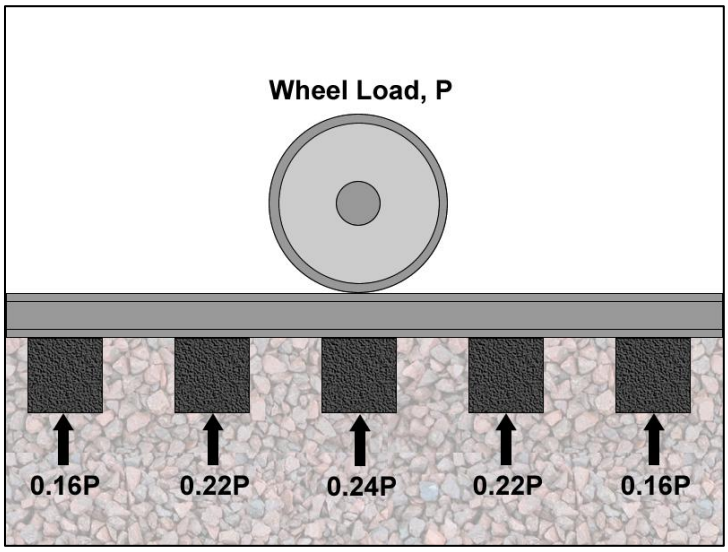

Figure 5.2b. Ballast-tie reaction from wheel load using FE analysis and 5 ties.

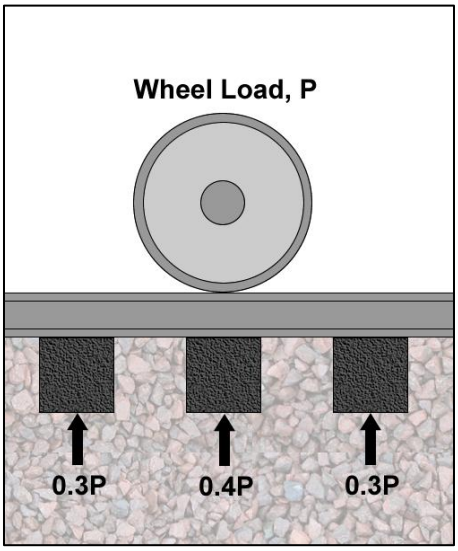

Figure 5.2c. Ballast-tie reaction from wheel load using FE analysis and 3 ties.

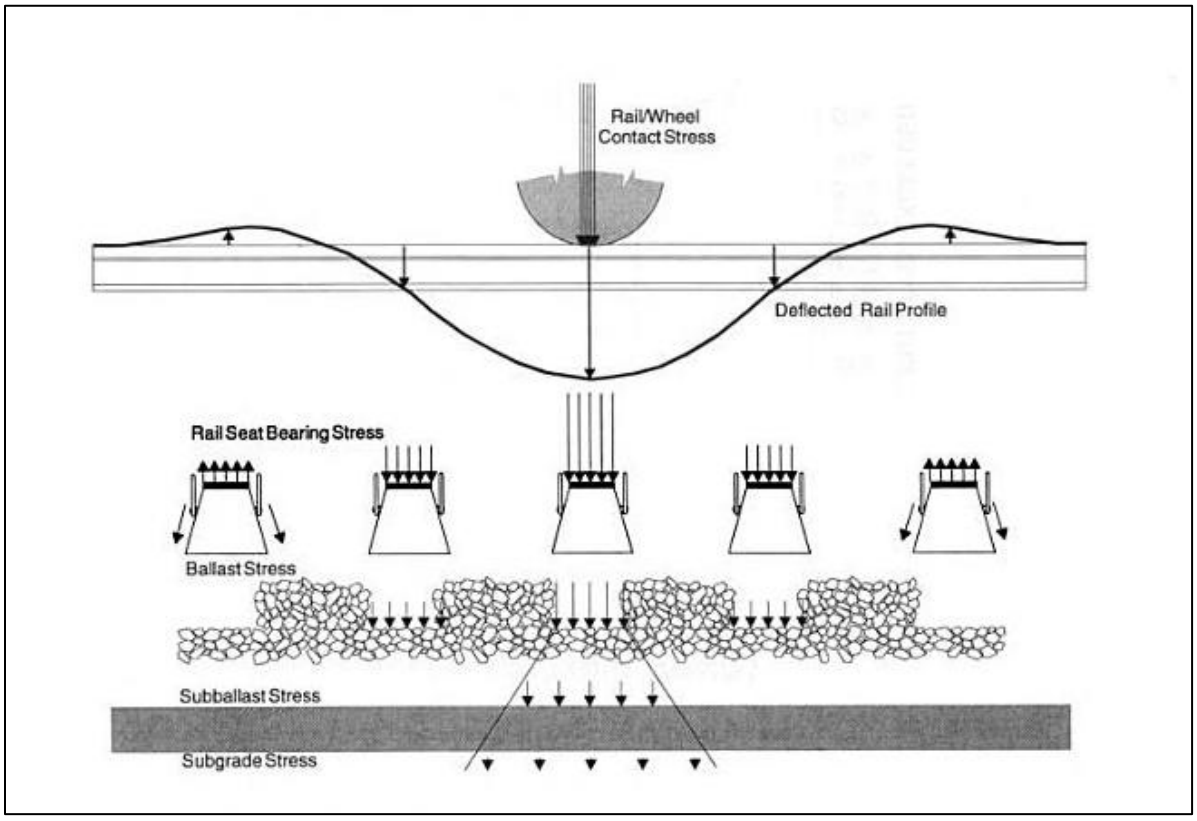

Figure 5.2d. Rail deflection and stress distribution profile (Selig and Waters, 1994).

5.3 Finite Element Analysis

5.3.1 Mesh/Elements

5.3.1.1 Unreinforced

The unreinforced model consisted of 19946 elements and 7387 nodes (*figure 5.4a*). Greatly coarser meshes provided lower, more conservative settlements.

A large majority of these elements were placed in the railway substructure, as its behavior was of utmost interest and the most deformation was expected in the area. It was modeled with 17318 tetrahedral, 4-noded reduced integration elements (C3D4R), which are necessary to mesh the relatively irregular geometry of the ballasted embankment. This implies that the element size would have an approximate diameter of approximately 4.4 cm (1.75”), which falls within the range for ballast grain sizes commonly used according to standard AREMA gradation specifications.

5.3.1.2 With Geocell

The reinforced model consisted of 41388 elements and 11075 nodes.

A large majority of these elements were placed in the railway substructure and geocell, as its behavior was of utmost interest and the most deformation was expected in the area. It was modeled with 17318 tetrahedral, 4-noded reduced integration elements (C3D4R), which are necessary to mesh the relatively irregular geometry of the ballasted embankment infilled with diamond-shaped geocell (*figure 5.4b, 5.4c*). This implies that the element size would have an

approximate diameter of approximately 3.7 cm (1.5”), which falls within range for ballast grain sizes commonly used according to standard AREMA gradation specifications.

5.3.1.3 Railroad and Ties

The railroad/tie instance was meshed with only 378 hexahedral, 8-noded reduced integration elements (C3D8R) because it’s deformation was not of concern due to its much higher stiffness in comparison to the ballast and foundation soils. The foundation was also modeled coarsely to focus computational memoryon the ballast embankment, containing 2250 C3D8R elements. Higher mesh density was specified for the area closest to the ballast embankment-subgrade interface in order to study subgrade stresses resulting from wheel loads.

5.3.1.4 Interaction

Planar interface elements were assigned to the surfaces where ballast and geocell were in contact, including the inside, outside, top and bottom of the geocell-ballast interface. They were modeled as contact where tangential properties were frictional (i.e. $\delta=(2/3\Phi)=30°$) and normal contact was “hard”, that is the walls of geocell could not be penetrated. The same type of interface was assigned for contact between the railroad ties and ballast.

5.3.1.5 Symmetry

Due to the symmetry of the model, the simulated half was then mirrored in both the X and Y directions to show the full structure for visualization purposes (*figure 5.5*).

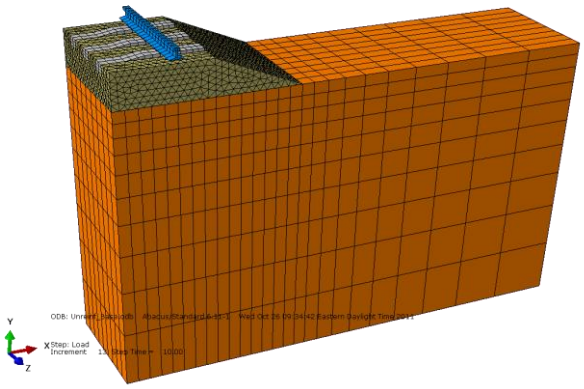

Figure 5.4a. Mesh of ballasted railway track and foundation.

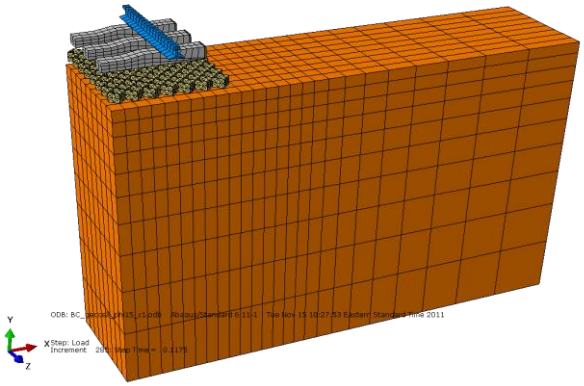

Figure 5.4b. Mesh of rail, geocell and foundation (ballast removed for illustration).

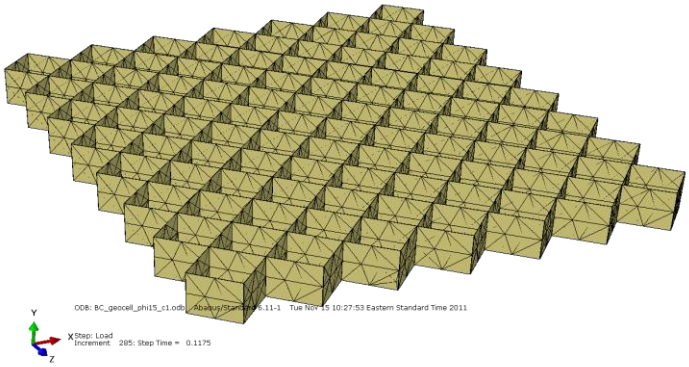

Figure 5.4c. Mesh of embedded geocell.

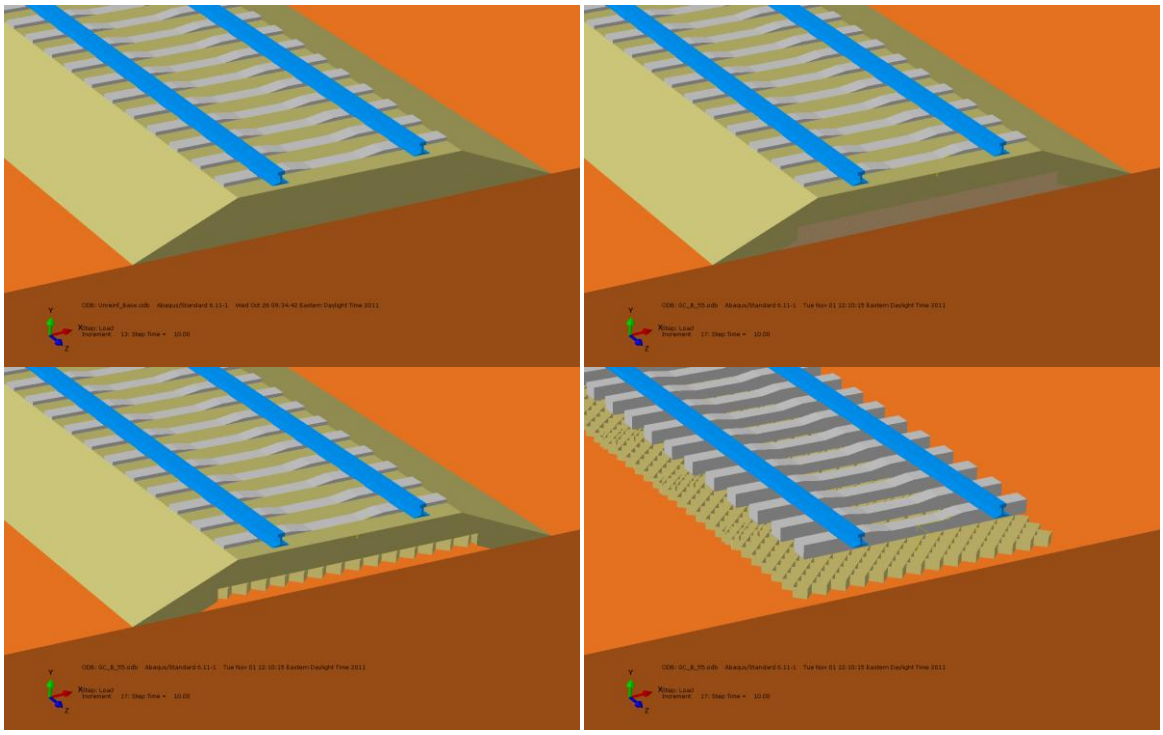

Figure 5.5a. Various views of the unreinforced railroad embankment (top left) and components of the reinforced railroad embankment when mirroring symmetry.

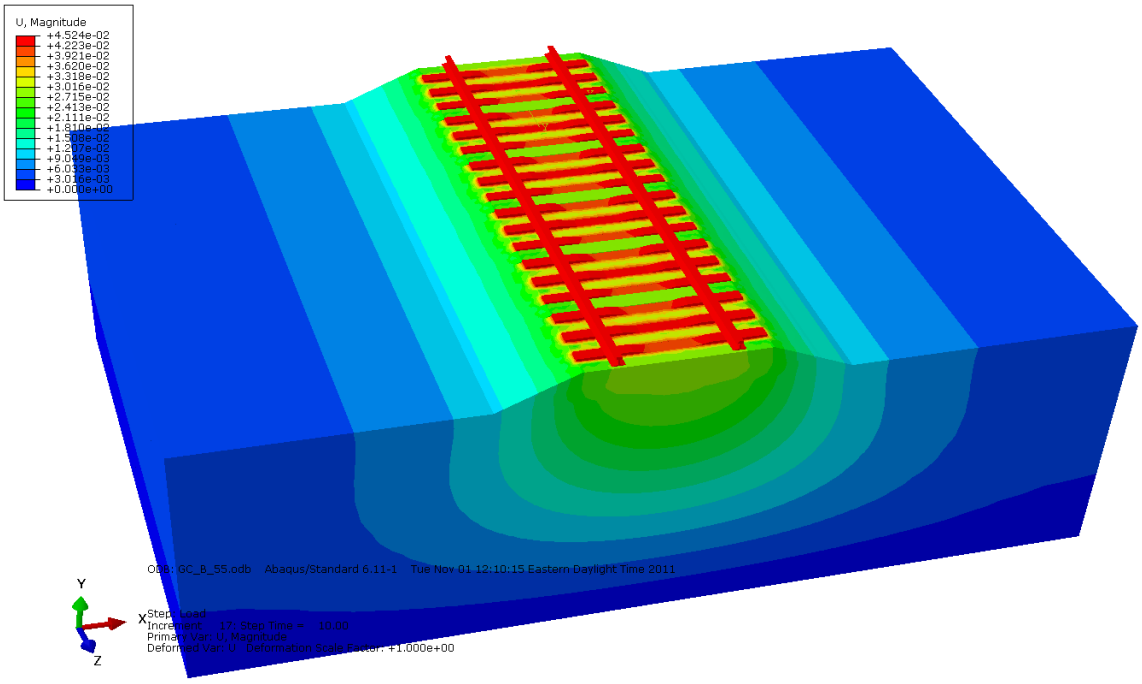

Figure 5.5b. The model is mirrored due to its symmetry and can therefore allow visualization of embankment behavior (displacement shown) in a more intuitive way.

5.3.2 Boundary Conditions

The plane strain slice of half of the ballasted railroad embankment and foundation was assigned several boundary conditions meant to reduce boundary effects, take advantage of symmetry and simulate reality. The vertical planes under the centerline of the railroad and along the outer edge of the foundation were constrained from displacing laterally in the X-direction (*figure 5.6*). The same constraint was affixed to the the Z-X planes to prevent lateral displacement in the Y-direction. The base of the model was restricted from any displacement.

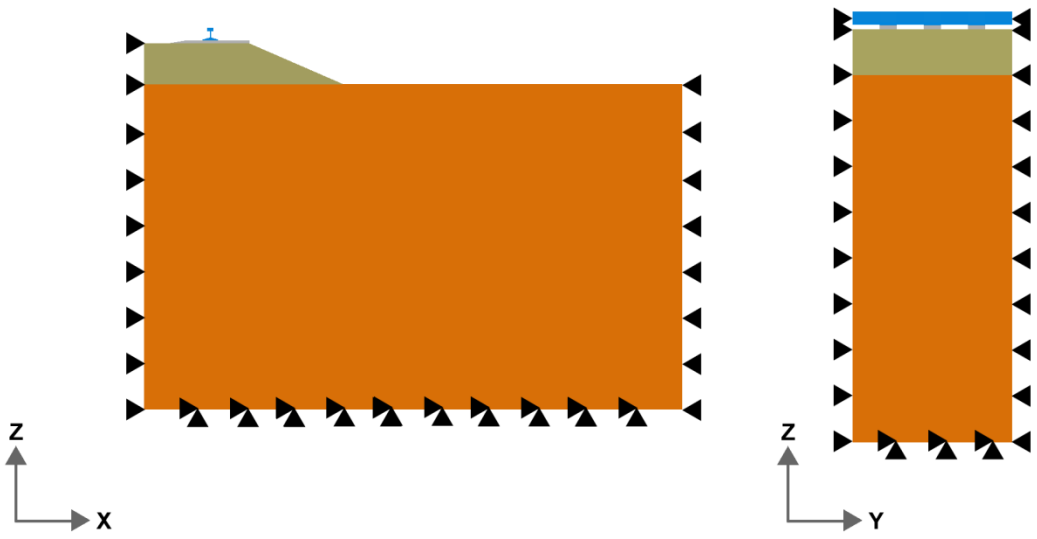

Figure 5.6. Boundary conditions of the FE model.

5.4 Material Properties

The material properties used in the analysis were based on results of experimental data from previous tests, well-established properties and demonstrative parametric data (*Table 5.1*).

The ballast and subballast were modeled using the same models (Drucker-Prager, *Appendix B*) and techniques as used to simulate the laboratory tests. The circumscribed circle of the model, based on the compressive strength properties of the soil, was used. Again, the model was chosen due to its simplicity, a possible drawback, but deemed acceptable in order to ignore multiple, complicated parameters necessary for more complex models.

The foundation was modeled as an elastic material to simply demonstrate the effects of a soft or loose soil that has settled greatly without any pore pressure or time-related behavior (undrained and/or consolidation).

The geocell was modeled as an elastic material again since experimental results suggested that the geocell rarely underwent large strain during testing. Additionally, the geocell has essentially failed when it has begun to undergo large plastic strain.

Both the concrete and steel were modeled as elastic materials as their stiffness values are well-defined. However, the high magnitude of these material properties in comparison to those of the ballast, foundation or geocell material simulated near-rigidity for the track structure.

Properties	**Ballast**	**Subballast**	**Foundation**	**Geocell**	**Rail/Tie Plates**	**Ties**
Mass Density, ρ (kg/m3)	1520	1520	1700	1500	2000	2000
Elastic Modulus, E (MPa)	2	2	20	2070	200000	30000
Poisson's Ratio, ν	0.35	0.35	0.35	0.35	0.3	0.25
Internal Angle of Friction, ϕ	45°	45°	-	-	-	-
Angle of Dilation, ψ	15°	15°	-	-	-	-
Cohesion, c' (kPa)	1	1	-	-	-	-

Table 5.1. FE material properties.

5.5 Loading

The wheel load chosen for the geometry was very conservative in order to demonstrate track behavior under the worst conditions possible. That is, the load corresponds to two wheels, each having a wheel load representative of a double stack of containers on a flatcar, equivalent to a wheel load of 50,000 lbs, or 25 tons (USACOE Railroad Design Manual). Therefore, the equivalent load is 100 kip (450 kN), placed on a small area of the steel railroad track to represent approximate point-loading of a wheel on a rail. The loading was applied monotonically above the central tie in the 1.8 meter-wide, plane-strain slice as it provides the most conservative representation by distributing the loads over a slightly smaller group of ties, in turn, applying a larger load generally encountered. The choice of width for the slice is based on the element allowance (20,000 elements maximum) and necessary geometry to demonstrate the behavior of the ballast embankment, with and without geocell. The density of the mesh did not show extreme variations when the number of elements was greater (approaching 20,000), but showed significant differences when the meshing was coarse (<5,000 elements).

5.6 Parametric Study

A series of simulations were performed on the railway geometry in order to determine the effects of foundation compressibility, ballast strength and geocell stiffness. In order to compare the results, each scenario was run with both geocell reinforcement and no reinforcement for comparison. During the simulation, displacements, stresses and strains were observed throughout the rail substructure in order to determine the behavior and improvement due to geocell reinforcement.

5.6.1 Foundation Compressibility

The effects of foundation compressibility were studied by varying the elastic modulus of the subgrade from very soft foundation, 2 MPa, to very stiff material at 1 GPa. As previous studies implied, geocell confinement is particularly useful when the railway substructure overlies a soft foundation. The "mattressing" effect of the geocell/ballast composite allows for a more even distribution of stress, increasing bearing capacity and reducing settlement.

It is essential to mention that the soft foundation was modeled as simply an elastic, which is not a perfect representation of the very complex, coupled flow-time consolidation problem that may occur. It is meant to demonstrate how the use of geocell may change the distribution of vertical subgrade stresses and thus reduce settlements. Further analyses are necessary to study the effects of the coupled time-pore pressure (or undrained) problem that occurs when considering consolidation. In such analyses the foundation soil would be idealized by a robust clay model such as the Modified Cam-Clay model.

One great advantage of the geocell was its redistribution of stress over a wider area (*figures 5.7a* and *5.7b*). Not only did use of geocell over a very soft foundation (2 MPa) distribute the stress more evenly; it reduced the magnitude of the subgrade stresses. The peak stress was reduced by approximately 15% when using geocell. Additionally, the difference between the middle and peak stresses under the tie was reduced significantly; that is, by 33 KPa (16%) and 15 KPa (10%) for the peak and middle stresses, respectively. The distribution of the rail loads over a wider area is also advantageous as it mobilizes more of the subgrade's strength and resistance, unlike the singular peak loads that induce shear when no reinforcement is present.

The use of geocell confinement reduced the vertical settlement, although it was not as significant as expected (*table 5.2*). This is likely due to the large stresses transferred to the subgrade, with or without the geocell. The geocell, however, does assist in redistributing the stresses more evenly, possibly preventing development of high shear strains and failure. The largest reduction in settlement occurred when the ballast embankment overlaid a very stiff subgrade, where much of the vertical settlement was due to lateral spreading and squeeze in the ballast. The confinement mechanism of the geocell was effective in preventing this occurrence, reducing the geocell settlement by about 23% (from 2 cm to 1.6 cm). However, the effects of the reinforcement were demonstrated in all cases of varying subgrade stiffness by reduction of settlement.

Intuitively, lowering the magnitude of vertical stresses occurring on the subgrade, especially when composed of soft, loose soils, reduces vertical and lateral displacements of the railway structure. Use of geocell in the base of the ballasted embankment reduced the magnitude of lateral spreading by 67% and also caused the largest lateral spreading to occur just by the crest, near the ties (*figures 5.8a* and 5.*8b*). The use of the geocell confinement contributes resistance to spreading above the reinforcement itself, likely through restraint by the composite mattress. The prevention of lateral spreading is especially pronounced when the railroad substructure overlies softer subgrades.

The geocell encountered small strains in all of the cases, generally within the elastic range of its material properties, varying between 0.8% and 2.5% for the stiffest and softest foundations, respectively. The highest concentrations of strain generally occurred in the region of geocell underlying the tie plates and outer edge of the ties. The portion of geocell lying outside of this

area generally encountered lower strains and stresses, suggesting that it may not be necessary to attain the benefits of the ballast-geocell composite.

Table 5.2. Results of parametric study varying foundation stiffness.

	Settlement under Tie (m)		
Young's Modulus (MPa)	**Geocell**	**None**	**Reduction (%)**
2	0.268	0.285	5.6
10	0.069	0.076	8.0
20	0.043	0.048	10.7
100	0.021	0.026	18.1
200	0.018	0.023	20.3
1000	0.016	0.020	22.4

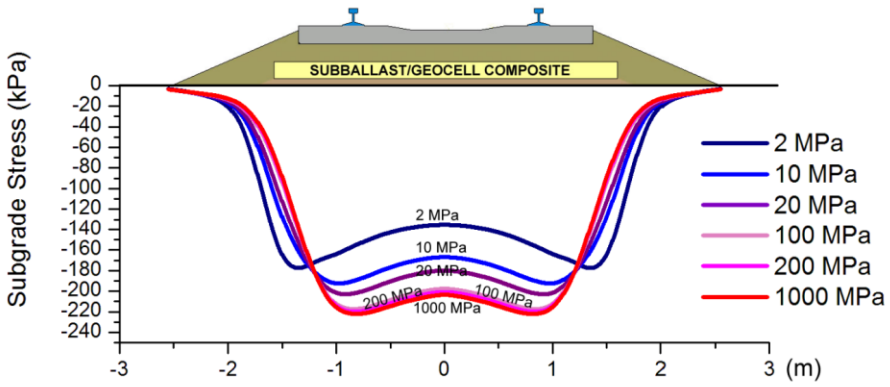

Figure 5.7a. Vertical subgrade stress distribution below geocell-reinforced embankment.

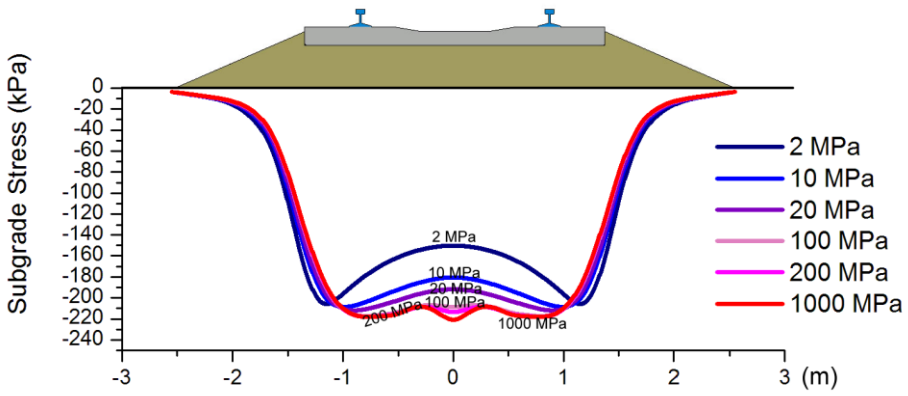

Figure 5.7b. Vertical subgrade stress distribution below unreinforced embankment.

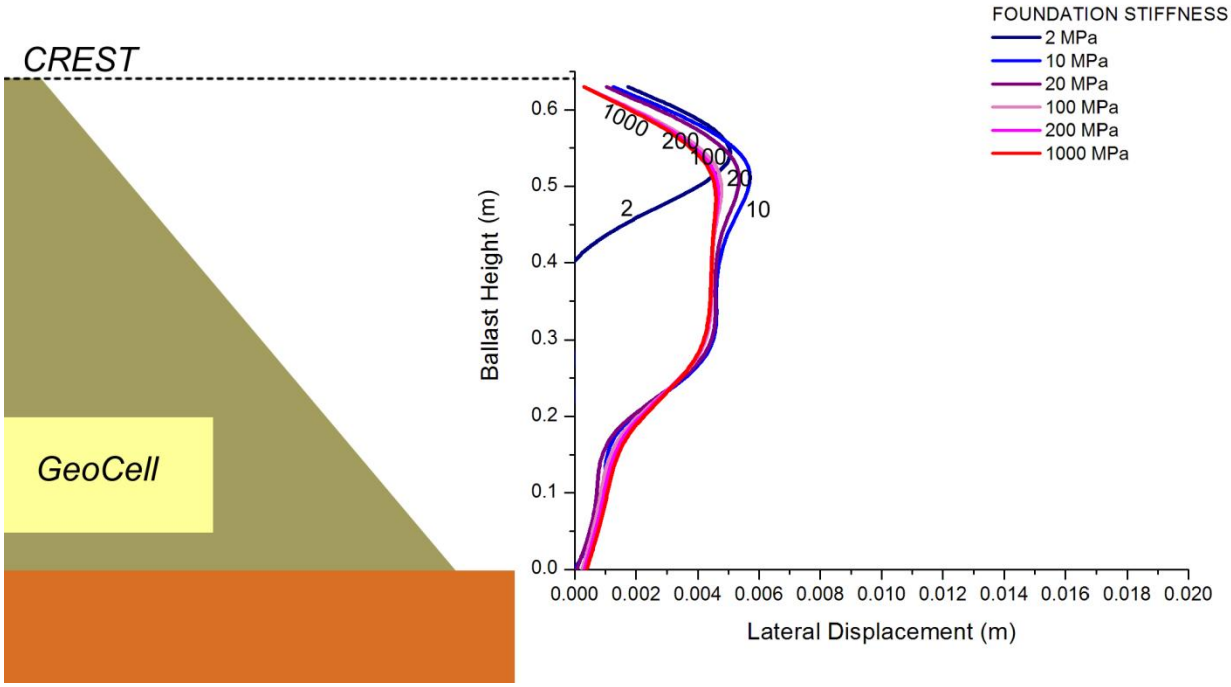

Figure 5.8a. Lateral displacement at slope of geocell-reinforced embankment.

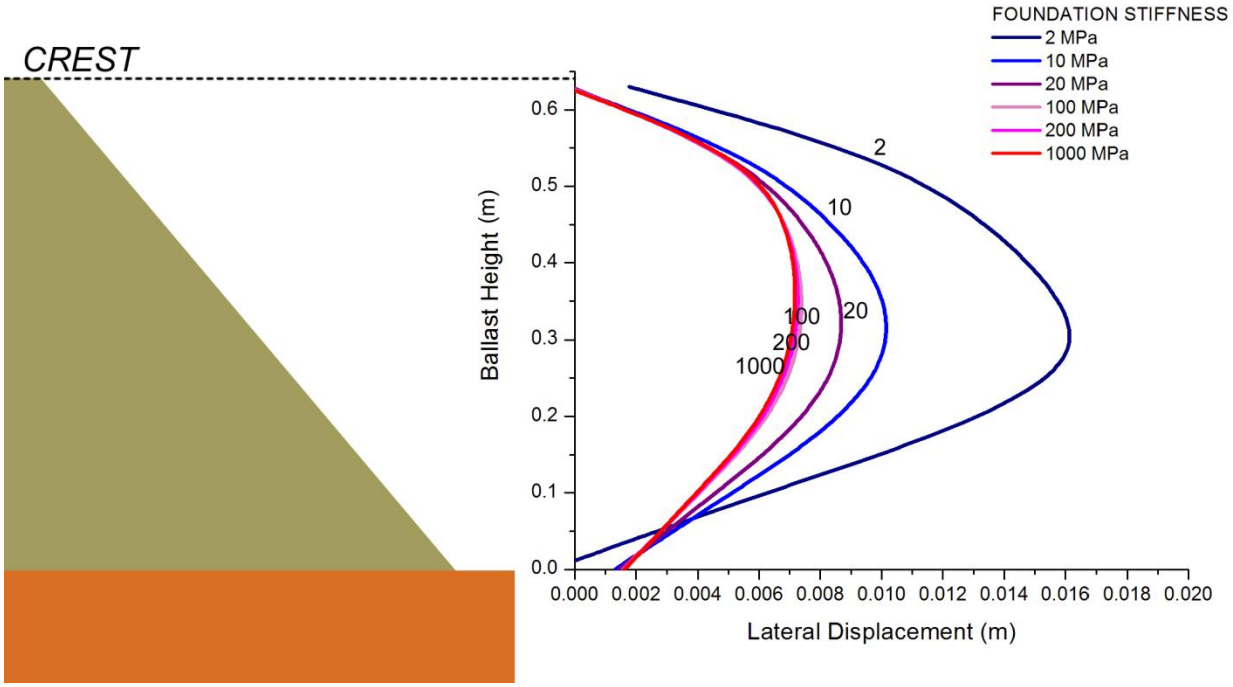

Figure 5.8b. Lateral displacement at slope of unreinforced embankment.

5.6.2 Ballast Strength

Over many loading cycles, often measured in Millions of Gross Tons (MGT), ballast can deteriorate through abrasion and fracture due to asperities and faults (Inraratna, 2003). This "rounding" of particles and loss of resistance due to a reduction in angularity reduces the critical strength property of ballast, i.e., its internal friction angle. Therefore, it is relevant to see what benefits geocell would provide the railway substructure, especially when deteriorated, perhaps representing old ballast or even showing promise for recycled ballast. To simulate the effects of confinement for a variety of materials with varying strengths, the internal friction angle of the ballast and subballast varied from 25° to 55°, representing the peak friction angle of fresh ballast (Indraratna, 2006). The subgrade stiffness was kept constant at 20 MPa throughout the different simulations.

The confinement of the ballast using geocell was quite effective in reducing vertical and lateral deformations, especially when low-quality material was used (*Table 5.3*). This is very encouraging, especially considering that ballast with strength properties less that are sub-standard could be used for the substructure, potentially at a lower cost. When the strength of the gravel was very low (ϕ=25°), the use of geocell reinforcement reduced vertical settlement by almost 23%, from 6.6 cm to 5.1 cm below the tie. Also, a more realistic strength value of ϕ=35° demonstrates similar behavior with a reduction in tie settlement from 5.1 cm to 4.4 cm, a decline of 13%. Higher shear strength of the ballast reduces the need for reinforcement, eliminating the need for substructure improvement as demonstrated by the similar settlement values for the reinforced and unreinforced scenarios.

In addition to reducing vertical displacement below the track structure, the lateral spreading and "squeeze" effects on the substructure profile were greatly affected by application of the geocell. This was demonstrated by the significant reduction in horizontal displacements along the slope of the ballasted foundation, especially at or below the level of the confined layer (*figures 5.10a* and *5.10b*). As expected, the larger displacements occurred in weaker materials (i.e. $\phi < 45°$), but were greatly reduced in magnitude as the spreading was diminished by almost 44% (2.25 cm to 1.25 cm) and 50% (4.9 cm to 2.4 cm), for the ϕ =35° and ϕ =25° cases, respectively. Intuitively, this prevention of spreading consequentially reduces vertical settlements as well, especially when the ballast overlies a stiff foundation, as the substructure materials will not squeeze horizontally under heavy loads. The effect of the geocell is demonstrated by not only the reduction in lateral deformations in comparison to the unreinforced ballast foundation, but also the location of the spreading along the embankment profile. The most spreading occurs above the layer of geocell placed at a safe, constructible clearance below the railroad ties. When the confinement is absent,

the center of the embankment displays much more spreading behavior along the middle and lower portions of slope near the toe, in addition to significantly larger magnitudes of deformation. An added advantage of the prevention of displacements is the increase in strength and stiffness of the railroad substructure due to the confinement of the geocell.

Another factor that preserves the structural integrity of the ballasted embankment is a more uniform transmission of train loads to the subgrade underlying the substructure (*figures 5.9a* and *5.9b*). The use of geocell confinement adds this advantageous behavior through its "mattressing" effect, as demonstrated by the subgrade stress distributions from the analysis. The use of geocell in conjunction with weaker ballast results in a significant decrease in vertical stress upon the subgrade, reducing its peak by almost 18% in magnitude (290 kPa to 240 kPa) and 10% (240 kPa to 215 kPa) for ϕ =25° and ϕ =35°, respectively. Additionally, the area that the elevated vertical stresses are distributed to is wider than that found without application of geocell, increasing the width of the transmitted load in the subgrade from approximately 1.4 meters to 1.9 meters for the ϕ =25° case, a gain of 26%. The increase in the area of this effective subgrade reaction results in the mobilization of more shear resistance and strength in the foundation and reduces the probability for "punching" failure in underlying foundation.

The geocell encountered small strains in all of the cases, generally within the elastic range of its material properties, varying between 0.9% and 1.3% for the strongest and weakest ballast friction angles, respectively. The highest concentrations of strain generally occurred in the region of geocell underlying the tie plates and outer edge of the ties. Similar to the previous study, the portion of geocell lying outside of this area generally encountered lower strains and stresses, suggesting that it may not be necessary to attain the benefits of the ballast-geocell composite.

Table 5.3. Results of parametric study varying ballast strength.

	Settlement under Tie (m)		
Internal Angle of Friction (°)	**Geocell**	**No Geocell**	**Reduction (%)**
25	0.05096	0.06571	22.4
35	0.044269	0.05086	13.0
45	0.04286	0.047971	10.7
55	0.042312	0.046721	9.4

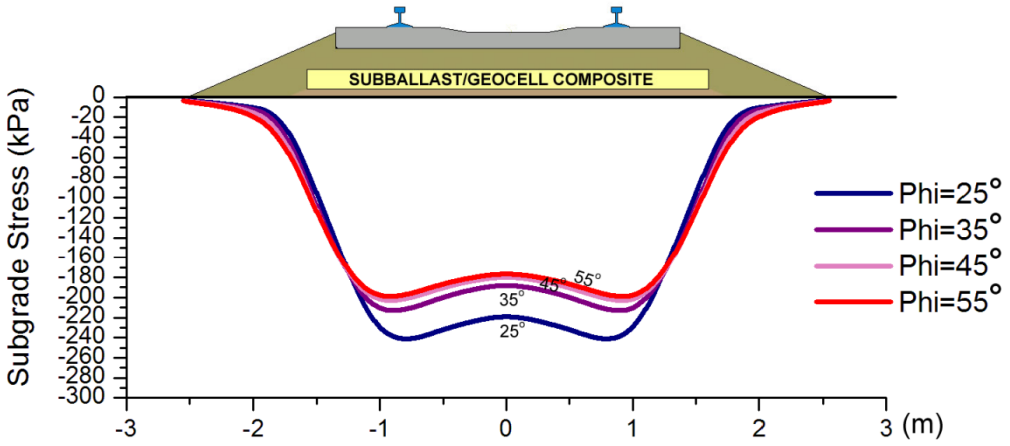

Figure 5.9a. Vertical subgrade stress distribution below geocell-reinforced embankment.

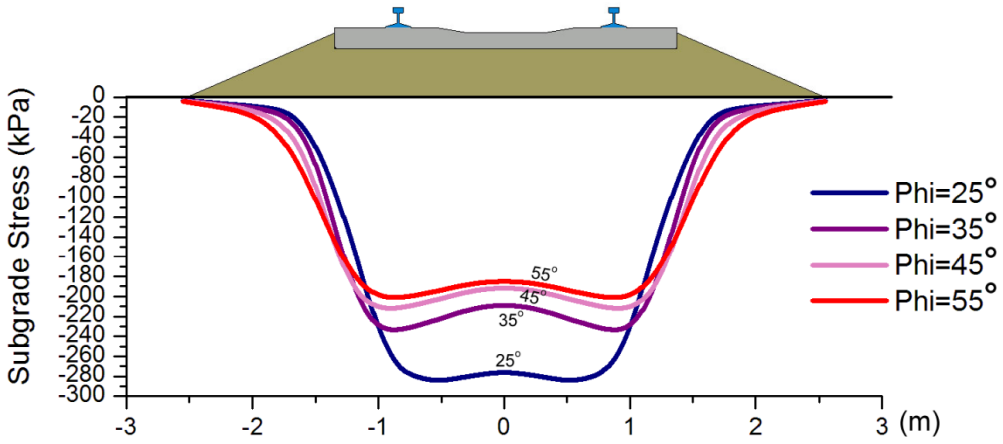

Figure 5.9b. Vertical subgrade stress distribution below unreinforced embankment.

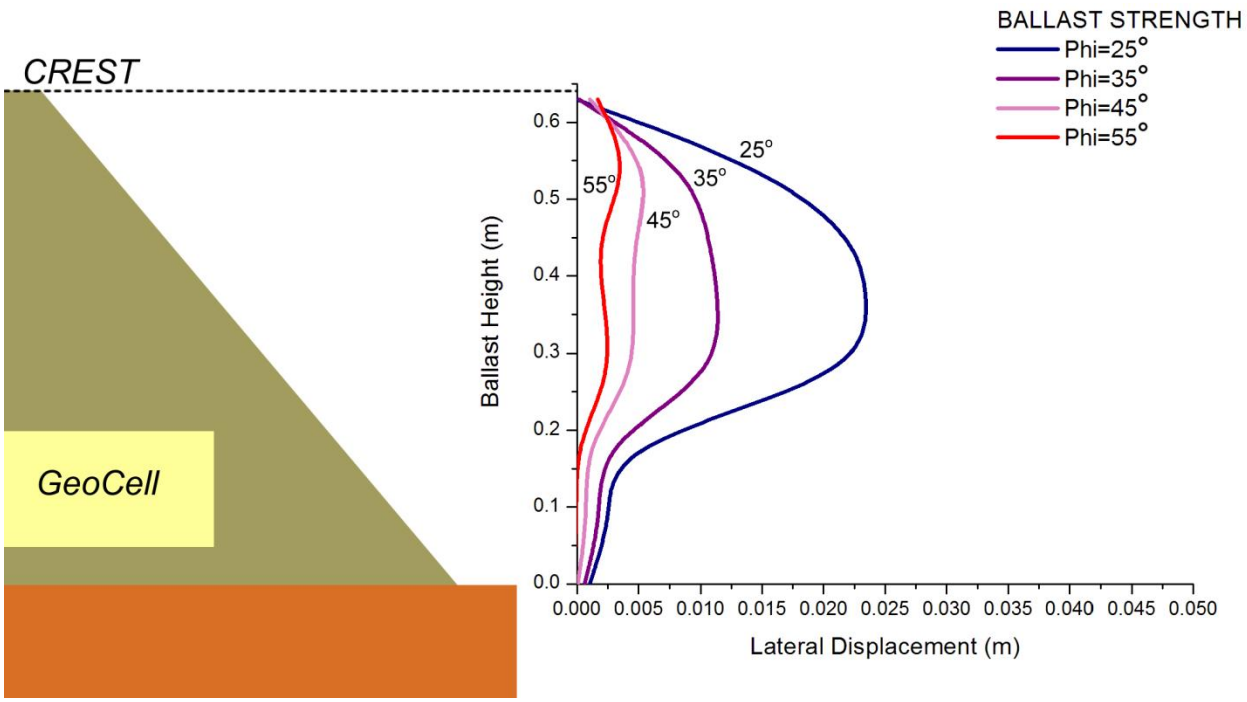

Figure 5.10a. Lateral displacement at slope of geocell-reinforced embankment.

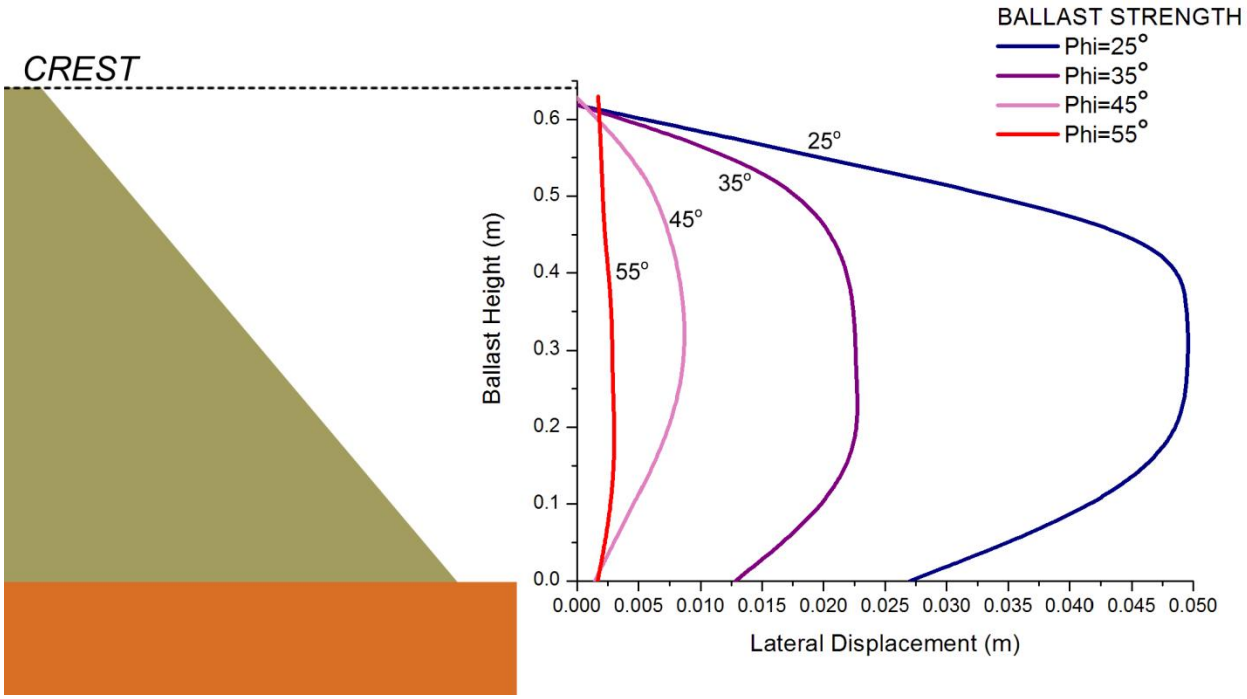

Figure 5.10b. Lateral displacement at slope of unreinforced embankment.

5.6.3 Geocell Stiffness

An important factor in the behavior of ballasted railway embankments that use geocell confinement is the effects of the stiffness of the geocell material. Geocell is made with a variety of materials, including High Density Polyethylene (HDPE) and Novel Polymeric Alloy (NPA), which both have Young's Moduli in the same order of magnitude. The implications of being able to utilize significantly inferior materials for geocell while still attaining the same benefits is enticing, especially from an economical viewpoint. In order to address this issue, similar FE analyses to those previously simulated were performed on the same ballasted embankment with geocell confinement. However, the stiffness of the geocell was altered using a variety of values that ranged from the very low Young's Modulus of rubber, 0.1 GPa, to very high values like that of Structural Steel, 200 GPa and in between (0.5, 1, 2.07, and 100 GPa). To demonstrate its effects in varying foundation conditions, this study was performed on both a very soft foundation (2 MPa) and a soft foundation (20 MPa). The study of the effects of geocell material on the embankment behavior demonstrates that the stiffness of the reinforcement does not have a significant effect on the performance of the substructure.

The reduction in vertical settlement under the ties and lateral deformation along the slope of the embankment are not highly affected by reasonable geocell materials, as demonstrated by the relatively similar vertical settlements and lateral deformations attained from the numerical simulations (*Tables 5.4* and *5.5*). In fact, the reduction of settlement when comparing a reinforced embankment to an unreinforced embankment is only 2.4% and 5.6% when overlying a 2 MPa foundation and 4% and 10.6% when overlying a 2 MPa foundation for rubber geocell or NPA geocell, respectively. Additionally, the use of varying reinforcement materials

demonstrates little practical gain in the prevention of lateral spreading, one of the main additions to structural and performance integrity for the railroad substructure. The range in magnitudes for peak lateral displacements on the slope of the ballasted embankment only varies between 0.25 cm and 1 cm as well as 0.35 cm and 0.65 cm when comparing steel and rubber overlying a 2 MPa foundation 20 MPa foundation, respectively (*figures 5.12a* and *5.12b)*. These differences are not exceptionally significant in practical terms. Even during use of less stiff reinforcement materials, the benefit of the geocell was still significant and likely more cost-efficient and practical than using very stiff materials like steel. Although use of structural steel did almost eliminate lateral deformations, fabrication, installation and economics of such a material in geocell would likely by prohibitive. Additionally, its effectiveness may not be completely utilized due to a lack on strain in the geocell and inability to allow easy filling of pockets with infill.

The effect of geosynthetic stiffness yields little effect on the vertical subgrade stress distribution (*figures 5.11a* and *5.11b*). Intuitively, the confining effect causes the geocell-ballast infill composite to act as a stiffer, yet flexible "mattress", allowing a reduced and more uniform stress distribution to be transmitted to the subgrade. Little variation in vertical and lateral deformations as well as near-congruent subgrade stress distributions suggests that the stiffness of the geocell has little effect on the effectiveness of the confining mechanism. Comparison of subgrade stress distributions when using NPA (the material used in experiments) and low stiffness materials like rubber show increases of only 9% and 4% for peak stresses when overlying 2 MPa and 20 MPa foundations respectively. Such differences may not be considered significant, especially when account for cost-effectiveness of material choice. Actually, simulations suggest that use of more

rigid materials like steel yield less uniform stress distributions due to the stiffness of the geocell-ballast composite.

Materials that are commonly used in geosynthetic reinforcements like HDPE and NPA have Young's Moduli that lie in the same order of magnitude. Simulations make it evident that they yield near-identical results, suggesting that development of ultra-stiff and strong materials for geocell confinement are not necessary as the confining mechanism does not heavily rely on high stiffness. However, it is important to indicate that the simplified analysis that occurred only accounts the geocell as an elastic material since the strains that occurred in the experimental phase were mostly elastic and the condition of geocell after loads was generally good. Certain materials might encounter plasticity at higher/lower strains and have different creep, temperature and electro-chemical properties than those tested in laboratory experiments.

As expected, the geocell encountered a large range of strains, depending on the stiffness of the chosen reinforcement material. As expected, for a low-stiffness, hyper-elastic material (0.1 GPa), the strain was 8.8% and 5.9% overlying a 2 MPa and 20 MPa foundation, respectively. When the stiffness was representative of HDPE, the strains encountered were 4.8% and 1.3% for a 2 MPa and 20 MPa foundation, respectively. This suggest behavior within the elastic range of HDPE when overlying a stiffer foundation, but mobilizing the geocell confinement more when a soft subgrade was present. When the geocell was made of "steel", the strain was negligible, remaining around 0.05% for both subgrades. Again, The highest concentrations of strain generally occurred in the region of geocell underlying the tie plates and outer edge of the ties. Similar to the previous study, the portion of geocell lying outside of this area generally

encountered lower strains and stresses, suggesting that it may not be necessary to attain the benefits of the ballast-geocell composite.

Table 5.4. Results of parametric study varying geocell stiffness overlying very soft foundation (2 MPa).

	Settlement under Tie (m)		
Geocell Stiffness (MPa)	**Geocell**	**None**	**Reduction (%)**
100	0.277602	0.284536	2.4
500	0.273676	0.284536	3.8
1000	0.271319	0.284536	4.6
2070	0.268476	0.284536	5.6
100000	0.25799	0.284536	9.3
200000	0.257586	0.284536	9.5

Table 5.5. Results of parametric study varying geocell stiffness overlying soft foundation (20 MPa).

	Settlement under Tie (m)		
Geocell Stiffness (MPa)	**Geocell**	**None**	**Reduction (%)**
100	0.04605	0.047971	4.0
500	0.044335	0.047971	7.5
1000	0.043577	0.047971	9.1
2070	0.04286	0.047971	10.6
100000	0.039879	0.047971	16.9
200000	0.039662	0.047971	17.3

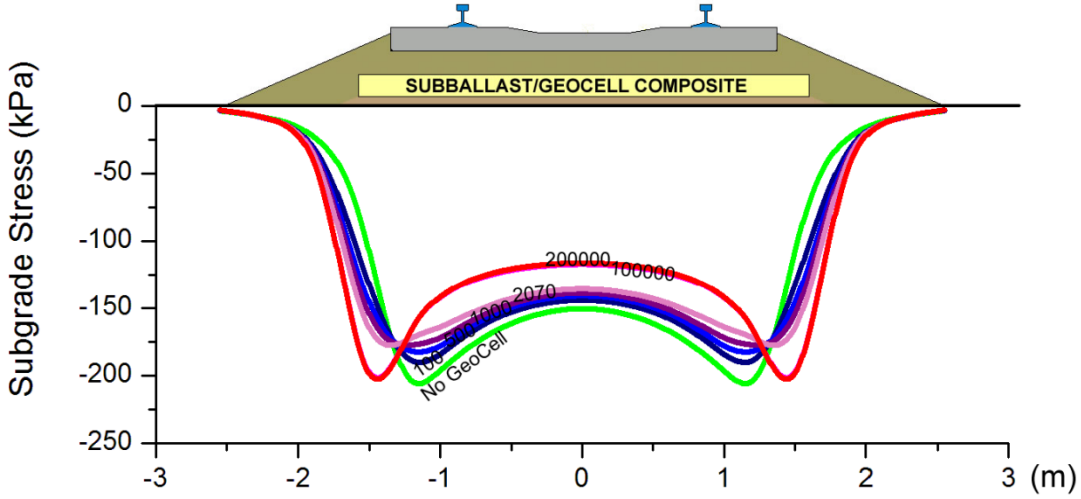

Figure 5.11a. Subgrade stress distribution below geocell-reinforced embankment overlying very soft foundation (2 MPa).

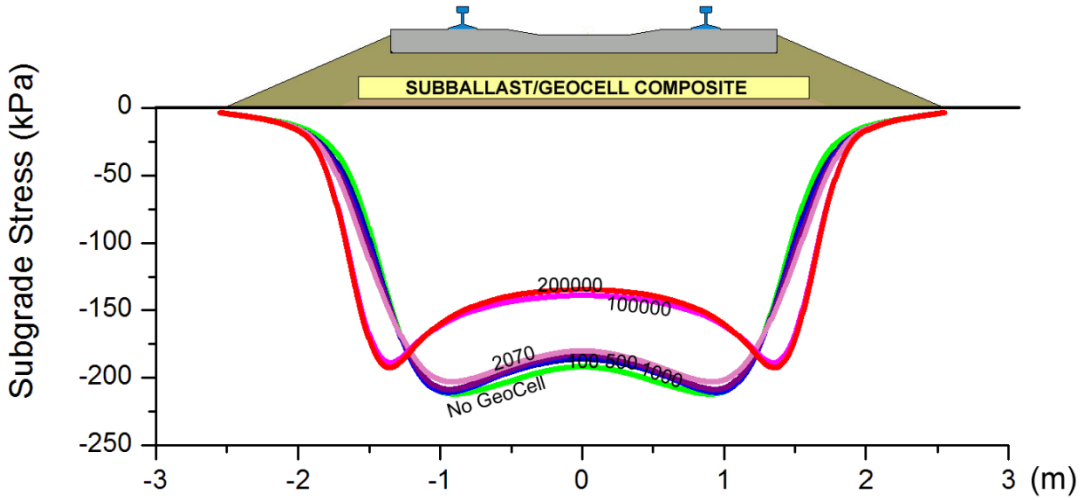

Figure 5.11b. Subgrade stress distribution below geocell-reinforced embankment overlying soft foundation (20 MPa).

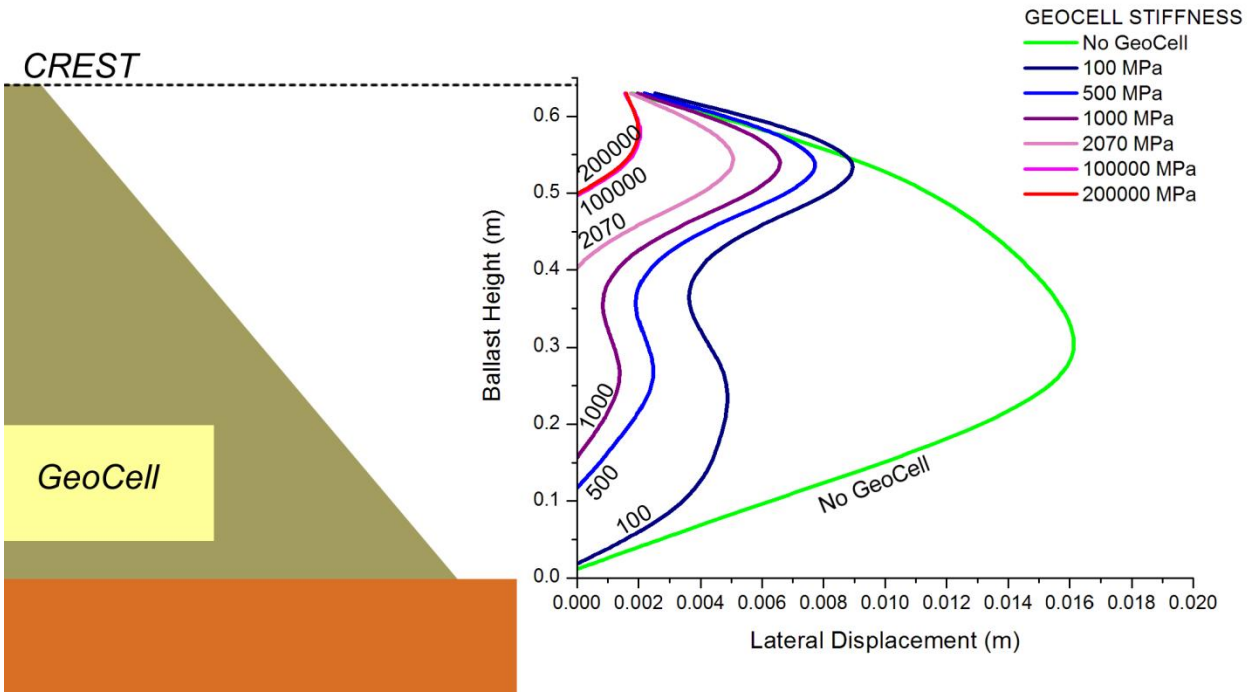

Figure 5.12a. Lateral displacement at slope of geocell-reinforced embankment overlying very soft foundation (2 MPa).

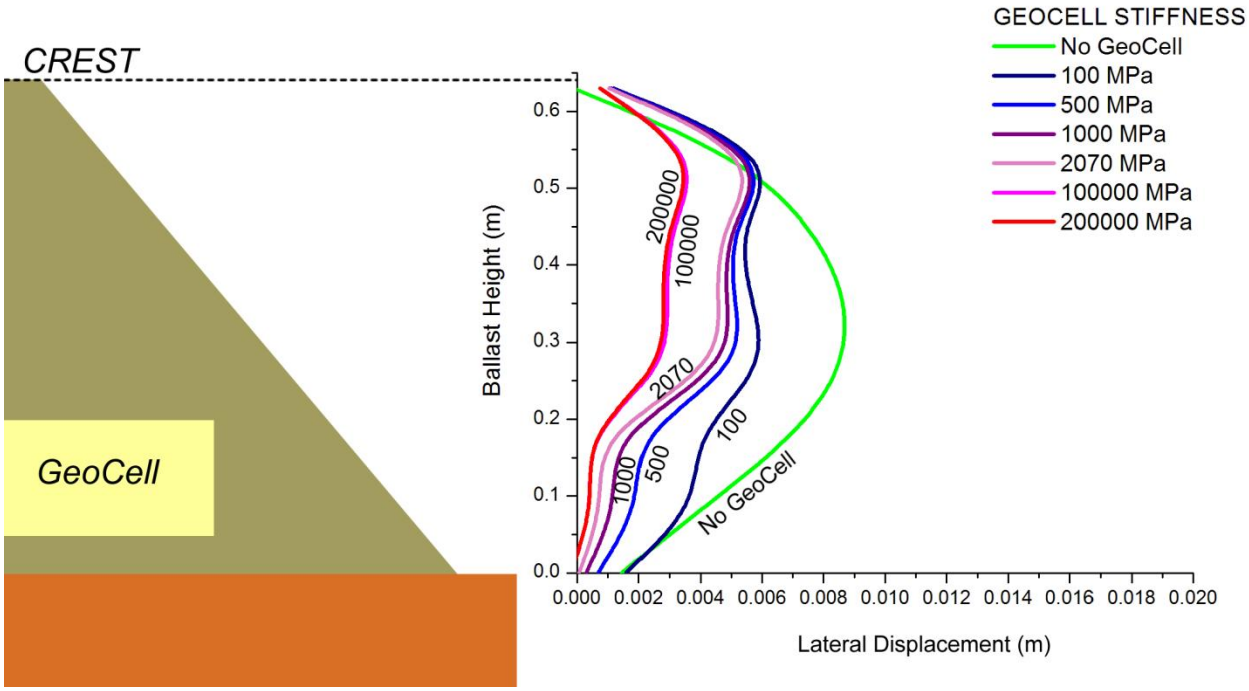

Figure 5.12b. Lateral displacement at slope of geocell-reinforced embankment overlying soft foundation (20 MPa).

5.7 Conclusions and Summary

Experimental data and validation and calibration through FE analysis allowed for further studies, including a parametric study on the experimental geometry which had implications on design and performance of geocell placed within ballast. Further simulations and practical inferences could be made from applying the geocell to the actual geometry of a ballasted railroad substructure. Performing a parametric study on realistic geometry and applications could allow insight into its performance in actual railroads. Again, analyses were performed by varying ballast strength to simulate inferior track material, foundation stiffness to simulate soft subgrades, and geocell stiffness to observe the effect of reinforcement material on overall performance. Conclusions made from numerical modeling of geocell applied to a railroad scenario include:

1) The confinement of the ballast using geocell was quite effective in reducing vertical deformations, especially when low-quality material was used. Higher shear strength of the ballast reduces the need for reinforcement, eliminating the need for substructure improvement. This is promising when considering the possibility for using weaker ballast materials like recycled ballast or well-graded particles.

   The use of geocell confinement reduced the vertical settlement, although it was not as significant as expected. This is likely due to the large stresses transferred to the subgrade, with or without the geocell. The geocell, however, did assist in redistributing the stresses more evenly, possibly preventing development of high shear strains and failure. Upon

stiffer foundations, the geocell prevents vertical settlement by reducing lateral squeeze of the ballast due to high loading.

2) Lateral spreading along the slope of the railroad substructure was greatly reduced with application of confinement to the ballast. The prevention of lateral spreading is especially pronounced when the railroad substructure overlies softer subgrades and when weaker ballast materials are used. This was demonstrated by the significant reduction in horizontal displacements along the slope of the ballasted foundation, especially at or below the level of the confined layer. The use of the geocell confinement likely contributes resistance to spreading above the reinforcement through frictional resistance of the composite mattress.

3) The geocell allowed for a more uniform subgrade stress distribution. In addition to being more uniform, the magnitudes of stresses were reduced significantly in addition to distribution of stresses to a wider area, in turn, mobilizing more of the subgrade's shear strength and preventing shear failure. Not only did use of geocell distributed the stress more evenly; it reduced the magnitude of the subgrade stresses when placed over a very soft foundation or in an embankment consisting of weak ballast.

4) Again, for materials commonly used as geosynthetic reinforcements, the benefit of using superior geocell materials are not pronounced, suggesting that the confinement mechanism does not necessitate expensive, top-grade polymers or alloys to function adequately. In fact, even use of materials with low Young's Moduli like rubber

demonstrate an improvement of performance likely because the stiffness of ‘weak’ reinforcement materials are still orders of magnitude stiffer than the ballast surrounding it. However, it is important to note that certain materials might encounter plasticity at higher/lower strains and have different creep, temperature and electro-chemical properties than those tested in laboratory experiments.

CHAPTER 6: CONCLUSION

6.1 Conclusions and Recommendations

In this study, tests were performed on gravel embankments with and without geocell reinforcement in monotonic and cyclic loading conditions to observe the stress, stiffness and deformation behavior. The experimental results from these tests were used to validate numerical models on ballast structures confined by geocell. Acceptable agreement between the vertical load-deformation behavior in the FE simulation of experimental data necessitated further studies of the effects of various material properties involved in the testing. Lateral deformation was not especially accurate due to numerical modeling deficiencies. A series of parametric studies is performed on similar geometry to that used in experimental load testing and FE simulation, except properties like ballast strength, geocell stiffness, and compressibility of foundation were altered to demonstrate the effects of geocell confinement on embankment behavior. Finally, another series of parametric studies was performed on realistic ballasted railroad embankment geometry with and without geocell reinforcement. This study provided implications of use of geocell in various practical situations in a railroad substructure. These phases of study were able to demonstrate several important trends.

- Lateral and vertical displacements were reduced due to geocell confinement. Lateral displacements were especially reduced at, and below the level of geocell placement. This phenomenon was captured in both laboratory experiments and various scenarios using numerical modeling, although it was less accurately modeled using finite element

analysis due to model deficiencies and complex soil behavior (e.g. anisotropy, dilation, etc.) that was not necessarily properly accounted for by the constitutive models used.

- The bearing capacity and effective stiffness increases due to the use of geocell, likely due to the composite, "mattressing" effect and the prevention of lateral spreading, subgrade shear and vertical settlement.

- Numerical modeling demonstrates that use of geocell helps to distribute stresses to the subgrade more uniformly, both reducing its peak stress and distributing the the load to a wider area, hence mobilizing more subgrade soil strength. Such effects are especially apparent when weaker ballast is used or the ballast structure overlies a soft subgrade.

- Cyclic deformation was reduced when geocell was used to confine the ballast. A stabilization effect and gain of resilience was reached in embankments reinforced with geocell, unlike those without, which was demonstrated in both laboratory testing and Finite Element modeling.

- The geocell walls were generally within low tensile strains that were recoverable during all stages of loading. Such strains suggest that most of the loading in laboratory testing and numerical simulations was within a working load for the geocell material, as shown by strain gauges placed on geocell. However, this does not account for weaknesses in the seam connecting cells.

- The elastic nature of the geocell material did not have a significant effect on the performance of the ballast structure, as demonstrated by a variety of numerical simulations. Young's Moduli for a variety of materials commonly used in geosynthetics all generally performed similarly, suggesting use of higher grade material is not necessary in all situations.

These implications are valuable to the nature of the study, but are based on a few assumptions and drawbacks. The anisotropic nature of the material used in experimentation, prevented perfect matching of some displacements under loading. Additionally, the behavior of polymers is complex as it involves many factors that are difficult to model, including behavior under creep, high or low temperatures, UV exposure and electrochemical resistance. Therefore, the following assumptions and drawbacks are addressed.

- The behavior of granular materials, especially under low confinements is very complex. However, the general benefits of geocell can be demonstrated with the simplicity of the non-linear, Drucker-Prager plasticity conditions, which was considered acceptable for this numerical study. The application of plasticity to the ballast provides basic insight into geocell confinement, as it is reliant on the material friction angle, which governs the behavior of the infill within the geocell and the confinement mechanism. However, the model had significant drawbacks that must be considered for future analyses, including a possible overestimate of lateral displacements due to anisotropy and higher dilation angles, and inability to capture the true hysteretic, cyclic nature of ballast behavior.

- The plastic behavior of geocell is reliant on too many factors to simulate very complex mechanisms (e.g. creep, temperature) in this analysis, but such factors may not be relevant to show the beneficial nature of geocell in such an application, especially when considering the non-plastic strains endured in the material during experimental testing. Therefore, the geocell was modeled as an elastic material as it generally does not encounter very high strains under realistic loading of the surrounding soil.
- Further model tests should be performed to ensure consistency in results. Single tests in each configuration/loading scheme were performed due to time and laboratory constraints, but additional model testing would allow for more confidence in the experimental data.
- In the parametric studies, a basic design geometry was provided based on design constraints commonly used by AMTRAK for construction of unreinforced ballast foundations. There is no design critieria for railway substructures reinforced with geocell, but according to AMTRAK and literature, a minimum clearance between the ties and top lip of the geocell was recommended.

6.2 Practical Issues

One practical concern about the use of geocell is the installation of the material in the substructure. Commonly, such reinforcement requires workers to spread the material out to its specified length, and drive stakes into the outer cells, keeping the geocell honeycomb structure in tension. Then, ballast must be place within by means of pouring the granular material from a specified height, and ensuring that a layer of at least 25 cm overlies the top lip of the infilled geocell. This provides a cushion for tamping and compaction of the ballast. Due to the poorly-graded nature of ballast and subballast (for drainage reasons), the ballast often reaches a high

relative density with very little more than placement, suggesting the compaction of infill may not be a critical issue. When placing the ballast on soft foundations, construction can also be a concern with geocell. In such cases, a sacrificial geogrid or membrane could be placed above the soft layer to facilitate compaction and construction upon problem soils.

Related and important to the construction issues with geocell is the concern of maintenance problems with installation of geocell. If the geocell were installed just below the railroad ties, removal and replacement or cleaning of the fouled ballast would be an issue as it would interfere with maintenance equipment. However, placement of the geocell at a minimum of 25 cm below the ties allows safe removal of fouled ballast overlying the geocell-ballast composite, while leaving the confined ballast undisturbed. However, such technicalities may not be of concern if the geocell manages to extend the lifespan of the railroad substructure long enough to justify fewer maintenance cycles, a possible justification for its application to ballast railroad embankments.

The cost of geocell can also certainly play a role of whether it is a sustainable solution for railway substructure reinforcement. Depending on the material used for the reinforcement, cost-effectiveness should be a concern. However, lower-grade geocell materials can still serve a purpose effectively, as suggested by the implications of the parametric study. Therefore, geocell may still be a sustainable and economic solution, especially relevant to railroad right-of-way with high traffic, high wheel loads, poor soil conditions and sensitive surroundings. Geocell generally helps distribute subgrade stresses more evenly and prevents deformation, so it could prolong the lifespan of a railway embankment that sustains high traffic and therefore cannot encounter frequent service. It also assists performance for ballast embankments overlying soft

foundations, which can result in recurring and expensive maintenance issues for railways. The increased deformation performance that geocell adds to a ballasted embankment could be beneficial in situations where space is limited and surroundings are sensitive (roadway overpasses, near utilities, drainage canals, retaining walls). Use of such a solution could possibly be beneficial in cost-effectiveness considering the reduced maintenance cycles, or prolonged lifespan that could provide to railways, especially in sensitive or problem areas.

The material used to manufacture is also a concern not just economical reasons, but for performance requirements. One of the main concerns in design with such materials in railway substructure application would be that of creep. Millions of train passes and high stresses resulting from these loads could contribute to significant creep strains and deterioration. These are especially relevant in places that are prone to higher temperatures, where often heat can induce lower strengths, plastic strains and creep. Alternatively, some materials are prone to different deteriorations of the electro-chemical variety, including deterioration due to exposure to acids, bases, UV radiation or other environmental conditions. Such aspects should be a concern of the designer and geosynthetic manufacturer, however, the addition of very modest confinement can still be advantageous despite these concerns, which may not be relevant anyway depending on the design life of the substructure.

6.3 Suggested Further Studies

The implications of these experiments and simulations are promising, but could use further justification from real field testing. The performance of such an application of geocell in actual railroad foundations would be an essential step in demonstrating the various benefits provided by the geocell-ballast composite. This is especially true for railroad overlying soft foundations and

railroads in sensitive or constrained right-of-ways. These tests would need to be compared to identical track geometry and similar site conditions for appropriate comparison. Field testing is in the process of being arranged in conjunction with FRA and AMTRAK.

Further studies could provide insight upon the effects of placement and dimensions of geocell within a ballast embankment. Practical constraints like construction and maintenance should be considered, but more complex railroad foundations could be consider in addition to applying the material to the subgrade or in wider or narrower cases.

One important aspect of geocell that could be investigated and has significant implications on performance is the effects of aspect ratio of the pocket size and effects of ratio of ballast size to pocket size of the geocell. Use of geocell pockets that are not large enough in comparison to the grain size of the infill would not provide the advantageous “confining” effect that the geocell applies to the ballast. Further parametric studies on these effects and its optimization would be insightful and have economic implications.

Further complex analyses that could be performed is effects of geocell on degradation of ballast. Also, further studies could elucidate the important observations on the creep behavior of geocell over time and its effects on the behavior of the railroad embankment.

Material modeling of both the ballast and geocell material using more advanced plasticity models could simulate more accurate railway behavior at the expense of more elaborate laboratory tests. These tests could also include full-scale railway geometry and loading patterns representative of exact train wheel passes. Some possible added factors for these models are to capture the deterioration, anisotropy or angularity of the ballast.

REFERENCES

Chrismer, S. (1997). "Test of Geoweb® to Improve Track Stability over Soft Subgrade." *Association of American Railroads Railway Technology Department*. TD 97-045.

Desai, C.S. and Siriwardane, H.J. Constitutive Laws for Engineering Materials with Emphasis of Geologic Materials. Englewood Cliffs, NJ: Prentice-Hall, Inc., 1984.

Giroud, J.P. and Han, J. (2004). "Design method for geogrid-reinforced unpaved roads, Part I theoretical development." *ASCE Journal of Geotechnical and Geoenvironmental Engineering*. 130(8), 776-786.

Han, J., Leshchinsky, D., Parsons, R.L., Rosen, A, and Yuu, J (2008). "Technical Review of Geocell-Reinforced Base Courses over Weak Subgrade." *The First Pan-American Conference and Exhibition.* Vol. 1.1, Cancun: 1022-1030.

Hibbitt, Karlsson and Sorensen Inc. (2007). ABAQUS User's Manual, Version 6.7, Pawtucket, R.I.

Indraratna, B., Christie, D., Khabbaz, H. and W. Salim (2006). "Geotechnical Properties of Ballast and the Role of Geosynthetics in Rail Track Stabilisation." *Ground Improvement,* Vol. 10, No.3, 91-101.

Indraratna, B., Ionescu, D. and D. Christie (1998). "Shear Behaviour of Railway Ballast based on Large Scale Triaxial Testing." *Journal of Geotechnical and Geoenvironmental Engineering.* 124(5), 439-449.

Indraratna, B., S. Nimbalkar, D. Christie, C. Rujikiatkamjorn and Vinod, J (2010). "Field Assessment of the Performance of a Ballasted Rail Track with and without Geosynthetics." *ASCE Journal of Geotechnical and Geoenvironmental Engineering*. 136, 907-917.

Indraratna, B. and Salim, W (2002). "Modelling of particle breakage of coarse aggregates incorporating strength and dilatancy." *Proceedins of the Institution of Civil Engineers, Geotechnical Engineering*. Issue 4, 243-252.

Indraratna, B. and Salim, W. (2003). "Deformation and degradation mechanics of recycled ballast stablised with geosynthetics." *Japanese Geotechnical Society: Soils and Foundations,* Vol. 43, No. 4, 35-46.

Koerner, R. Designing with Geosynthetics, 5th Edition. Upper Saddle River, NJ : Prentice Hall, 2005.

Lackenby,J, Indraratna, B., G. McDowell and D. Christie (2007). "Effect of confining pressure on ballast degradation and deformation under cyclic triaxial loading." *Géotechnique*. 57, No. 6, 527-536.

Lai, M., Rubin, D. and Krempl, E. Introduction to Continuum Mechanics. Burlington, MA: Butterworth-Heinemann, 1993.

Leshchinsky, B. (2011) "Enhancing Ballast Performance Using Geocell Confinement." *Proceedings of Geo-Frontiers 2011*. 4693-4072.

Pokharel, S., Han, J., Manandhar, C., Yang, X., Leshchinsky, D., Halami, I. and Parsons, R. (2011). "Accelerated Pavement Testing of Geocell-Reinforced Unpaved Roads over Weak Subgrade." *Journal of the Transportation Research Board*, No. 2204, *Low-Volume Roads*. Vol. 2, 67-75.

Raymond, G. P. (2001). "Failure and reconstruction of a gantry crane ballasted track." *Canadian Geotechnical Journal*, 38(3), 507-507-529.

Selig, E. and Waters, J. Track Geotechnology and Substructure Management. London, England: Thomas Telford Books, 1994.

US Army Corps of Engineers Track Design Manual (2000), TI-850-02, AIR FORCE AFMAN 32-1125(I).

Webster, S.L. and Alford, S.J. (1977). "Investigation of Construction Concepts for Pavement across Soft Ground," *Report S-77-1. Soils and Pavements Laboratory*, U.S. Army Engineer Waterways Experiment Station, Vicksburg, MS.

Yang, X. (2010). *Numerical Analyses of Geocell-Reinforced Granular Soils under Static and Repeated Loads.* Ph.D., University of Kansas, United States.

Zhou, H. and Wen, X. (2008). "Model studies on geogrid- or geocell-reinforced sand cushion on soft soil." *Geotextiles and Geomembranes*. 26, 231-238.

APPENDIX A: LINEAR ELASTICITY CONSTITUTIVE MODEL

Linear-elastic behavior was used in the analysis since it is the simplest elasticity model available and would suffice to simulate their material. This material model is dependent on several parameters, including Poisson's Ratio (ν) and Young's Modulus (E), which were assigned to every material in the analysis based on real experimental data. Using these parameters and Generalized Hooke's Law, the stress-strain relationship based on this model can be defined as:

$$\varepsilon_{11} = \frac{1}{E}[\sigma_{11} - \nu(\sigma_{22} + \sigma_{33})]$$
$$\varepsilon_{22} = \frac{1}{E}[\sigma_{22} - \nu(\sigma_{11} + \sigma_{33})]$$
$$\varepsilon_{33} = \frac{1}{E}[\sigma_{33} - \nu(\sigma_{11} + \sigma_{22})]$$
$$\varepsilon_{12} = \frac{\sigma_{12}}{2G}$$
$$\varepsilon_{13} = \frac{\sigma_{13}}{2G}$$
$$\varepsilon_{23} = \frac{\sigma_{23}}{2G}$$

This model simulates strains as recoverable, that is, when load is removed, the strain returns to 0 as well unless any model for plasticity is applied to the material as well and yield criteria are reached. One such example is soil, which does not act as solely an elastic material.

APPENDIX B: DRUCKER-PRAGER PLASTICITY CONSTITUTIVE MODEL

The constitutive model chosen to simulate the plasticity behavior of soils in the numerical analyses was the Drucker-Prager elastic-perfectly plastic material law. This material law is advantageous because of its general simplicity and dependence on similar material properties than those used for Mohr-Coulomb Failure criteria (ϕ, c), yet its yield surface is rounded, avoiding the anomalous behavior that could arise from the Mohr-Coulomb yield surface (see *figure B.1*). Drucker-Prager Yield Criteria, also known as "Extended Von Mises" plasticity, is defined as:

$$f = \sqrt{J_2} - \alpha J_1 - k$$

Where the yield surface is dependent upon the second invariant of deviatoric stress, J_2, the first invariant of deviatoric stress, J_1, as well as α and k, which are dependent on the friction angle and cohesion of the material as follows:

$$J_2 = (\sigma'_1 - \sigma'_2)^2 + (\sigma'_2 - \sigma'_3)^2 + (\sigma'_3 - \sigma'_1)^2$$

$$J_1 = \sigma'_1 + \sigma'_2 + \sigma'_3$$

Conventional Triaxial compression:

$$\alpha = \frac{2\sin\phi}{\sqrt{3}(3 - \sin\phi)}$$

$$k = \frac{6c\cos\phi}{\sqrt{3}(3 - \sin\phi)}$$

Plane Strain compression:

$$\alpha = \frac{\tan\phi}{(9 + 12\tan^2\phi)^{0.5}}$$

$$k = \frac{3c}{(9 + 12\tan^2\phi)^{0.5}}$$

The yield surface is also dependent upon a flow rule, which uses a differential equation a constant of proportionality that describes the relationship of the stress increment to the yield function. However, since the material model was kept simplified due to limitations in material testing, the flow stress ratio, the constant of proportionality, was kept as unity, implying isotropy.

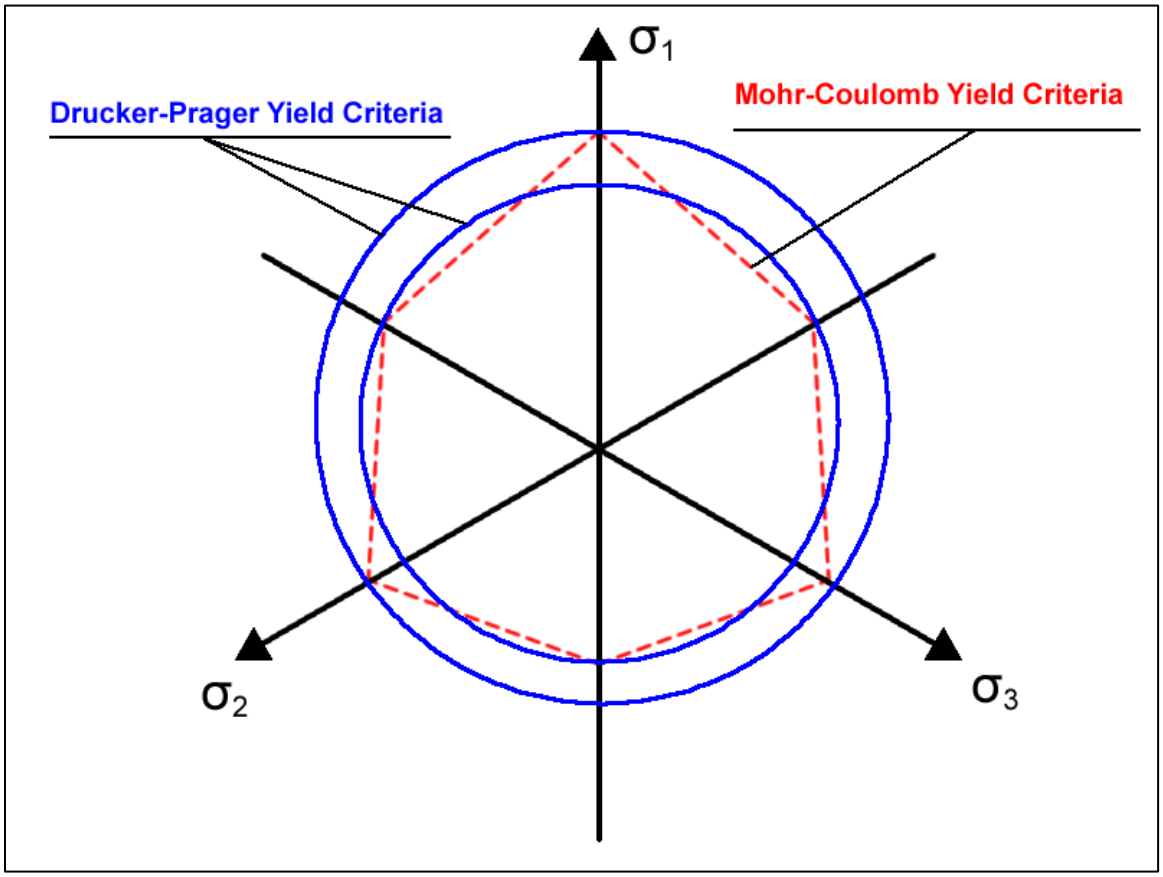

Figure B.1: Comparison of Drucker-Prager yield surfaces to Mohr-Coulomb yield surfaces.